

# Stress-Activated Kinase MKK7 Governs Epigenetics of Cardiac Repolarization for Arrhythmia Prevention

**Running Title:** Chowdhury *et al.*; MKK7 deficiency induces ventricular arrhythmias

Sanjoy K. Chowdhury, MBBS, PhD<sup>\*1</sup>; Wei Liu, MD, PhD<sup>\*†1</sup>; Min Zi, MD<sup>1</sup>; Yatong Li, MD, PhD<sup>1</sup>; Shunyao Wang, MSc<sup>1</sup>; Hoyee Tsui, PhD<sup>1</sup>; Sukhpal Prehar, MSc<sup>1</sup>; Simon Castro, PhD<sup>2</sup>; Henggui Zhang, PhD<sup>2</sup>; Yong Ji, MD, PhD<sup>3</sup>; Xiuqin Zhang, MD, PhD<sup>4</sup>; Ruiping Xiao, MD, PhD<sup>4</sup>; Rongli Zhang, MD<sup>5</sup>; Ming Lei, MD, PhD<sup>6</sup>; Lukas Cyganek, PhD<sup>7</sup>; Kaomei Guan, PhD<sup>7</sup>; Catherine B. Millar, PhD<sup>1</sup>; Xudong Liao, PhD<sup>5</sup>; Mukesh K. Jain, MD<sup>5</sup>; Mark R. Boyett, PhD<sup>1</sup>; Elizabeth J. Cartwright, PhD<sup>1</sup>; Holly A. Shiels, PhD<sup>1</sup>; Xin Wang, MD, PhD<sup>†1</sup>



<sup>1</sup>Faculty of Biological, medical and Health, University of Manchester, Manchester, UK; <sup>2</sup>School of Physics and Astronomy, University of Manchester, Manchester, UK; <sup>3</sup>Atherosclerosis Research Centre, Nanjing Medical University, Jiangsu, China; <sup>4</sup>Institute of Molecular Medicine, Peking University, Beijing, China; <sup>5</sup>Case Cardiovascular Research Institute, Case Western Reserve University, Cleveland, OH; <sup>6</sup>Department of Pharmacology, University of Oxford, Oxford, UK; <sup>7</sup>Department of Cardiology and Pneumology, University Medical Center Göttingen, Göttingen, Germany.

\* These authors are joint first authors

† Equal senior authors

## Address for Correspondence:

Xin Wang, MD, PhD  
Faculty of Life Sciences  
The University of Manchester  
Michael Smith Building  
Oxford Road, Manchester  
M13 9PT, UK  
Tel: +44-161-2755616  
Fax: + 44-161-2755082  
Email: [xin.wang@manchester.ac.uk](mailto:xin.wang@manchester.ac.uk)

**Journal Subject Terms:** Basic Science Research; Translational Studies; Heart Failure; Hypertrophy; Arrhythmias

## Abstract

**Background**—Ventricular arrhythmia is a leading cause of cardiac mortality. Most antiarrhythmics present paradoxical pro-arrhythmic side effects, culminating in a greater risk of sudden death.

**Methods**—We describe a new regulatory mechanism linking mitogen-activated kinase kinase-7 (MKK7) deficiency with increased arrhythmia vulnerability in hypertrophied and failing hearts using mouse models harbouring MKK7 knockout or overexpression. The human relevance of this arrhythmogenic mechanism is evaluated in human induced pluripotent stem cells-derived cardiomyocytes (iPSC-CMs). Therapeutic potentials by targeting this mechanism are explored in the mouse models and human iPSC-CMs.

**Results**—Mechanistically, hypertrophic stress dampens expression and phosphorylation of MKK7. Such MKK7 deficiency leaves histone deacetylase-2 (HDAC2) unphosphorylated and filamin-A (FLNA) accumulated in the nucleus to form a complex with Krüppel-like factor-4 (KLF4). This complex leads to KLF4 disassociation from the promoter regions of multiple key potassium channel genes (Kv4.2, KChIP2, Kv1.5, ERG1 and Kir6.2) and reduction of their transcript levels. Consequent repolarization delays result in ventricular arrhythmias. Therapeutically, targeting the repressive function of the KLF4/HDAC2/FLNA complex with the HDAC2 inhibitor Valproic acid (VPA) restores K<sup>+</sup> channel expression and alleviates ventricular arrhythmias in pathologically remodelled hearts.

**Conclusions**—Our findings unveil this new gene regulatory avenue as a new anti-arrhythmic target where repurposing of anti-epileptic drug VPA as an antiarrhythmic is supported.

**Key-words:** arrhythmia; heart failure; gene expression/regulation; drug; treatment; Drug repurposing

## Clinical Perspective

### What is new?

- We discover a new mechanism linking mitogen-activated kinase kinase-7 (MKK7) deficiency with increased arrhythmia vulnerability in pathologically remodelled hearts.
- Mechanistically, MKK7 deficiency in the hypertrophied heart leaves histone deacetylase-2 (HDAC2) unphosphorylated and filamin-A (FLNA) accumulated in the nucleus, which forms an association with Krüppel-like factor-4 (KLF4), preventing its transcriptional regulation of Kchip2, Kcnd2, Kcnh2, Kcna5 and Kcnj11.
- Diminished K<sup>+</sup> channel reserve causes repolarization delays, resulting in ventricular arrhythmias.
- Targeting the KLF4/HDAC2/FLNA complex with the HDAC2 inhibitor Valproic acid (VPA) restores K<sup>+</sup> channel expression, therefore alleviating ventricular arrhythmias.

### What are the clinical implications?

- Supported by functional characterization and human relevant data, our study not only discovers a unique mechanism underlying arrhythmogenesis, but also demonstrates a repurposing possibility of an anti-epileptic drug VPA for anti-arrhythmic application.
- Wider pursuit of existing drugs for new therapeutic indications is anticipated to encounter a low regulatory hurdle and rapid progression to patient benefits, which is eagerly sought by healthcare systems.
- Furthermore, our work provides exciting insights in developing a new class of anti-arrhythmics specifically targeting signal transduction cascades to replenish repolarization reserve for the treatment of ventricular arrhythmias, a leading cause of cardiac mortality.

## Introduction

Sudden cardiac arrest from ventricular arrhythmias accounts for approximately 1 in 5 deaths worldwide. A common mechanism underlying fatal ventricular arrhythmias is prolonged repolarization, measured on the ECG as increased QT interval<sup>1</sup>. Excessive lengthening of repolarization can incite early after-depolarisations (EADs). On a suitable substrate, this triggers action potentials that propagate aberrantly through re-entry circuits producing arrhythmias<sup>2</sup>. Prolonged repolarization is common in congenital mutations of genes coding for ion-flux proteins (e.g. long QT syndrome)<sup>3-5</sup>, in adverse responses for various drugs (e.g. anti-arrhythmics, antipsychotics, antibiotics, antihistamines)<sup>6,7</sup> and most prevalently, in acquired conditions like cardiac hypertrophy and heart failure<sup>8-11</sup>. In the last case, substantially impaired 'repolarization reserve' due to widespread ion-channel remodeling places the heart at a greater risk of life-threatening rhythm disorders.

Ventricular arrhythmia is difficult to cure, treat or even prevent. Current treatment choices include defibrillation, which is immensely useful for acute restoration of normal rhythm; catheter ablation, which is becoming more commonplace; and anti-arrhythmic drugs for adjunctive, maintenance, or preventive use depending on the clinical diagnosis<sup>12</sup>. Implantable defibrillators or ablation, despite significantly reducing mortality in indicated cases, come with inherent risks ranging from infection to invasive hazards, defibrillator storm, heart perforation, or even exacerbation of heart failure<sup>13,14</sup>. On the other hand, the outcome of anti-arrhythmic drug treatment is disappointing too, including in patients with failing hearts<sup>15,16</sup>. Apart from beta-blockers, most available anti-arrhythmics are primarily ion-channel blockers having paradoxical pro-arrhythmic side-effects that can be terminal for failing hearts. These pro-arrhythmic effects

of anti-arrhythmics are difficult to control since they often result from direct alteration of ion channel activities, the very mechanism of their therapeutic purpose<sup>16</sup>.

Acknowledging this serious situation, enormous effort has been devoted to understanding the mechanisms underlying ion-channel expression and function, including transcriptional regulation, epigenetic make-up, mRNA processing, protein quality control and trafficking, and subunit assembly into macromolecular complexes<sup>17</sup>. A new concept emerging is the targeting regulatory mechanisms to replenish repolarization reserve, which may hold the key to developing a completely new class of anti-arrhythmics with improved efficacy and a reliable safety profile.

We describe here a new regulatory mechanism linking MKK7 stress signaling with repression of cardiac potassium ( $K^+$ ) channel expression and increased arrhythmia susceptibility. Targeting this signal transduction pathway with the class-I HDAC inhibitor Valproic acid (VPA) shows therapeutic benefit in alleviation of ventricular arrhythmias in animal models. Thus, we propose this new gene regulatory avenue as an anti-arrhythmic target and provide evidence in support of repurposing the anti-epileptic drug VPA as a novel anti-arrhythmic approach.

## Methods

Detailed methods are available in the online Data Supplement.

## Animal models

Mice and rats in this study were maintained in a pathogen-free facility at the University of Manchester. Animal studies were performed in accordance with the United Kingdom Animals (Scientific Procedures) Act 1986 and were approved by the University of Manchester Ethics Committee. The experimental protocol for non-human primate was approved by the Institutional

Animal Care and Use Committee of Peking University and was in accordance with the principles of laboratory animal care of China National Academy of Sciences/National Research Council.

### **Valproic acid (VPA) treatment**

VPA (200mg/kg/day, Sigma Aldrich P4543) or equal volume of water (vehicle) for 3 days along with transverse aortic constriction (TAC), or 4 days followed 3 days TAC, or 2 weeks followed 3 weeks TAC were applied to various mouse models, thereafter the mice were subjected to a range of assessments.

### **Single-cell electrophysiological study**

Patch pipettes (Harvard apparatus) had resistances of 1.1-2.3m $\Omega$  for mouse cardiomyocyte or 5.5-6.5m $\Omega$  for human induced pluripotent stem cells-derived cardiomyocytes (iPSC-CMs) when filled with respective pipette solution. Current- and voltage-clamping were achieved in the whole cell configuration, and data were analyzed using pClamp software (version 10.6, Axon Instruments Inc.). Action potentials (APs) were elicited in current-clamp by injecting square pulses of 1-2ms width and 1.5 times of threshold current at 1Hz using current clamp. 100 consecutive APs were recorded at 37°C. Liquid junction potential of -12 mV was corrected offline in the AP data analysis.

### **Immunoprecipitation**

To investigate the association of KLF4, HDAC2 and FLNA, immunoprecipitations were performed with Pierce Protein A/G Magnetic Beads (Thermo Scientific) following the manufacturer's instruction.

### **Experimental design and statistical analysis**

Sample sizes were calculated based on available comparable data to achieve 80% power at a 5% significance level. Data are expressed as mean  $\pm$  S.E.M. and analyzed using Student's t-test for

comparisons between two groups or one- or two-way ANOVA with Bonferroni post-hoc tests for comparisons among multiple groups. P values  $p < 0.05$  were considered statistically significant. When measuring 19 ion channel genes, Bonferroni correction for multiple testing was applied.

## Results

### **MKK7 deficiency is associated with stress-induced ventricular arrhythmias**

Our previous work identified MKK7 as a critical signal transducer to prevent hypertrophic remodeling<sup>18</sup>. In the current study we observed that MKK7 phosphorylation was increased along with acute stress by pressure overload (from 1 day to 7 days), and then its expression and phosphorylation level rescinded in chronic (5 weeks) pressure-overloaded mouse hearts. In a consistent observation, MKK7 abundance and phosphorylation were decreased in hypertrophied primate hearts (Supplementary Fig. 1), which clearly indicates MKK7 deficiency underlying pathological hypertrophy. We then tested whether its deficiency is involved in ventricular arrhythmias commonly harboured in hypertrophied and failing hearts. Cardiac MKK7-deficient (MKK7-CKO) mice were used to mimic the MKK7 deficiency of pathologically remodelled hearts. 8-10 week old male MKK7-CKO mice and their littermate controls (MKK7-Flox) were subjected to pressure overload by transverse aortic constriction (TAC) to investigate primary electrophysiological remodeling events preceding the development of overwhelming hypertrophy. After 3-day TAC, the MKK7-CKO hearts were enlarged but without overt functional failure (Supplementary Fig. 2). Interestingly, MKK7-CKO mice displayed prolonged rate-corrected QT intervals (QTc) in surface ECGs (Fig. 1A, Supplementary Fig. 3). Next, we examined whether such prolonged QTc correlated with arrhythmia vulnerability using programmed electrical stimulation (PES) applied to in-vivo and ex-vivo preparations of MKK7-

CKO and MKK7-Flox hearts. In contrast to controls (0 of 10 mice), markedly high incidences of ventricular tachycardia (VT), often preceded by early after-depolarisations (EADs), were seen in MKK7-CKO hearts (5 out of 10 mice) (Fig. 1B-1C). Consistently, monophasic action potentials (MAPs) recorded from the ex-vivo Langendorff-perfused hearts of these mice showed prolonged repolarisation at 90% action potential durations (APD<sub>90</sub>) (Fig. 1D). APDs recorded from isolated single cardiomyocytes confirmed this prolongation (Fig. 1E). Furthermore, arrhythmia susceptibility was examined in response to adrenergic stimulation. MKK7-CKO and MKK7-Flox mice were challenged by mini-pump delivery of Isoprenaline (ISO, 10mg/kg/day) for 2 weeks. Prolonged APD<sub>90</sub> and frequent arrhythmic events induced by the S1S2 extrastimulus-pacing programme were recorded in Langendorff-perfused MKK7-CKO hearts (5 out of 6 hearts). Conversely, no MKK7-Flox hearts displayed frequent arrhythmia episodes and their MAP durations were in the normal range (Supplementary Fig. 4).

A gain-of-function model of cardiac-specific MKK7 transgenic (MKK7-Tg) mice was brought in to further assess the link between MKK7 and arrhythmogenesis. As anticipated, none of the MKK7-Tg mice displayed arrhythmic episodes after 3-day or 7-day TAC stress (Supplementary Fig. 5A). Their MAP durations and cardiac function remained within the normal range (Supplementary Fig. 5B-5E). We then stressed MKK7-Tg mice more aggressively to evaluate the protective role of MKK7 against hypertrophy and arrhythmia by 5 weeks of TAC. In contrast to wild-type control mice, which developed considerably hypertrophic remodeling attendant with impaired cardiac function and increased arrhythmia sensitivity, MKK7-Tg mice manifested strong resilience against pathological hypertrophic remodeling with preserved contractility (Supplementary Fig. 5F-5G). MKK7-Tg mice exhibited no sign of ventricular tachycardia and action potentials remained normal (Supplementary Fig. 5A).



The cumulative evidence suggested a pro-arrhythmic affiliation of MKK7 deficiency and its protective role against arrhythmias, which led us to study the upstream signaling pathways underlying the acquired ventricular arrhythmia susceptibility of remodelled hearts.

### **MKK7 controls KLF4-HDAC2 signaling regulation of K<sup>+</sup> channel expression**

To discern the signaling mechanism responsible for delayed repolarization, we measured a wide range of ion-channels and found significant down-regulation of *Kcnip2* (coding for KChIP2), *Kcnd2* (coding for Kv4.2), *Kcnh2* (coding for ERG1), *Kcna5* (coding for Kv1.5) and *Kcnj11* (coding for Kir6.2) in the TAC stressed or ISO challenged MKK7-CKO myocardium but not in the MKK7-Tg counterpart (Fig. 2A and Supplementary Fig. 6A-6B). In addition, reduced mRNA levels of the K<sup>+</sup> channels were also observed in the C57BL/6N hearts after 5-week TAC, as well as in the hypertrophied primate hearts (Supplementary Fig. 6C-6D). Furthermore, expression and phosphorylation of MKK7 were examined in 3-day TAC stressed MKK7-Flox hearts versus MKK7-CKO hearts (Supplementary Fig. 7). Meanwhile KChIP2 was chosen as a candidate to evaluate its protein expression, and we found a reduced protein level correlated with its decreased mRNA expression (Supplementary Fig. 7). Importantly, transcript levels of other ion transporters crucial for cardiac action potential and Ca<sup>2+</sup> cycling remained unchanged (Supplementary Fig. 8). The reduction in the selective K<sup>+</sup> channel genes was recapitulated in neonatal rat cardiomyocytes (NRCMs) as a consequence of stress following MKK7 knockdown (Supplementary Fig. 9). In-silico analysis revealed a cluster of consensus Krüppel-like factor (KLF) binding sites on the proximal promoter regions of the 5 K<sup>+</sup> channel coding genes (Supplementary Fig. 10) and we found that the stress-responsive KLF isoform 4 (KLF4) influenced their transcript levels. Shown in Fig. 2B, knockdown of KLF4 caused a down-regulation of the K<sup>+</sup> channel expression in NRCMs stressed by ISO (10μM). Consistently, a

similar reduction in expression of the K<sup>+</sup> channels was detected in KLF4 cardiac-deleted (KLF-CKO) mouse hearts after 3-day TAC (Fig. 2C). As a consequence, QTc was 33% prolonged in the KLF4-CKO hearts ( $111.94 \pm 12.76$  ms) in comparison with the  $\alpha$ MHC-CRE controls ( $75.12 \pm 3.23$  ms) (Fig. 2D). To ascertain the transcriptional role of KLF4 on these 5 K<sup>+</sup> channels, we chose *Kcnip2* and *Kcnh2* for quantitative chromatin immunoprecipitation (ChIP) assays. ChIP analyses of ventricular extracts showed considerably reduced binding of KLF4 at the promoter regions of *Kcnip2* and *Kcnh2* of the MKK7-CKO hearts following 3-day TAC (Fig. 2E).

Meanwhile, we also discovered that local H3 acetylation (H3ac) in the promoter regions of *Kcnip2* and *Kcnh2* was markedly decreased in TAC-stressed MKK7-CKO hearts (Fig. 2E). This reduction in H3ac suggested a gene repression mechanism involving histone deacetylases (HDACs). Given the pro-hypertrophic effects of class-I HDACs<sup>19–21</sup>, we probed for the prospective involvement of HDAC1 and/or HDAC2. Subsequent immunoprecipitation experiments clearly demonstrated that endogenous HDAC2, but not HDAC1, was associated with KLF4 in both 3-day TAC-stressed MKK7-CKO myocardium and ISO-treated MKK7-deficient NRCMs (Fig. 2F). Meanwhile we did not find HDAC2 association with KLF15, another cardiac-active KLF isoform (Fig. 2F). Of note, HDAC2 binding at the promoter regions of *Kcnip2* and *Kcnh2* in the MKK7-CKO hearts after 3-day TAC was not changed by ChIP (Fig. 2G). Interestingly, HDAC2 phosphorylation status regulated its interaction with KLF4. We also observed that phosphorylation of JNK1/2 and HDAC2 was increased following hypertrophic stimuli (Supplementary Fig. 11). Furthermore, with over-expression of JNK1 in NRCMs, HDAC2 became profoundly phosphorylated, thereby disrupting its association with KLF4 regardless of the absence of MKK7 (Fig. 2H). Collectively, these data illustrate that MKK7 deficiency leads to loss of HDAC2 phosphorylation. Unphosphorylated HDAC2 then associates

with KLF4 for leading to reduced  $K^+$  channel transcript levels. HACD2 *per se* does not directly bind with the promoter regions of the 5  $K^+$  channel genes.

### **Filamin A as scaffold for KLF4-HDAC2 association**

In hypertrophied hearts, structural remodeling caused by inflammation, apoptosis and fibrosis can contribute toward arrhythmogenesis. We next investigated the molecular extent of myocardial remodeling and screened for possible alterations in cytoskeleton proteins, such as actin, actinin, tubulin and filamin A (FLNA); fibrotic marker  $\alpha$ -smooth muscle actin (SMA); apoptotic markers such as Bcl2, Bax, and Bad; and inflammation markers TGF $\beta$ 1 and Smad2 (Fig. 3A). Intriguingly, we found that protein expression of FLNA, but not its transcript, was substantially higher in MKK7-CKO hearts of 3-day TAC, and that this increase in FLNA protein was in the nuclear fraction (Fig. 3A-3C). This prompted us to test whether increased FLNA might be involved in the association of KLF4 and HDCA2. Indeed, we found FLNA interacted with both KLF4 and HDAC2 by co-immunoprecipitation and proximity ligation assay (Fig. 3D and Supplementary Fig. 12). Of note, such an interaction of FLNA with KLF4 and HDAC2 was not detected in myocardium of MKK7-Tg mice after 3-day or 7-day TAC (Supplementary Fig. 13). When we knocked down FLNA in MKK7-deficient NRCMs, HDAC2-KLF4 failed to associate despite unchanged protein levels (Fig. 3E). Strikingly, transcript levels of the 5  $K^+$  channel genes were increased in the context of FLNA knockdown (Fig. 3F). Double knockdown of FLNA and HDAC2 did not give additive effects on restoring the 5  $K^+$  channel expression (Fig. 3F), consistent with them acting through the same pathway. We explored further if the MKK7/JNK pathway is involved in FLNA protein turnover with over-expression of JNK1 in MKK7-deficient NRCMs. We observed that JNK1 over-expression led to a reduction of accumulated FLNA expression (Fig. 3G). Cysteine protease inhibitor (E-64D), but not

proteasome inhibitor (MG132), prevented such a reduction in presence of protein biosynthesis inhibitor Cycloheximide (Fig. 3H). Furthermore, we performed immunoprecipitation with a series of FLNA fragments to locate FLNA direct binding with KLF4 and HDAC2, respectively, and found that FLNA (aa2196-aa2436) was required for binding with KLF4, whereas fragment (aa1716-aa1955) was in association with HDAC2 (Fig. 3I). These results suggest that FLNA protein turnover is subject to MKK7/JNK1 regulation via a proteolytic mechanism, and that in the absence of MKK7, FLNA accumulates in the nucleus and acts as scaffold for HDAC2-KLF4 association to repress  $K^+$  channel expression.

### **The HDAC2 inhibitor Valproic acid alleviated ventricular arrhythmias**

Finally, we attempted translation of the above-described signaling mechanism to derive therapeutic anti-arrhythmic effects. We reviewed the available cluster of class-I HDAC inhibitors, and were attracted to Valproic acid (VPA), a widely used anti-epileptic drug with a sound safety record showing substantial HDAC inhibitory effect<sup>22,23</sup>. VPA not only inhibited HDAC enzyme activity by 34%, but also significantly reduced HDAC2 expression, but not HDAC1, 3 and 8 expression in NRCMs and myocardium (Fig. 4A-4B). In-vitro attempts to restore the  $K^+$  channel mRNA levels in NRCMs were promising as they were up-regulated by VPA at an optimal dose of 20mM in MKK7-deficient NRCMs under ISO stimulation (Fig. 4C). Of note, VPA treatment did not introduce an additional increase in the  $K^+$  channel expression when both HDAC2 and MKK7 were knocked down in NRCMs, suggesting VPA effect on the restoration of the  $K^+$  channel expression is likely through the inhibition of HDAC2 (Fig. 4C). Interestingly, in KLF4 knockdown-NRCMs, VPA did not affect transcript levels of the 5  $K^+$  channels (Fig. 4D).

We then moved to test the in-vivo efficacy of VPA in our arrhythmia models. MKK7-CKO mice, stressed by 3-day TAC, received intra-peritoneal VPA injections (200 mg/kg/day) for 3 days. At the end of the treatment, ChIP assays showed increased KLF4 occupancy at the promoter regions of *Kcnip2*, *Kcnd2*, *Kcnh2*, *Kcna5* and *Kcnj11*, concomitant with an enhanced H3ac level in the VPA-treated group compared to the vehicle group (Supplementary Fig. 14). Consistently, mRNA levels of the 5 K<sup>+</sup> channels returned back to their normal levels with no significant changes in other critical ion-channels, including *Scn5a* and *Cacna1c*, or other key morphometric and functional parameters (Fig. 4E and Supplementary Fig. 15). Furthermore, no FLNA association with KLF4 and HDAC2 was detected in VPA-treated groups (Fig. 4F). More convincingly, whole-cell patch-clamp recordings of peak outward K<sup>+</sup> currents in isolated cardiomyocytes, primarily consisting of transient outward current I<sub>to</sub>, revealed an improved density profile in the VPA-treated group (Fig. 5A-5B). MAP durations at 50%-90% of repolarisations were reduced following VPA treatment while dV/dt<sub>max</sub> remained comparable throughout groups, and ex-vivo PES could not induce arrhythmic events in the VPA-treated group (Fig. 5C-5D).

To explore beneficial effects of VPA in exacerbated hypertrophy/heart failure and associated arrhythmias, we challenged MKK7-CKO mice for 7-day TAC and C57BL/6N mice for 5-week TAC. In both models, expression of cJun, KLF4 and HDAC2 remained unchanged (Supplementary Fig. 16), but we observed FLNA association with KLF4 and HDAC2 in their hearts (Fig. 6A), which experienced aggravated hypertrophic remodeling and significantly prolonged action potentials (Fig. 6B-6C and Supplementary Fig. 17-18). Sustained TAC stress predisposed MKK7-CKO (6 out of 7 hearts) and C57BL/6N (5 out of 6 hearts) mice to develop frequent VTs under ex-vivo PES stimulation. We then treated MKK7-CKO mice for 4 days of

VPA (200 mg/kg/day) commencing on the third day after TAC, and C57BL/6N mice undergoing TAC for 3 weeks were then administered VPA for 2 weeks. VPA treatment potently restored the  $K^+$  channel expression and noticeably shortened APD<sub>90</sub> (Fig. 6B-6E). Notably, no KLF4/HDAC2/FLNA complex was detected in VPA-treated groups (Fig. 6A). Furthermore, VPA ameliorated the widespread hypertrophic remodeling by reducing hypertrophic growth and fibrosis (Supplementary Fig. 17-18), paralleled by an improvement of cardiac function (Supplementary Fig. 19-20), which is in line with previously described anti-hypertrophic effects of VPA<sup>19,24,25</sup>.

Finally, we evaluated human relevance of the proposed  $K^+$  channel regulatory mechanism and beneficent effects of VPA in human iPSC-CMs (Fig. 7A). Knockdown of MKK7 in iPSC-CMs significantly lowered mRNA levels of *Kcnip2*, *Kcnh2*, *Kcna5* and *Kcnj11* in the condition of ISO stimulation, whereas VPA treatment markedly restored the expression of the  $K^+$  channels (Fig. 7B). Consistently, associations of FLNA with KLF4 and HDAC2 were detected in iPSC-CMs deficient of MKK7 under ISO stress; however, VPA treatment disrupted these associations (Fig. 7C). Furthermore, functional outcomes of VPA effects were measured using whole-cell patch-clamp recordings of APD<sub>90</sub> in isolated iPSC-CMs. APD<sub>90</sub> of MKK7-deficient iPSC-CMs was noticeably longer when stressed by ISO, this APD<sub>90</sub> prolongation ( $402.31 \pm 40.49$ ms) was significantly shortened to  $313.5 \pm 18.96$ ms by VPA treatment (Fig 7D).

Together, our evidence from mouse models to human iPSC-CMs supports the proposed mechanism of KLF4/HDAC2/FLNA signaling for repression of  $K^+$  channel expression. Anti-arrhythmic therapeutic potential of VPA is evident by disrupting the KLF4/HDAC2/FLNA complex, which allows expression of the 5  $K^+$  channel genes being restored and alleviate stress-induced ventricular arrhythmias (Fig. 8).

## Discussion

Pathological remodeling in hypertrophy and heart failure is often associated with prolonged repolarization due to suppression of  $K^+$  currents<sup>26–29</sup>, which triggers ventricular arrhythmias responsible for 80–95% of sudden cardiac deaths<sup>30</sup>. Following observation of transcript-level down-regulation of the  $K^+$  channels in TAC-stressed MKK7-CKO mice, our molecular and cellular data identified KLF4 as a key transcription factor regulating the expression of the  $K^+$  channels. KLF4 is a cardiac-active KLF isoform, whose functional importance in the heart was demonstrated by a highly TAC-sensitive detrimental phenotype<sup>31</sup>. In a very consistent manner, 3-day TAC stressed KLF4-CKO hearts displayed prolonged QTc intervals and altered expression of a group of ion channels, including down-regulation of the 5  $K^+$  channels, which was reminiscent of electrical remodeling in MKK7-CKO hearts after 3-days of TAC. This finding strengthens the notion that KLF4 plays an important role in regulating cardiac  $K^+$  channels. Our data further show that KLF4-based regulation is elicited through the involvement of HDAC2.

HDAC2 is a member of class-I HDACs notable for their pro-hypertrophic functions<sup>19–21</sup>.

In an early study, cardiac-specific double deletion of HDAC1 and HDAC2 caused mice to die during the postnatal stage<sup>32</sup>. Prior to death mice were predisposed to arrhythmias and cardiomyopathy with an up-regulation of *Cacna1h* and *Cacna2d2* transcript expression<sup>32</sup>. Notably, expression of other important  $Ca^{2+}$  handling proteins remained unaltered, while *Kcnd2* was down-regulated in these post-natal hearts<sup>32</sup>. Interestingly, neither HDAC1- nor HDAC2-specific deletion in mouse hearts produced noticeable changes in cardiac function<sup>32</sup>. Our data shows that HDAC2 knockdown or VPA treatment is able to restore the expression of the 5  $K^+$  channels, including *Kcnd2*. This incongruity in the  $K^+$  channel expression may be related to the



fact that the transcriptome of post-natal hearts is different to the adult ones. For example, *Cacna1h* is expressed differentially in embryonic hearts versus in adults<sup>32</sup>.

In this study, we unveiled a regulatory role of cytoskeletal protein FLNA by mapping out its distinct binding sites with KLF4 and HDAC2. The evidence that KLF4 cannot associate with HDAC2 when FLNA is knocked down implicates FLNA as a scaffold for KLF4 and HDAC2. Further data showing unchanged HDAC2 binding at the *Kcnip2* and *Kcnh2* promoter and knockdown of FLNA and HDAC2 giving no additive effects on restoring the K<sup>+</sup> channel expression indicates that HDAC2 does not directly bind with the promoter regions and the effect of HDAC2 on promoter chromatin is exerted through the KLF4/HDAC2/FLNA complex. On a separate note, an adverse effect of excessive FLNA in MKK7-CKO hearts was similarly documented in an animal model of periventricular heterotopia, in which MKK7-activator MEKK4 deficiency resulted in accumulation of FLNA that impeded neuronal migration<sup>33</sup>. We reason that MKK7 regulation of FLNA turnover by a protease-mediated mechanism may occur in multiple organs, like heart and brain.

MKK7 is a stress-activated MAP kinase. Facing a stress challenge, MKK7 rapidly becomes activated, which enables it to prevent the formation of the KLF4/HDAC2/FLNA complex, as we observed in Flox mice undergoing TAC stress (3 days to 1 week). Evidence from MKK7-Tg mice also supports this notion that MKK7 overexpression and increased JNK activation allowed MKK7-Tg hearts to be resilient against pathological hypertrophy and associated arrhythmias under 5-week TAC. However, sustained stress like that imposed by 5 weeks of TAC on C57BL/6N mouse hearts, dampened endogenous MKK7 expression and activation, therefore the KLF4/HDAC2/FLNA complex was formed. To establish a direct link between MKK7 deficiency and cardiac electrical remodeling, we used an experimental model of



MKK7-CKO mice. The lack of MKK7 in the heart predisposed mice to ventricular arrhythmias following TAC insult or adrenergic stress. However, MKK7 deficiency did not affect the 5 K<sup>+</sup> channel expression and repolarisation duration under the sham condition, reiterating that its role is confined to the response to stress stimulation. It is likely that other transcriptional regulation mechanisms for K<sup>+</sup> channel expression predominate in the absence of stress.

Benefiting from the discovery of the KLF4/HDAC2/FLNA regulation complex, we made attempts to explore therapeutic values of VPA in various TAC-induced arrhythmia models. VPA is a unique drug candidate because it induces proteasomal degradation of HDAC2<sup>34</sup>, alongside inhibiting class-I HDAC catalytic activity<sup>22</sup>. In our 3-day TAC model, we revealed an unambiguous anti-arrhythmic effect of VPA in MKK7-CKO mice based on an array of functional analyses. The expression of the K<sup>+</sup> channels restored by VPA treatment are functionally critical for replenishing the depleted 'repolarization reserve' of overload-stressed hearts. In our prolonged TAC models (MKK7-CKO mice of 1-week TAC and C57BL/6N mice of 5-week TAC) with exacerbated hypertrophy, VPA exerted salutary effects by alleviating arrhythmia occurrences and hypertrophic remodeling, which demonstrates the therapeutic value of VPA in a more clinically-relevant setting. By investigation of VPA mechanism of action, we believe that HDAC2 degradation by VPA treatment would cause a disruption of the association of KLF4 and FLNA, which allows KLF4 to access the promoter regions of the K<sup>+</sup> channels. Meanwhile, VPA-induced reduction in HDAC2 activity could indirectly increase H3ac level of the promoter regions. These effects in combination lead to restored expression of the 5 K<sup>+</sup> channels and salient anti-arrhythmia benefits. Worthy of noting, VPA did not introduce an additional increase in the 5 K<sup>+</sup> channel expression when HDAC2 was knocked down in MKK7-deficient NRCMs, suggesting VPA action is likely through the inhibition of HDAC2.

Remarkably, we realize that VPA is already a first-line drug for various neuro-psychiatric conditions without instance of significant cardiac side-effects. Although epidemiological data detailing cardiac effects of VPA exclusive of confounding conditions is lacking, a clinical study amongst bipolar patients revealed that VPA significantly reduces QT dispersion, implying a possible beneficial effect on human hearts<sup>35</sup>. Given its reliable safety profile and potential in alleviating both arrhythmias and hypertrophy, repurposing VPA for cardiac applications seems an attractive prospect that merits rapid and prioritized scrutiny.

The physiological differences and similarities between rodents and humans have been widely studied<sup>36</sup>. Mouse models contribute enormously to our current understanding of mammalian ion-channel functions, and are still the choice for investigating molecular mechanisms<sup>37</sup>. All of the  $K^+$  channels down-regulated in MKK7-CKO hearts have cardinal roles in human hearts too:  $I_{to}$  (Kv4 and KChIP2) is crucial for myocyte repolarization in many mammalian hearts<sup>11,38,39</sup>.  $I_{Kr}$  (ERG1) is essential for human cardiac repolarization, but less so in murine hearts<sup>11,38,39</sup> despite abundant transcript expression<sup>37</sup>.  $I_{Kur}$  (Kv1.5) is an important repolarizing current in human atrium<sup>11,38</sup>, and it is also present in rodent hearts<sup>37</sup>.  $I_{KATP}$  (Kir6.2) is particularly involved in ischaemia-response in both species<sup>11,38,39</sup>. The consensus KLF binding sites on the promoters of the above-listed genes are evolutionarily conserved. As such, it is very likely that MKK7 deficiency-induced transcription repression of  $K^+$  channel expression is conserved across species. Indeed, we took human iPSC-CMs as a translational model, which provides a series of molecular and functional evidence, comprising of mRNA expression profile of  $K^+$  channels, formation of KLF4/HDAC2/FLNA complex and action potential recordings that clearly demonstrate human relevance of this regulatory mechanism and beneficent effects of VPA.

In the current study, we did not investigate phosphorylation or hyper-oxidation of ion channels, so cannot exclude the possibility of posttranslational modifications altering function in the channels whose transcripts did not change. Indeed, as MKK7-CKO is a stress-activated pro-arrhythmic model we would expect phosphorylation of various excitation-contraction coupling proteins. In future work we plan on investigating the possible role of  $\text{Ca}^{2+}$  cycling proteins (in particular the SERCA and the RyR2) in the contractile and arrhythmogenic phenotype of our MKK7 models. However, the lack of a difference in upstroke velocity of the action potential in isolated cardiomyocytes is in keeping with the lack of significant posttranslational alterations in Na-channels. Furthermore, proteomic studies elucidating the KLF4/HDAC2/FLNA complex could uncover any additional members of the complex. A better understanding would be imperative for designing ideal small-molecule inhibitors to exclusively disrupt the complex formation without inhibiting any enzymatic activity or altering protein expression, therefore evading unpredictable side effects. Hopefully, a safe and effective new class of anti-arrhythmics specifically targeting molecular signal transduction is not far off.

### **Acknowledgments**

We thank M. Hardy (the University of Manchester) for technical support and reviewing the manuscript.

### **Sources of Funding**

This work was supported by the British Heart Foundation (PG/09/052/27833, PG/12/76/29852 and FS/15/16/31477), the Medical Research Council (G1002082, MC\_PC\_13070), American

Heart Association National Scientist Development grants (12SDG12070077 to X. Liao), and National Basic Research Program of China (2012CB518000 to R. Xiao).

## Disclosures

None.

## References

1. John RM, Tedrow UB, Koplan BA, Albert CM, Epstein LM, Sweeney MO, Miller AL, Michaud GF, Stevenson WG. Ventricular arrhythmias and sudden cardiac death. *Lancet*. 2012; 380:1520-1529.
2. Jalife J. Ventricular fibrillation: mechanisms of initiation and maintenance. *Annu Rev Physiol*. 2000; 62:25–50.
3. Marbán, E. Cardiac channelopathies. *Nature*. 2002; 415:213–218.
4. Giudicessi JR, Ackerman MJ. Potassium-channel mutations and cardiac arrhythmias—diagnosis and therapy. *Nat Rev Cardiol*. 2012; 9:319–332.
5. Hedley PL, Jørgensen P, Schlamowitz S, Wangari R, Moolman-Smook J, Brink PA, Christiansen M. The genetic basis of long QT and short QT syndromes: a mutation update. *Hum Mutat*. 2009; 30:1486-511.
6. Roden DM. Drug-induced prolongation of the QT interval. *N Engl J Med*. 2004; 350:1013-1022.
7. Kannankeril P, Roden DM, Darbar D. Drug-induced long QT syndrome. *Pharmacol Rev*. 2010; 62:760-781.
8. Haugaa KH, Bos JM, Borkenhagen EJ, Tarrell RF, Morlan BW, Caraballo PJ, Ackerman MJ. Impact of left ventricular hypertrophy on QT prolongation and associated mortality. *Heart Rhythm*. 2014; 11:1957–1965.
9. Kang YJ. Cardiac hypertrophy: a risk factor for QT-Prolongation and cardiac sudden death. *Toxicol Pathol*. 2006; 34:58–66.
10. Hart G. Exercise-induced cardiac hypertrophy: a substrate for sudden death in athletes? *Exp Physiol*. 2003; 88:639-644.
11. Tomaselli GF, Marban E. Electrophysiological remodeling in hypertrophy and heart failure. *Cardiovasc Res*. 1999; 42:270–283.
12. Zipes DP, A. Camm AJ, Borggrefe M, Buxton AE, Chaitman B, Fromer M, Gregoratos G, Klein G, Moss AJ, Myerburg RJ, Priori SG, Quinones MA, Roden DM, Silka MJ, Tracy C. ACC/AHA/ESC 2006 guidelines for management of patients with ventricular arrhythmias and the prevention of sudden cardiac death: a report of the American College of Cardiology/American Heart Association Task Force and the European Society of Cardiology Committee for Practice Guidelines (Writing Committee to Develop Guidelines for Management of Patients With Ventricular Arrhythmias and the Prevention

- of Sudden Cardiac Death) Developed in collaboration with the European Heart Rhythm Association and the Heart Rhythm Society. *Circulation*. 2006; 114:e385-e484.
13. Goldenberg I, Moss AJ, Hall WJ, McNitt S, Zareba W, Andrews ML, Cannom DS. Causes and consequences of heart failure after prophylactic implantation of a defibrillator in the multicenter automatic defibrillator implantation trial II. *Circulation*. 2006; 113:2810–2817.
  14. Moss AJ, Greenberg H, Case RB, Zareba W, Hall WJ, Brown MW, Daubert JP, McNitt S, Andrews ML, Elkin AD. Long-term clinical course of patients after termination of ventricular tachyarrhythmia by an implanted defibrillator. *Circulation*. 2004; 110:3760–3765.
  15. The Anti-arrhythmics Versus Implantable Defibrillators (AVID) Investigators. A comparison of antiarrhythmic-drug therapy with implantable defibrillators in patients resuscitated from near-fatal ventricular arrhythmias. *N Engl J Med*. 1997; 337:1576–1583.
  16. Roden DM. Antiarrhythmic drugs: from mechanisms to clinical practice. *Heart*. 2000; 84:339–346.
  17. Rosati B, McKinnon D. Regulation of ion channel expression. *Circ Res*. 2004; 94:874–883.
  18. Liu W, Zi M, Chi H, Jin J, Prehar S, Neyses L, Cartwright EJ, Flavell RA, Davis RJ, Wang X. Deprivation of MKK7 in cardiomyocytes provokes heart failure in mice when exposed to pressure overload. *J Mol Cell Cardiol*. 2011; 50:702–711.
  19. Trivedi CM, Luo Y, Yin Z, Zhang M, Zhu W, Wang T, Floss T, Goettlicher M, Noppinger PR, Wurst W, Ferrari VA, Abrams CS, Gruber PJ, Epstein JA. Hdac2 regulates the cardiac hypertrophic response by modulating Gsk3 beta activity. *Nat Med*. 2007; 13:324–331.
  20. Kee HJ, Eom GH, Joung H, Shin S, Kim JR, Cho YK, Choe N, Sim BW, Jo D, Jeong MH, Kim KK, Seo JS, Kook H. Activation of histone deacetylase 2 by inducible heat shock protein 70 in cardiac hypertrophy. *Circ Res*. 2008; 103:1259–1269.
  21. McKinsey TA, Olson EN. Cardiac histone acetylation-therapeutic opportunities abound. *Trends Genet*. 2004; 20:206–213.
  22. Bantscheff M, Hopf C, Savitski MM, Dittmann A, Grandi P, Michon AM, Schlegl J, Abraham Y, Becher I, Bergamini G, Boesche M, Delling M, Dümpelfeld B, Eberhard D, Huthmacher C, Mathieson T, Poeckel D, Reader V, Strunk K, Sweetman G, Kruse U, Neubauer G, Ramsden NG, Drewes G. Chemoproteomics profiling of HDAC inhibitors reveals selective targeting of HDAC complexes. *Nat. Biotechnol*. 2011; 29:255–265.
  23. Göttlicher M, Minucci S, Zhu P, Krämer OH, Schimpf A, Giavara S, Sleeman JP, Lo Coco F, Nervi C, Pelicci PG, Heinzl T. Valproic acid defines a novel class of HDAC inhibitors inducing differentiation of transformed cells. *EMBO J*. 2001; 20:6969–6978.
  24. Kook H, Lepore JJ, Gitler AD, Lu MM, Wing-Man Yung W, Mackay J, Zhou R, Ferrari V, Gruber P, Epstein JA. Cardiac hypertrophy and histone deacetylase-dependent transcriptional repression mediated by the atypical homeodomain protein Hop. *J Clin Invest*. 2003; 112:863–871.
  25. Cho YK, Eom GH, Kee HJ, Kim HS, Choi WY, Nam KI, Ma JS, Kook H. Sodium valproate, a histone deacetylase inhibitor, but not captopril, prevents right ventricular hypertrophy in rats. *Circ J*. 2010; 74:760–770.

26. Boyden PA, Jeck CD. Ion channel function in disease. *Cardiovasc Res.* 1995; 29:312–318.
27. Wickenden AD, Kaprielian R, Kassiri Z, Tsoporis JN, Tsushima R, Fishman GI, Backx PH. The role of action potential prolongation and altered intracellular calcium handling in the pathogenesis of heart failure. *Cardiovasc Res.* 1998; 37:312–323.
28. Näbauer M, Kääh S. Potassium channel down-regulation in heart failure. *Cardiovasc Res.* 1998; 37:324–334.
29. Swynghedauw, B. Molecular mechanisms of myocardial remodeling. *Physiol. Rev.* 1999; 79:215–262.
30. Huikuri HV, Castellanos A, Myerburg RJ. Sudden death due to cardiac arrhythmias. *N Engl J Med.* 2001; 345:1473–1482.
31. Liao X, Haldar SM, Lu Y, Jeyaraj D, Paruchuri K, Nahori M, Cui Y, Kaestner KH, Jain MK. Krüppel-like factor 4 regulates pressure-induced cardiac hypertrophy. *J Mol Cell Cardiol.* 2010; 49:334–338.
32. Montgomery RL, Davis CA, Potthoff MJ, Haberland M, Fielitz J, Qi X, Hill JA, Richardson JA, Olson EN. Histone deacetylases 1 and 2 redundantly regulate cardiac morphogenesis, growth, and contractility. *Genes Dev.* 2007; 21:1790–1802.
33. Sarkisian MR, Bartley CM, Chi H, Nakamura F, Torii KH, Torii M, Flavell RA, Rakic P. MEKK4 signaling regulates filamin expression and neuronal migration. *Neuron.* 2006; 52:789–801.
34. Krämer OH, Zhu P, Ostendorff HP, Golebiewski M, Tiefenbach J, Peters MA, Brill B, Groner B, Bach I, Heinzel T, Göttlicher M. The histone deacetylase inhibitor valproic acid selectively induces proteasomal degradation of HDAC2. *EMBO J.* 2003; 22:3411–3420.
35. Kurt E, Emul M, Ozbulut O, Guler O, Erdur F, Sağlam H, Gecici O. Is valproate promising in cardiac fatal arrhythmias? Comparison of P- and Q-wave dispersion in bipolar affective patients on valproate or lithium-valproate maintenance therapy with healthy controls. *J Psychopharmacol.* 2009; 23:328–333.
36. Kaese S, Verheule S. Cardiac electrophysiology in mice: a matter of size. *Front. Physiol.* 2012; 345:1–19.
37. Nerbonne JM, Nichols CG, Schwarz TL, Escande D. Genetic manipulation of cardiac K<sup>+</sup> channel function in mice: what have we learned, and where do we go from here? *Circ Res.* 2001; 89:944–956.
38. Furukawa T, Kurokawa J. Potassium channel remodeling in cardiac hypertrophy. *J Mol Cell Cardiol.* 2006; 41:753–761.
39. Nattel S, Maguy A, Le Bouter S, Yeh YH. Arrhythmogenic ion-channel remodeling in the heart: heart failure, myocardial infarction, and atrial fibrillation. *Physiol Rev.* 2007; 87:425–456.



## Figure Legends

**Figure 1.** MKK7-CKO mice are vulnerable to stress-induced ventricular arrhythmias. (A) Single surface-ECG beat (left) and mean rate-corrected QT intervals (right, Mitchell QTc) demonstrate QT prolongation following 3-day TAC (n=10 mice/group). (B) In-vivo PES protocol comprising of eight serial supra-capture-threshold stimuli (S1, at 100ms interval) followed by an extra-stimulus (S2) delivered at progressively shortened S1S2 delay was applied. Induced ventricular arrhythmias were observed in 50% of the knockouts after 3-day TAC but none of the controls (n=10 mice/group). (C) Ex-vivo PES traces show early-afterdepolarizations (EADs) and overt arrhythmias, observed in 67% of the MKK7-CKO/3d-TAC (7 out of 9 hearts) but none of the MKK7-Flox/3d-TAC heart preparations (n=9 mice/group). (D) Mean MAP durations at 90% (APD<sub>90</sub>) of repolarizations recorded from ex-vivo Langendorff perfused hearts (n=9 mice/group). (E) Action potential traces of ventricular cardiomyocytes isolated from MKK7-CKO/3d-TAC and MKK7-Flox/3d-TAC hearts by whole-cell patch clamping at 37°C (left panel), with APD<sub>50</sub>, APD<sub>90</sub>, dv/dt<sub>max</sub> and maximum repolarization velocity during phase 1 of the action potential, which is determined by the transient outward current in the right panel (15 cells/group). All bar graphs express mean ± S.E.M values, ns = not significant.

**Figure 2.** KLF4-HDAC2 signaling regulates K<sup>+</sup> channel expression. (A) Quantitative real-time PCR (qPCR) analyses of *Kcnip2*, *Kcnd2*, *Kcnh2*, *Kcna5* and *Kcnj11* in myocardium. Bonferroni multiple testing correction was applied for 19 ion channel genes, and two-way ANOVA with Bonferroni correction for post-hoc comparisons were used to analyze mRNA expression of the 5 K<sup>+</sup> channel genes (n=12 mice/group, normalized to Gapdh content). (B) qPCR analyses show

down-regulation of the K<sup>+</sup> channels upon KLF4 knockdown in NRCMs (n=4 independent experiments). (C) qPCR analyses of ion channel profiles in KLF4-CKO/3d-TAC hearts (n=5 mice/group, \*P<0.05 KLF-CKO/TAC versus  $\alpha$ MHC-Cre/TAC). (D) ECG analyses show 3-day TAC causing longer QTc in KLF4-CKO mice compared with that in  $\alpha$ MHC-CRE controls (n=5 mice/group). (E) Chromatin immunoprecipitation (ChIP) reveals reduced KLF4 binding and H3ac level at the promoter regions of *Kcnip2* and *Kcnh2* in the MKK7-CKO/3d-TAC ventricles (n=4 mice/group, data normalized to % input DNA and expressed as fold change relative to control). (F) Association of endogenous HDAC2, but not HDAC1, with KLF4 determined by immunoprecipitation from myocardium and NRCMs, respectively. Meanwhile, HDAC2 did not associate with KLF15. Quantitative measurements reflecting the association intensity in myocardium samples are presented as bar graphs (n=3 independent experiments). (G) ChIP failed to detect change in HDAC2 binding at the promoter regions of *Kcnip2* and *Kcnh2* in the MKK7-CKO/3-day TAC ventricles (n=4 mice/group). (H) JNK1 overexpression disrupted the HDAC2-KLF4 association in ISO-treated NRCMs. JNK1 increased phosphorylated-HDAC2 that failed to bind with KLF4. IgG used as control for nonspecific interaction and GAPDH used as loading control (n=3 independent experiments).

**Figure 3.** FLNA as a scaffold for KLF4/HDAC2 regulation of K<sup>+</sup> channels. (A) Immunoblots exhibit augmented FLNA expression (quantified in bar graph) in whole heart lysates from MKK7-CKO/3d-TAC mice, whilst other cytoskeleton proteins, fibrotic marker, apoptotic markers, or inflammation markers remains comparable (n=5 mice/group). (B) qPCR analyses demonstrate comparable transcript levels of FLNA between genotypes (n=8 mice/group, data normalised to *Gapdh* content). (C) Immunoblots on the nuclear fractions of myocardium or



NRCMs illustrate elevated FLNA level. Histone-3 (H3) used as loading control (n=5). (D) FLNA association with KLF4 and HDAC2 detected in MKK7-deficient NRCMs after ISO stimulation. IgG used as control for nonspecific interaction, GAPDH as loading control (n=3). (E) FLNA knockdown disrupted KLF4-HDAC2 interaction in ISO-treated MKK7-deficient NRCMs, whereas expression of KLF4 and HDAC2 remained unchanged (n=3). (F) Transcript levels of the 5 K<sup>+</sup> channels measured following knockdown of FLNA with or without HDAC2 (n=4 independent experiments). (G) Immunoblots show increased FLNA level in the nuclear fractions of ISO-treated MKK7-deficient NRCMs; while JNK1 overexpression reduced this augmented FLNA. H3 used as loading control for the nuclear fractions (n=3). (H) Cysteine protease inhibitor E-64D (5μM, 16 hours), but not proteasome inhibitor MG132 (2.5μM, 16 hours), inhibited this FLNA reduction. Pre-incubation with Cycloheximide (CHX, 10μg/ml for 4 hours) demonstrates that JNK1-induced FLNA reduction is via proteolysis (n=3). (I) Schematic diagram of flag-tagged FLNA fragments used in immunoprecipitation experiments (upper panel), ABD: actin binding domain, DD: dimerization domain. Immunoprecipitation experiments demonstrate the distinct region of FLNA required for association with KLF4 or HDAC2 (lower panel), n=3. All bar graphs present mean ± S.E.M. values, ns = not significant.

**Figure 4.** Valproic acid restores K<sup>+</sup> channel expressions by targeting HDAC2. (A) In-vitro HDAC activity was blunted (34% reduction) by VPA (4mM) in NRCMs (n=5 independent experiments). Pan-HDAC inhibitor (Trichostatin-A) was used as control for HDAC inhibitor activity. (B) Immunoblots show reduced expression of HDAC2 but not HDAC1, 3 and 8 upon VPA (20mM) in myocardium and NRCMs (n=5, GAPDH used as loading control). (C) qPCR analyses reveal increased transcript expression of the 5 K<sup>+</sup> channels by VPA treatment (20mM)

in MKK7-knockdown NRCMs under ISO stimulation (n=5 independent experiments). (D) qPCR analyses of transcript levels of the 5 K<sup>+</sup> channels in KLF4 knockdown-NRCMs upon VPA treatment (n=4). (E) qPCR analyses demonstrate restored myocardial transcript expression of the 5 K<sup>+</sup> channels by VPA treatment (n=8 mice/group). (F) Immunoblotting detection of FLNA association with KLF4 and HDAC2 in myocardium of MKK7-CKO/3d-TAC mice with VPA or vehicle treatment (n=4 mice/group). All bar graphs present mean  $\pm$  S.E.M. values, ns = not significant.

**Figure 5.** Valproic acid prevents ventricular arrhythmias. (A) Representative peak (arrows) outward K<sup>+</sup> current traces recorded from isolated adult cardiomyocytes. (B) Current-voltage relationship curves of peak outward K<sup>+</sup> currents. Combination of Tetrodotoxin (TTX) and CoCl<sub>2</sub> inhibited Na<sup>+</sup> and Ca<sup>2+</sup> channel activities, respectively, and isolation of K<sup>+</sup> currents subsequently confirmed by 4-aminopyridine (4-AP), n=14 cells/group. \*Flox/3d-TAC/veh versus CKO/3d-TAC/veh, #CKO/3d-TAC/veh versus CKO/3d-TAC/VPA, p<0.05. (C) MAP durations at 50% (APD<sub>50</sub>) and 90% (APD<sub>90</sub>) of repolarizations and maximum depolarisation velocity recorded from ex-vivo Langendorff perfused hearts (n=9 mice/group). (D) Ex-vivo PES traces show the absence of arrhythmic events in MKK7-CKO/3d-TAC mice following VPA treatment (n=9 mice/group). Data presented as mean  $\pm$  S.E.M, ns= not significant.

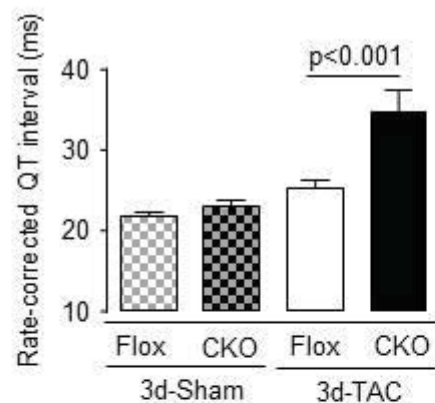
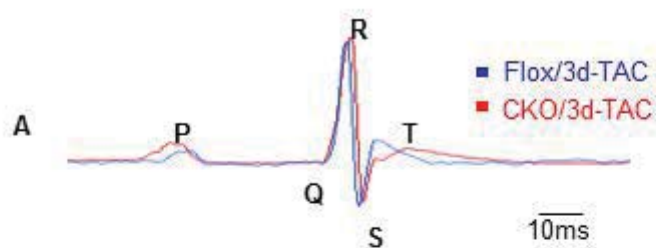
**Figure 6.** Valproic acid alleviates ventricular arrhythmias in heart failure. (A) Immunoblotting detection of FLNA association with KLF4 and HDAC2 in MKK7-CKO/7d-TAC hearts or C57BL/6N-5w-TAC hearts with or without VPA treatment (n=4 mice/group). (B) Ex-vivo MAP durations at 50% (APD<sub>50</sub>) and 90% (APD<sub>90</sub>) of repolarizations were markedly shortened by VPA

treatment in MKK7-CKO/7d-TAC hearts (n=7 mice/group). (C) APD<sub>50</sub> and APD<sub>90</sub> of ex-vivo heart preparations were significantly shortened by VPA treatment in C57BL/6N/5w-TAC hearts (n=6 mice/group). (D) qPCR analyses show VPA treatment increasing transcript expression of *Kcnip2*, *Kcnd2*, *Kcnh2*, *Kcna5* and *Kcnj11* in myocardium of MKK7-CKO/7d-TAC mice (n=7 mice/group, normalized to *Gapdh* content). (E) qPCR analyses show enhanced transcript expression of the K<sup>+</sup> channels by VPA treatment in C57BL/6N/5w-TAC hearts (n=6 mice/group). Data presented as mean ± S.E.M values.

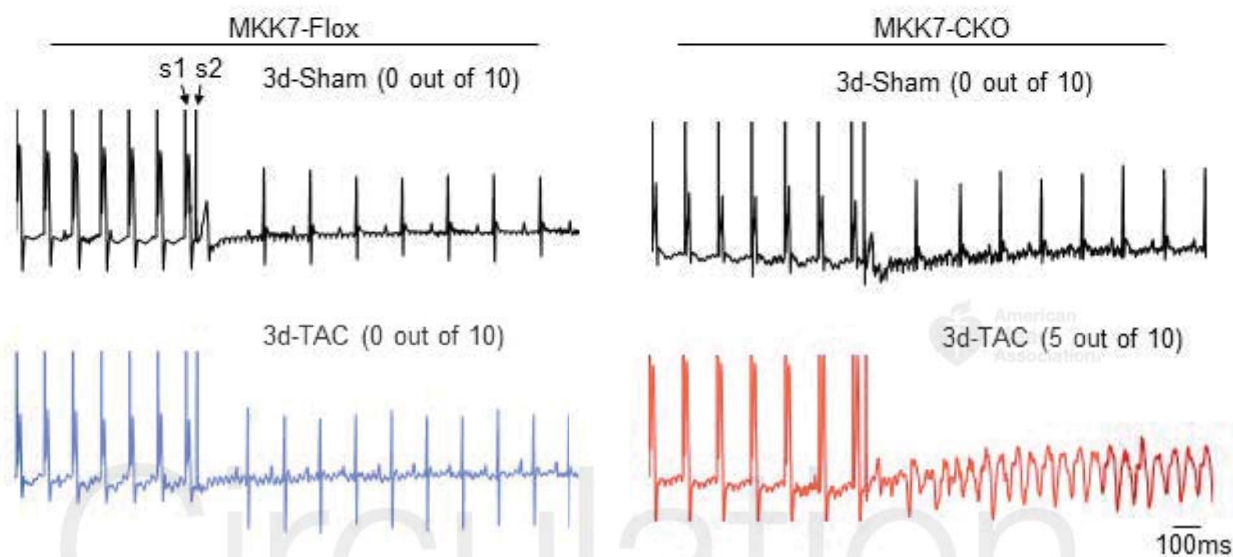
**Figure 7.** VPA effects on K<sup>+</sup> channel expression, KLF4/HDAC2/FLNA complex and action potentials in iPSC-cardiomyocytes. (A) Representative immunocytochemistry images confirm nature of iPSC-cardiomyocytes using alpha-actinin (red), Cx43 (green), and Alexa Fluor 555-Phalloidin (blue) (scale bar: 50µm). (B) qPCR analyses of *Kcnip2*, *Kcnh2*, *Kcna5* and *Kcnj11* in iPSC-cardiomyocytes with MKK7 knockdown followed by ISO (5µM) stimulation with or without VPA treatment (4mM) (n=4 independent experiments performed in triplicates, normalized to *Gapdh*). (C) Immunoblotting detection of FLNA association with KLF4 and HDAC2 in iPSC- cardiomyocytes with MKK7 knockdown following ISO stimulation with or without VPA treatment (n=3). (D) Representative action potential traces of isolated single iPSC-cardiomyocyte recorded by whole-cell patch clamping at 37°C (15 cells/group, upper panel), and 90% action potential durations (APD<sub>90</sub>) quantified in graph bar (lower panel). All bar graphs express mean ± S.E.M values.

**Figure 8.** The new regulatory mechanism linking MKK7-deficiency with increased arrhythmia susceptibility and therapeutic potential of VPA. KLF4 is involved in regulating the  $5 K^+$  channel expression in the healthy heart under stress. Loss of MKK7 in the hypertrophied heart (phenocopied by MKK7-CKO mice) leaves HDAC2 unphosphorylated and FLNA accumulated in the nucleus, where they form an association with KLF4. This complex leads to KLF4 dissociation from the promoter regions of the  $K^+$  channels and consequently reduced transcript levels. Diminished  $K^+$  channel reserves fail to cope with states of increased demand; resulting in repolarization delays and arrhythmias. Disrupting the repressive function of KLF4/HDAC2/FLNA complex by the HDAC2 inhibitor VPA not only restores  $K^+$  channel expression, but also confers therapeutic benefits of normalizing cardiac repolarization and reducing arrhythmia susceptibility in pathologically remodelled hearts. Ac: Acetyl.

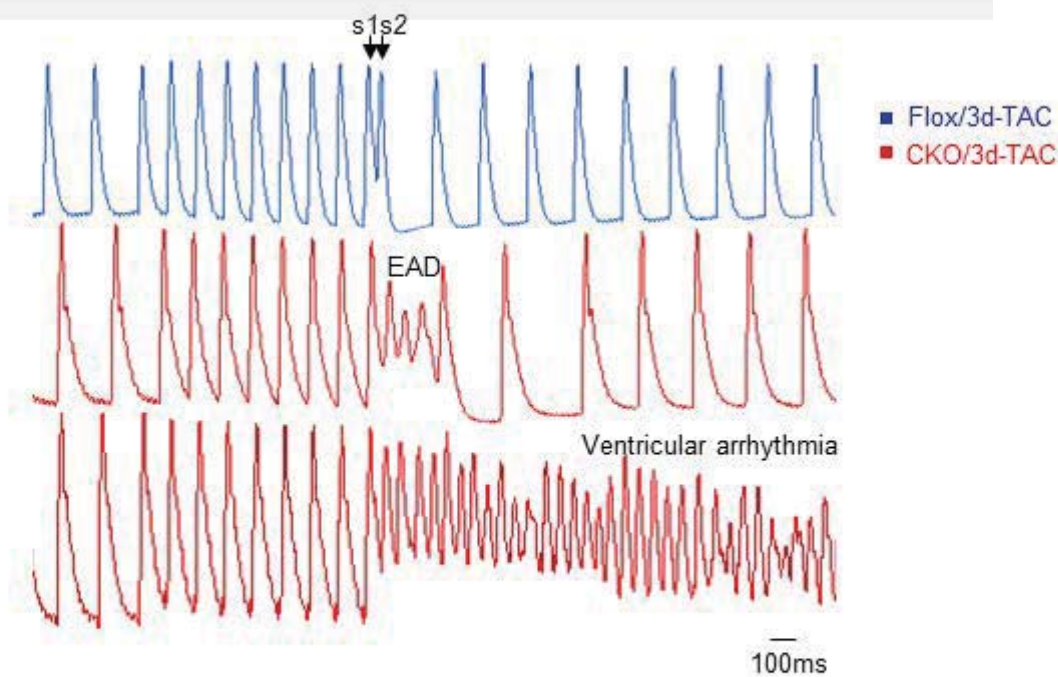
Circulation

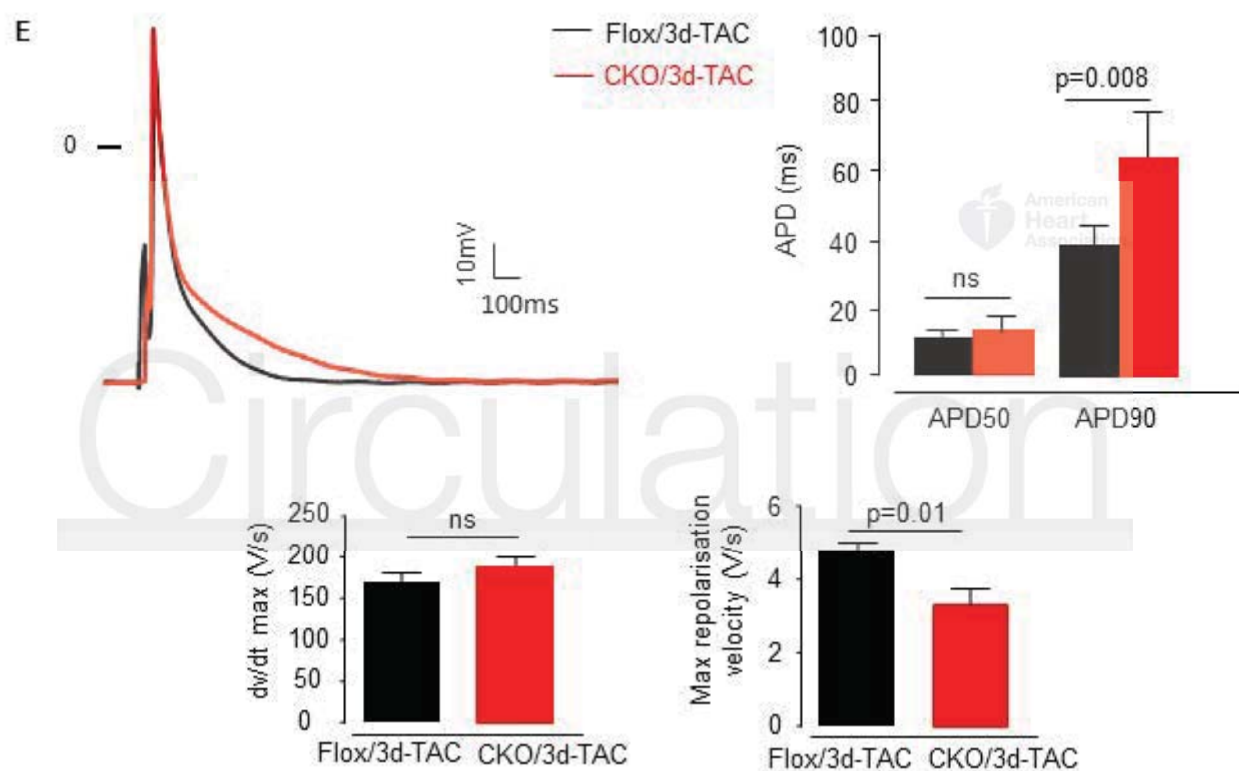
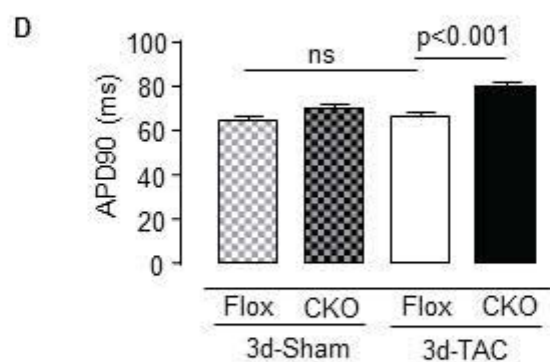


**B**



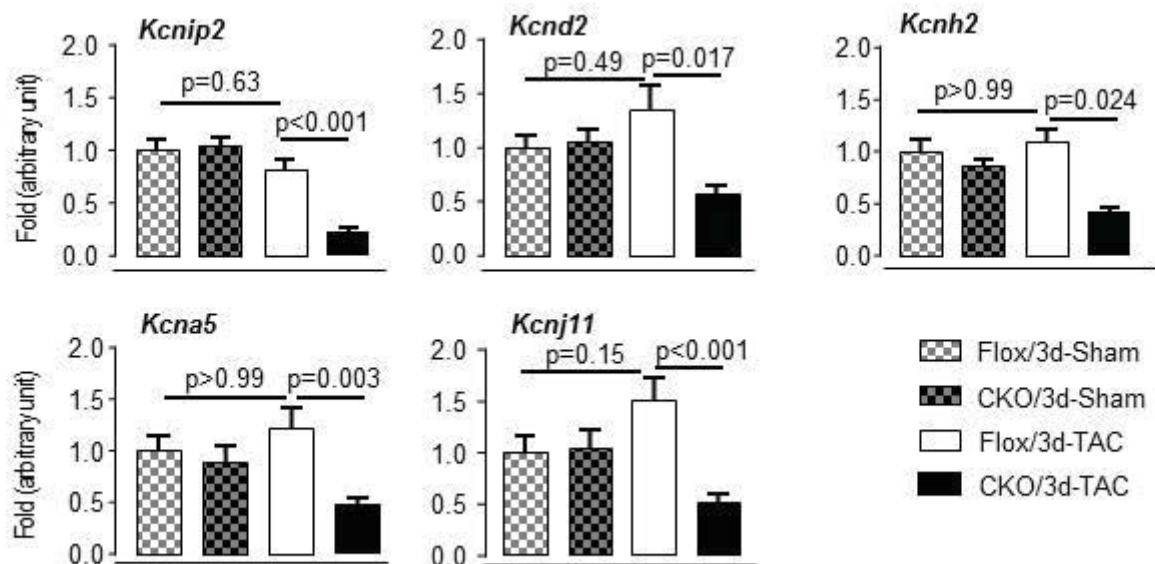
**C**



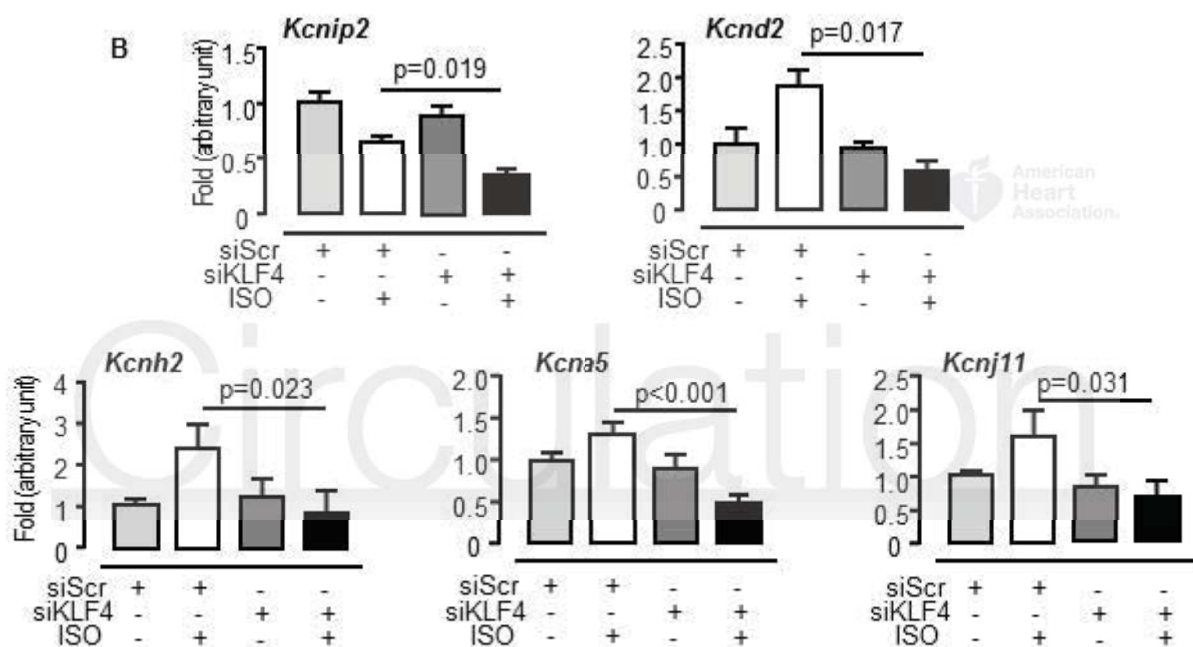




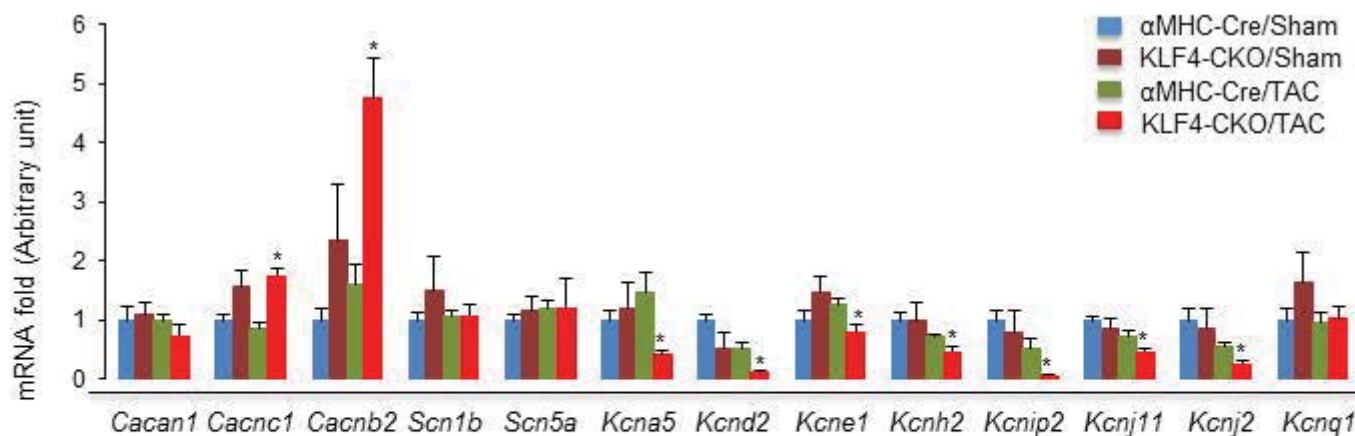
A

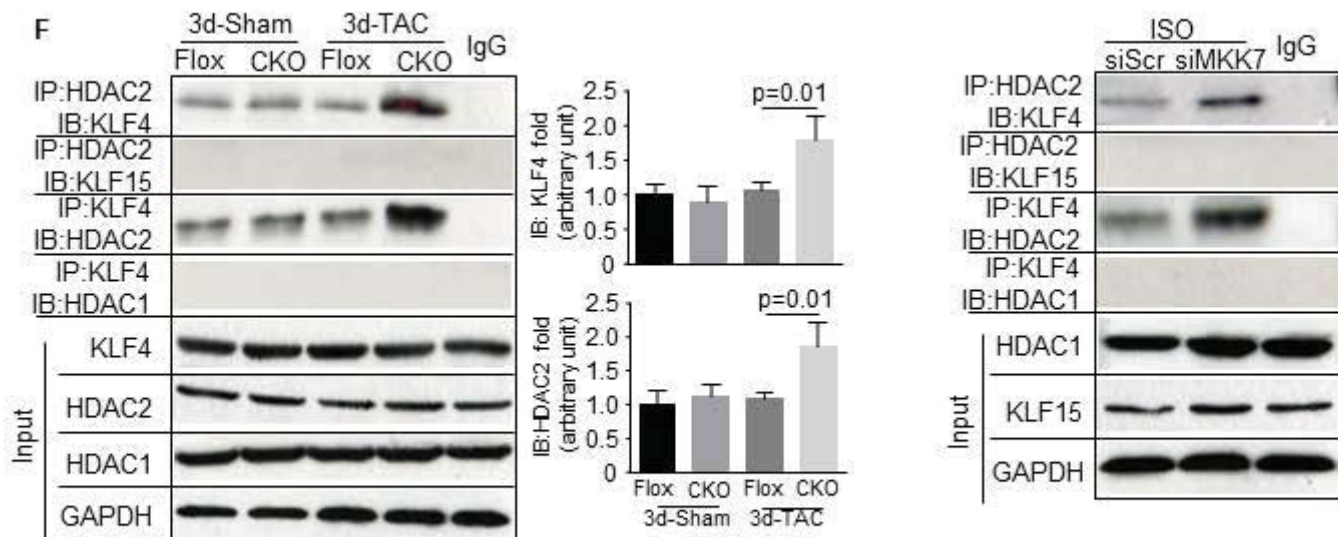
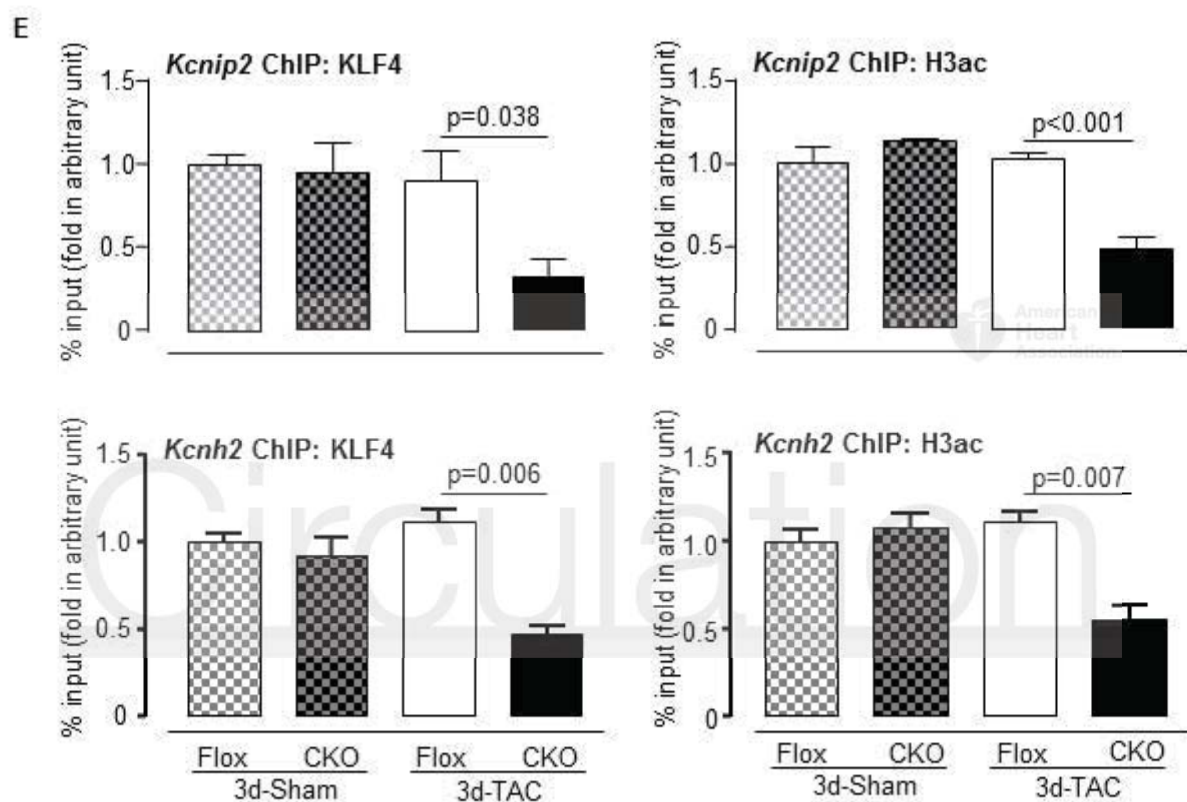
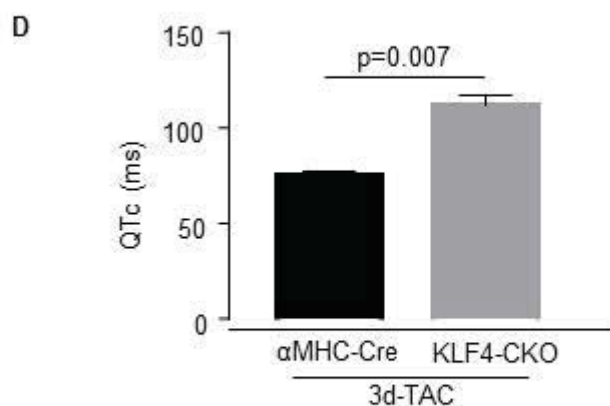


B



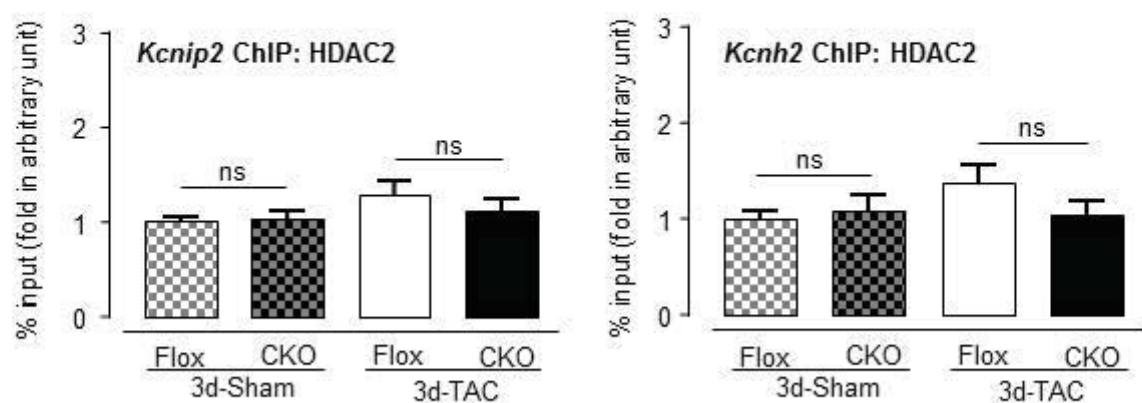
C



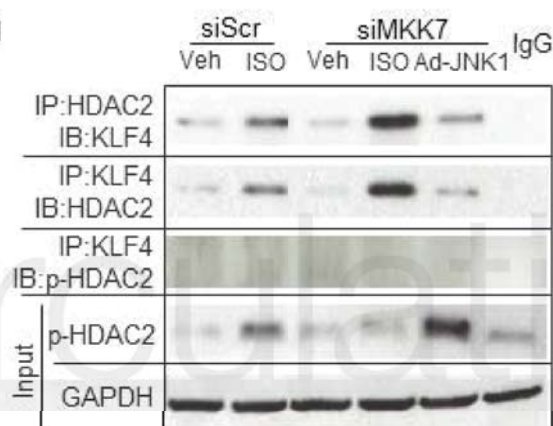


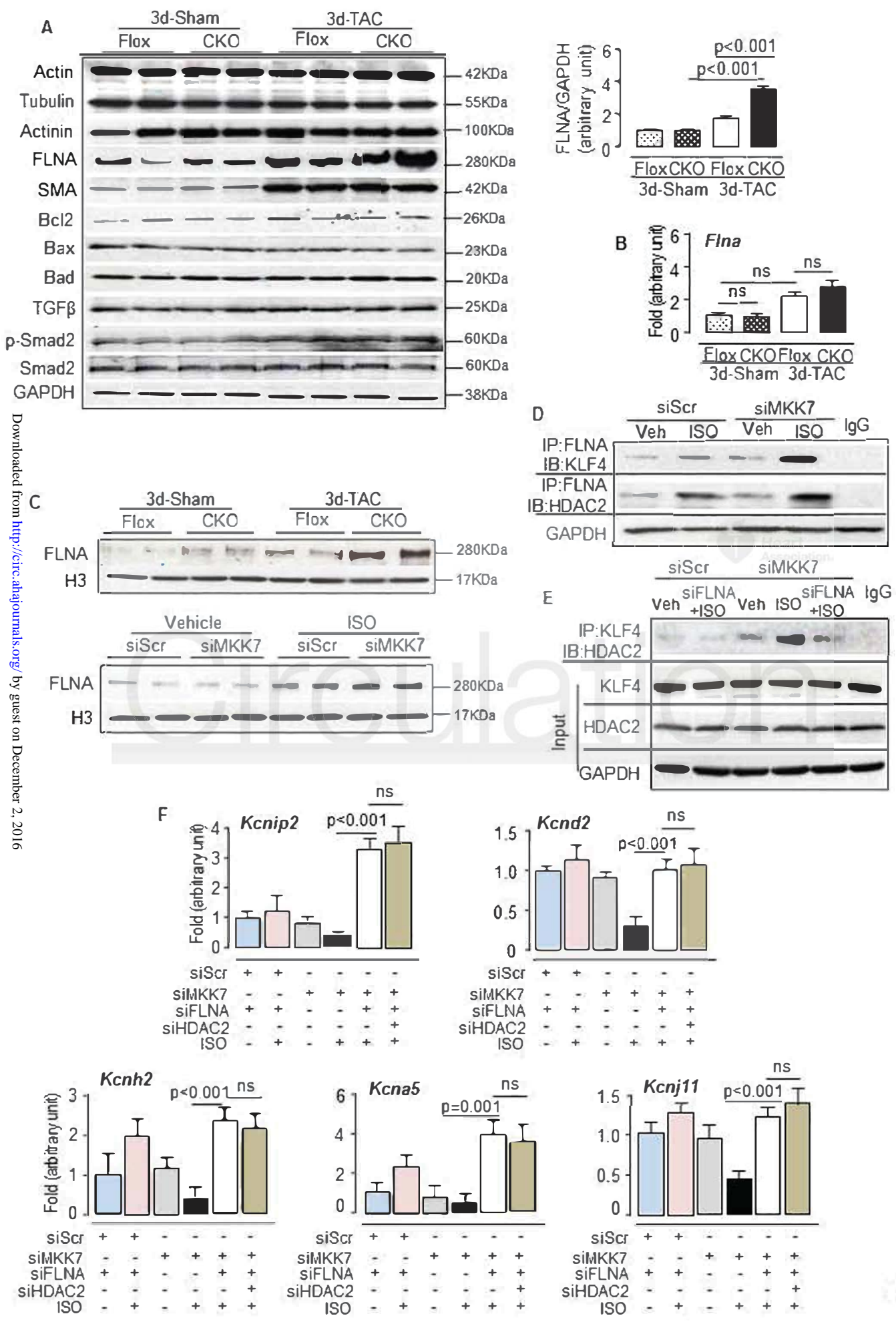


G

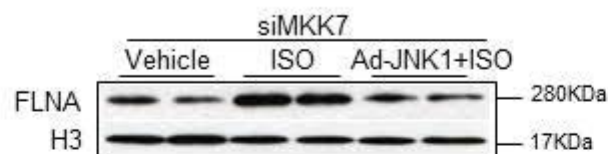


H

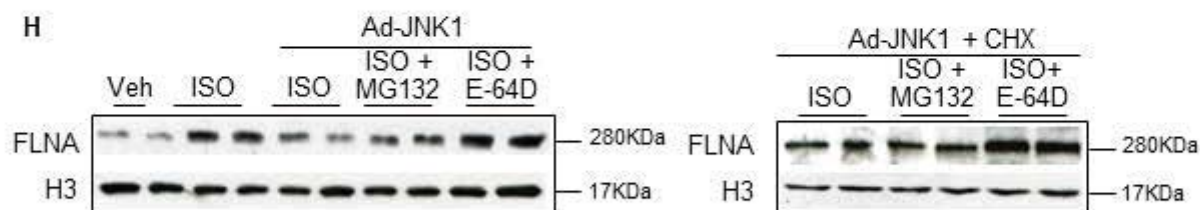




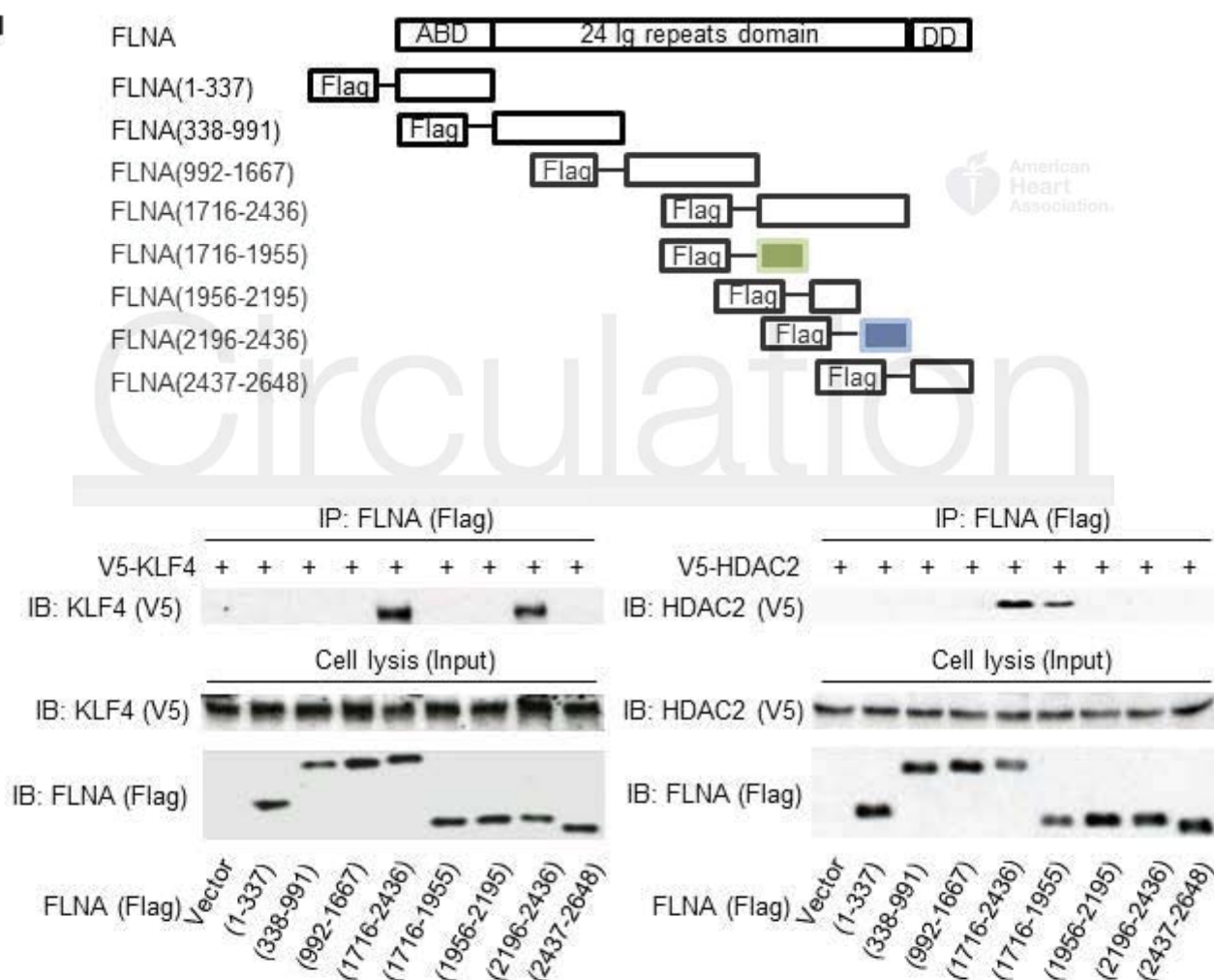
G

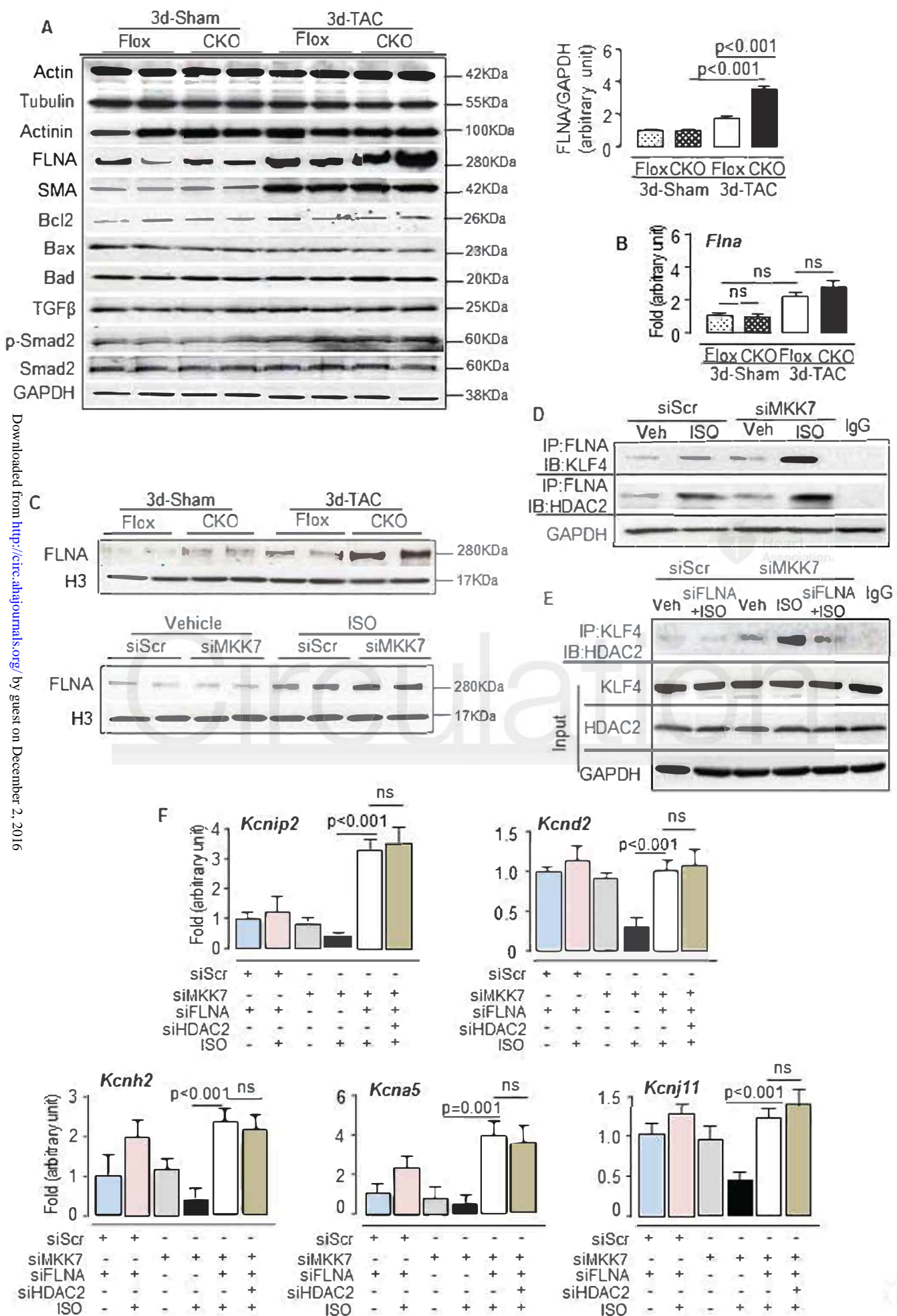


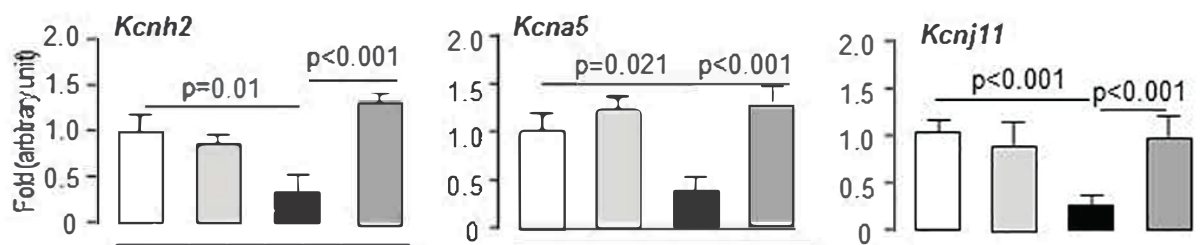
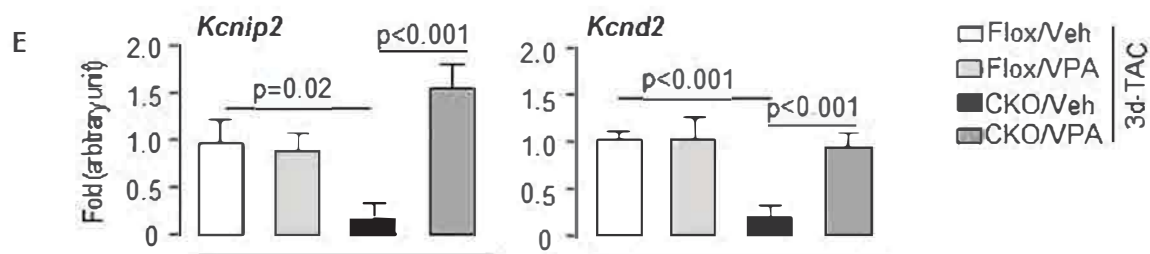
H



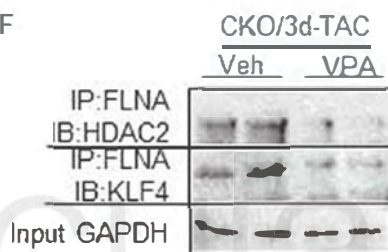
I





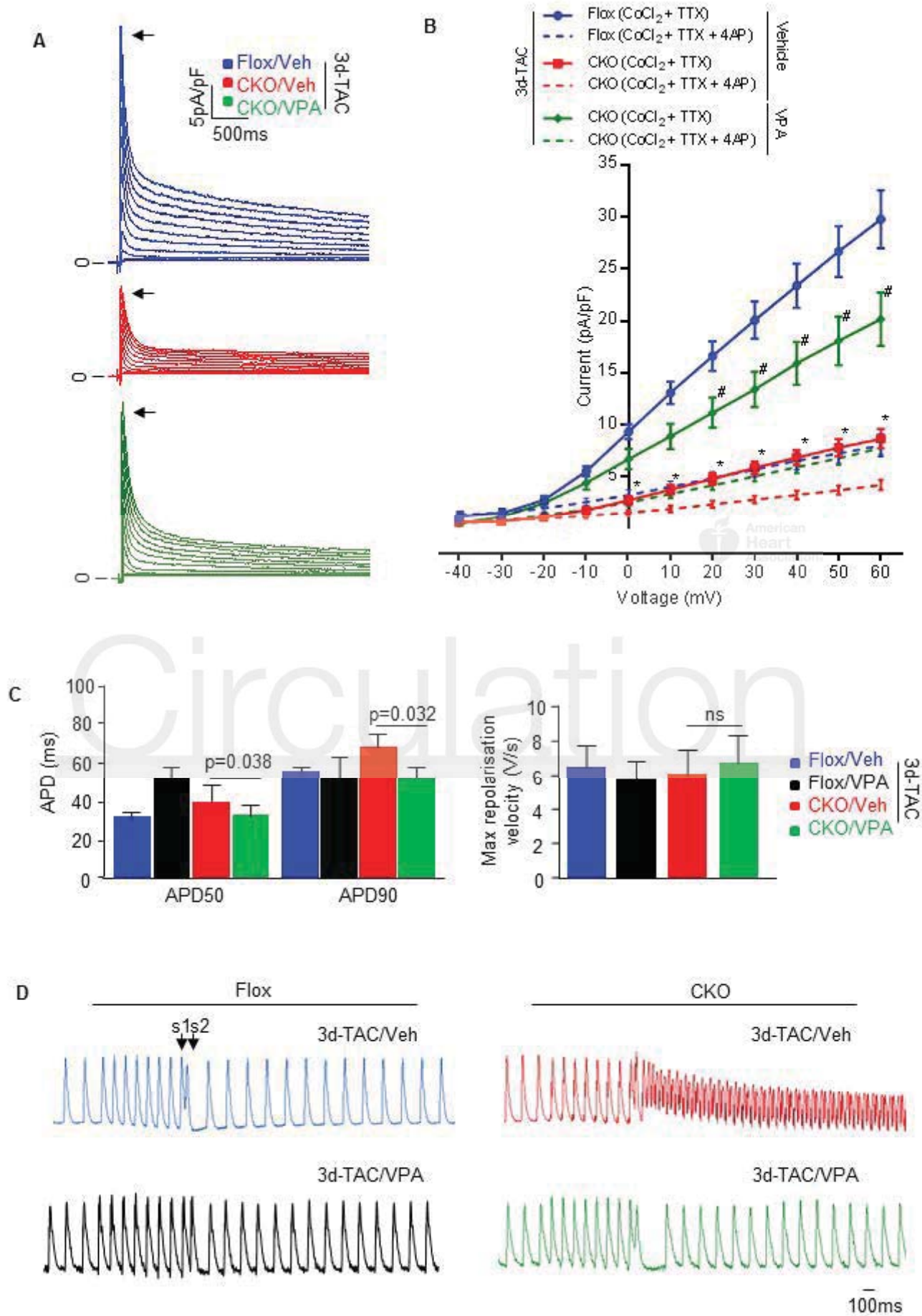


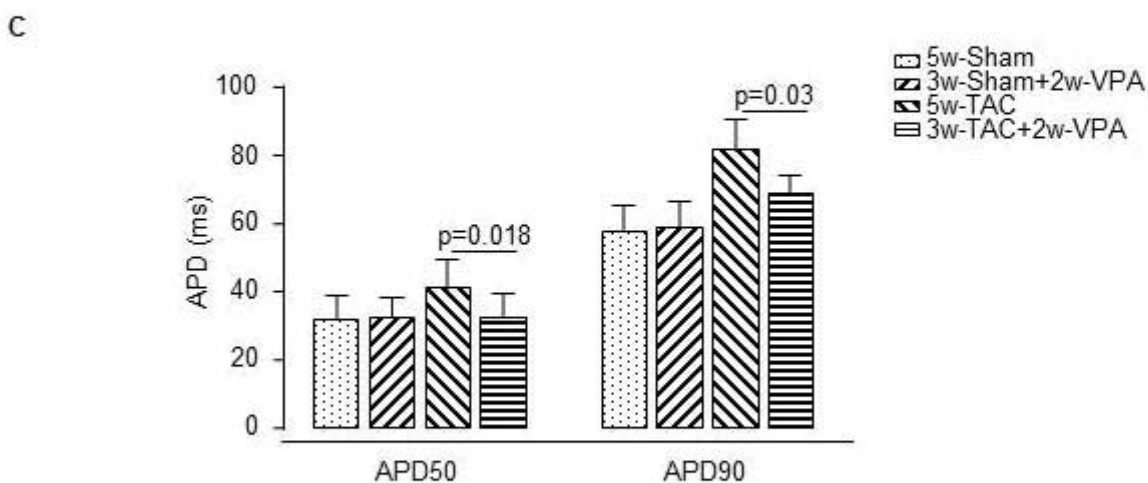
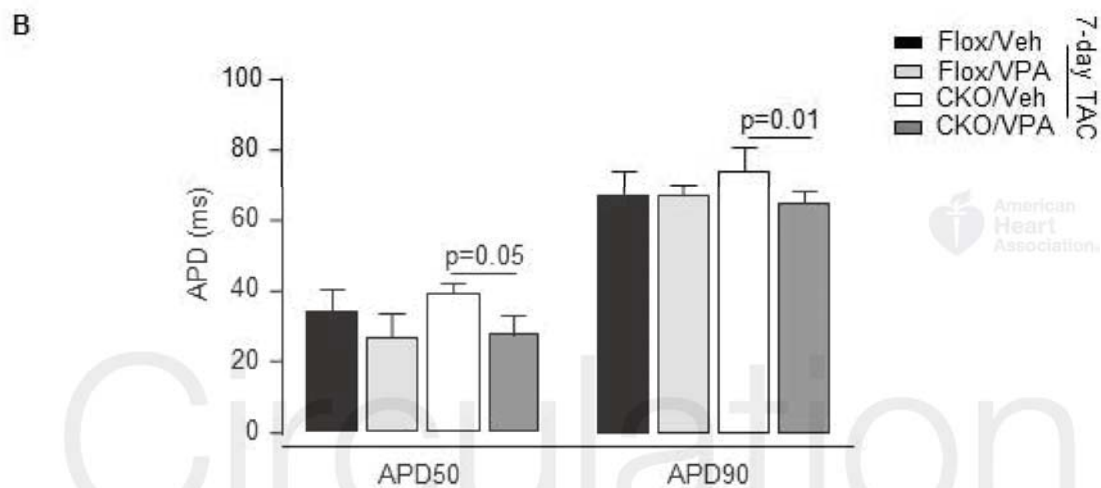
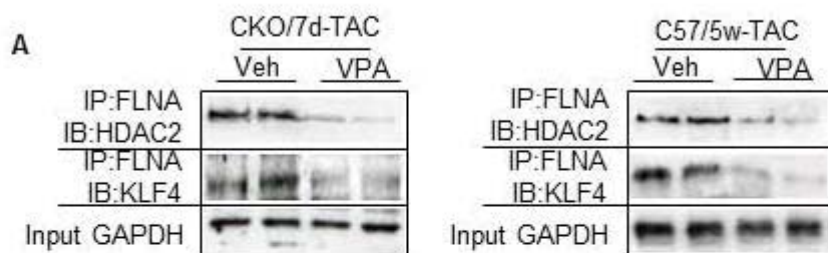
**F**

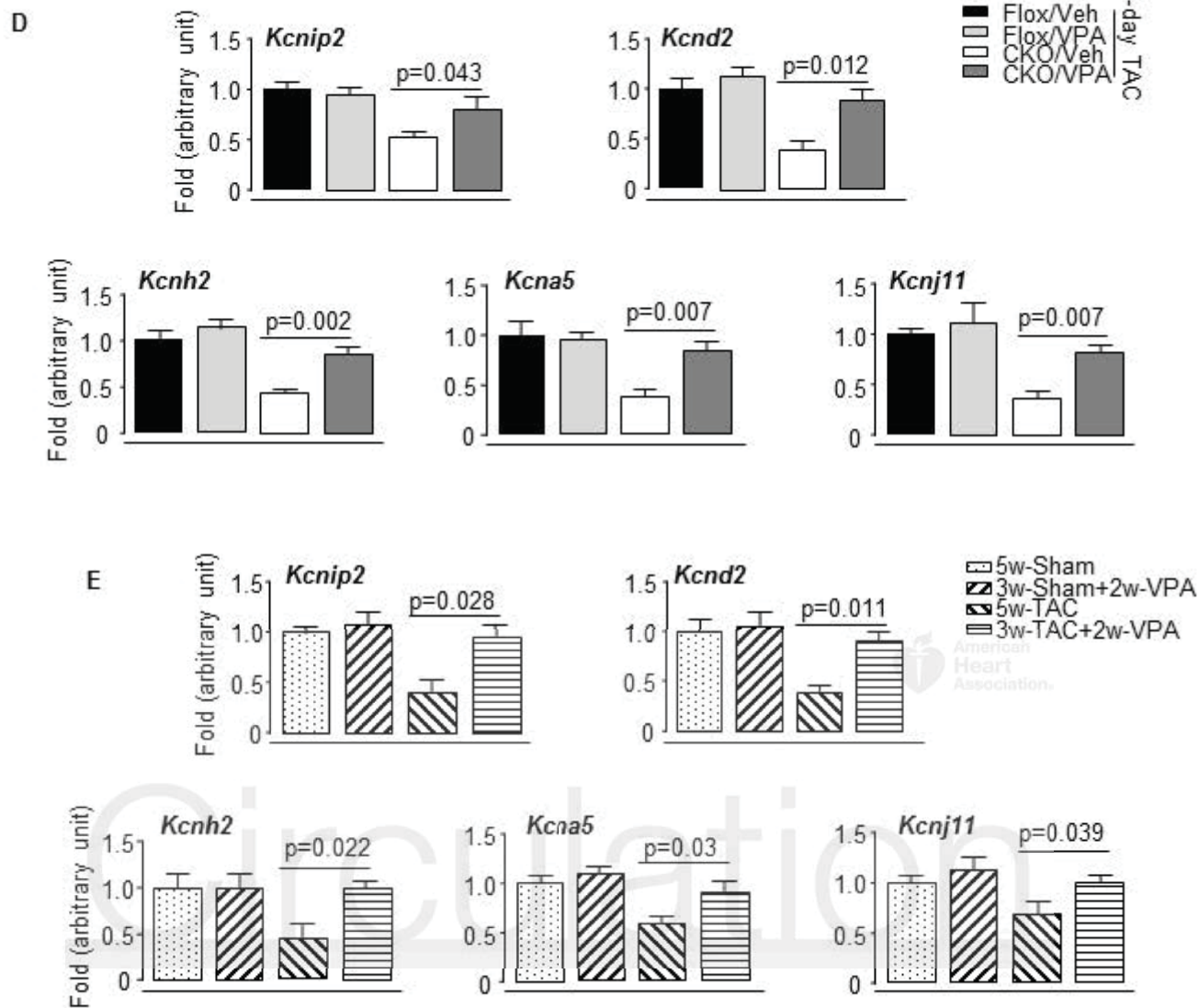


Circulation

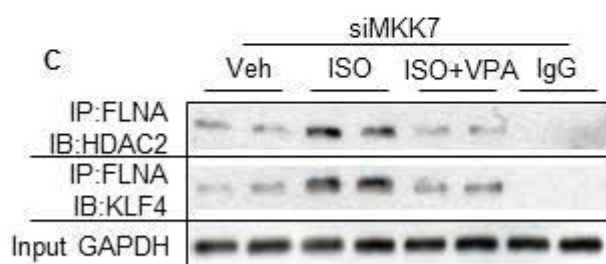
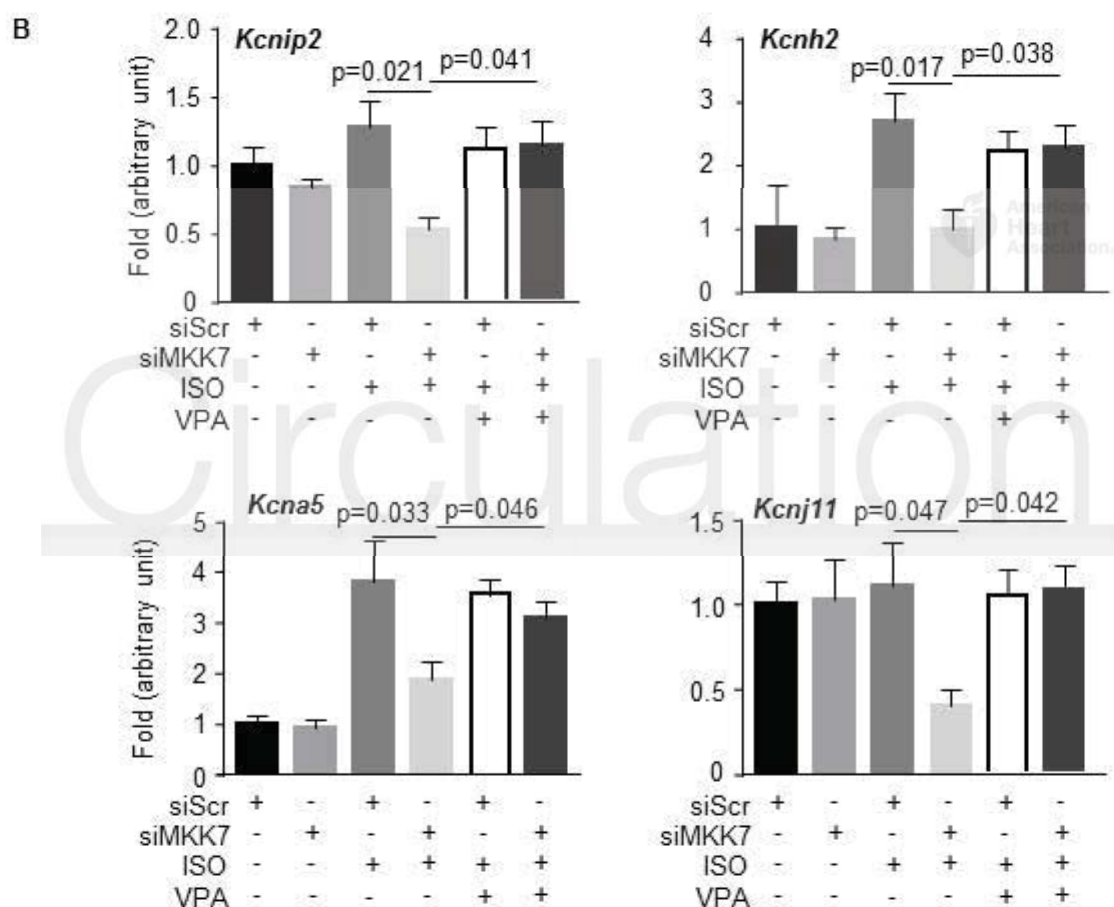
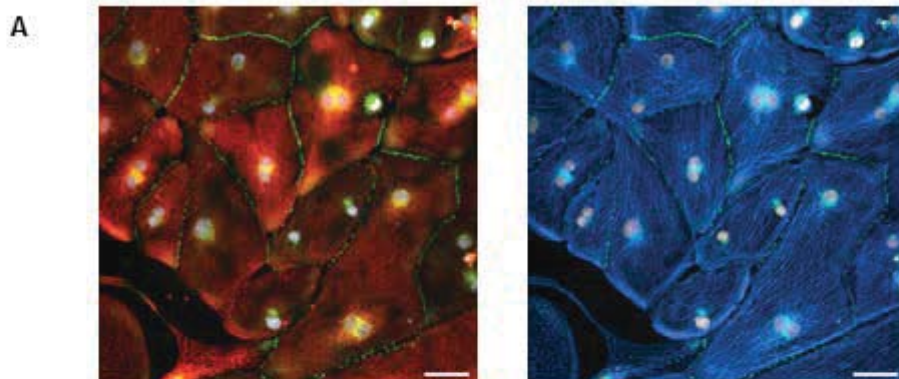


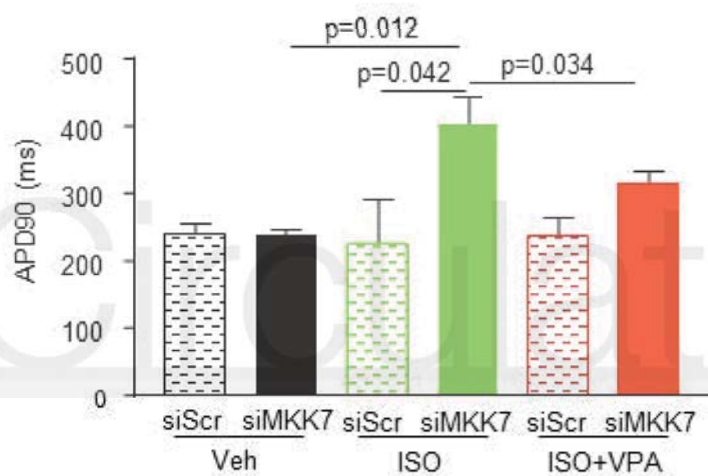
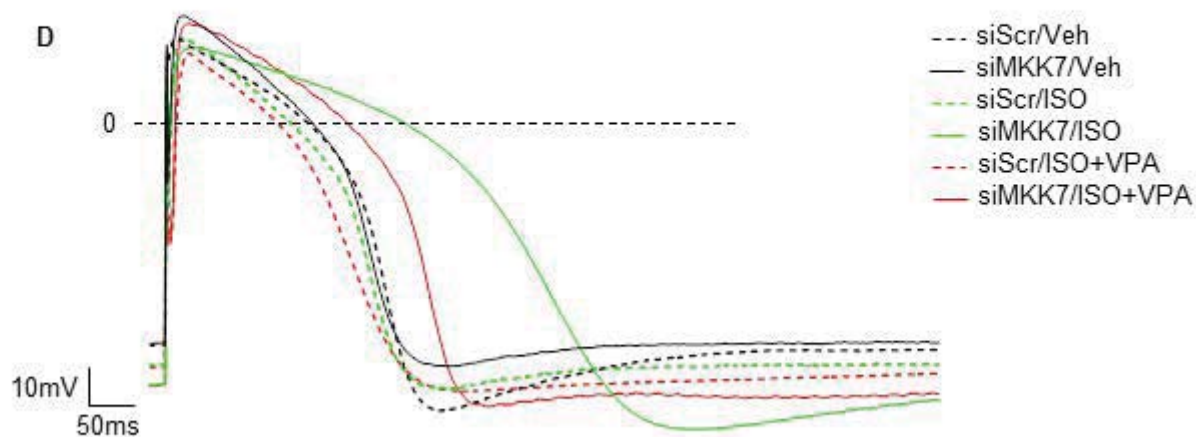


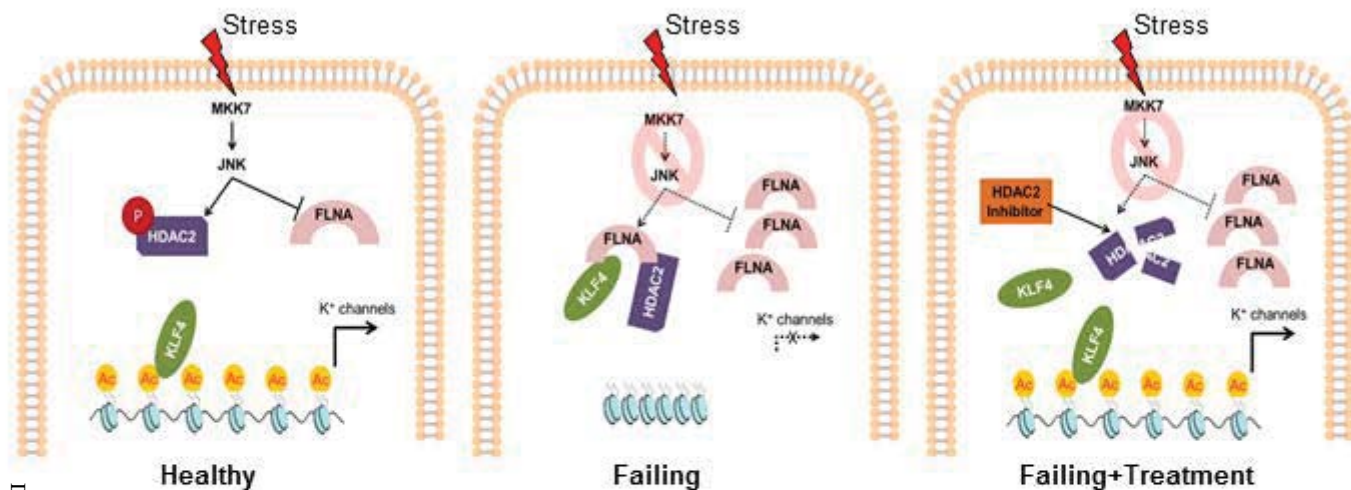












# Circulation

## Stress-Activated Kinase MKK7 Governs Epigenetics of Cardiac Repolarization for Arrhythmia Prevention

Sanjoy K. Chowdhury, Wei Liu, Min Zi, Yatong Li, Shunyao Wang, Hoyee Tsui, Sukhpal Prehar, Simon J. Castro, Henggui Zhang, Yong Ji, Xiuqin Zhang, Rui-ping Xiao, Rongli Zhang, Ming Lei, Lukas Cyganek, Kaomei Guan, Catherine B. Millar, Xudong Liao, Mukesh K. Jain, Mark R. Boyett, Elizabeth J. Cartwright, Holly A. Shiels and Xin Wang

*Circulation*. published online November 29, 2016;

*Circulation* is published by the American Heart Association, 7272 Greenville Avenue, Dallas, TX 75231

Copyright © 2016 American Heart Association, Inc. All rights reserved.

Print ISSN: 0009-7322. Online ISSN: 1524-4539

The online version of this article, along with updated information and services, is located on the World Wide Web at:

<http://circ.ahajournals.org/content/early/2016/11/28/CIRCULATIONAHA.116.022941>

Data Supplement (unedited) at:

<http://circ.ahajournals.org/content/suppl/2016/11/28/CIRCULATIONAHA.116.022941.DC1.html>

**Permissions:** Requests for permissions to reproduce figures, tables, or portions of articles originally published in *Circulation* can be obtained via RightsLink, a service of the Copyright Clearance Center, not the Editorial Office. Once the online version of the published article for which permission is being requested is located, click Request Permissions in the middle column of the Web page under Services. Further information about this process is available in the [Permissions and Rights Question and Answer](#) document.

**Reprints:** Information about reprints can be found online at:  
<http://www.lww.com/reprints>

**Subscriptions:** Information about subscribing to *Circulation* is online at:  
<http://circ.ahajournals.org/subscriptions/>

## Supplemental Material

### Animal models

All laboratory mice and rats in this study were maintained in a pathogen-free facility at the University of Manchester. Animal studies (mice and rats) were performed in accordance with the United Kingdom Animals (Scientific Procedures) Act 1986 and were approved by the University of Manchester Ethics Committee.

Generation of cardiomyocyte-specific MKK7 knockout mice (referred to as MKK7-CKO) was described in our previous study<sup>1</sup>. To achieve MKK7 deletion in cardiomyocytes, a transgenic Cre knock-in mouse (MLC2v-Cre)<sup>2</sup> was mated with MKK7-Flox mouse. In this transgenic mouse line, Cre expression is regulated by the ventricle specific isoform-2 of myosin light chain (MLC2v) promoter. General physiological parameters and cardiac morphological features at baseline or stress condition have previously been shown to be comparable between wild type (MKK7+/+), MKK7-Flox, MLC2v-Cre and MKK7-CKO mice by Liu et al<sup>1, 2</sup>. In this study, we further characterized ECG parameters, arrhythmia vulnerability by in vivo programmed electrical stimulation (PES) in MLC2v-Cre versus MKK7-Flox mice with or without transverse aortic constriction (TAC). Normal ECG parameters and no arrhythmic event were detected in MLC2v-Cre in Supplementary Fig. 21. An attempt was made to backcross MKK7-Flox and MKK7-CKO mice into a C57BL/6J background for 5 generations. MKK7-CKO mice and littermates MKK7-Flox mice as control were used to investigate specific impacts of MKK7 deletion in the heart.

MKK7 transgenic mice (referred to as MKK7-Tg), generated and described by Kaiser et al<sup>3</sup>, were obtained from the Jackson laboratory (stock number: 010584). Mouse Map2k7 cDNA expression was driven by the  $\alpha$ -myosin heavy chain (Myh6) promoter in this transgenic strain. The strain was maintained on a FVB/N background.

KLF4-cardiac deleted (referred to as KLF4-CKO) mice were generated by crossing KLF4-Flox mice with  $\alpha$  myosin heavy chain ( $\alpha$ MHC) Cre mice and was described in the previous study<sup>4</sup>.

Left ventricular tissues of non-human primate were prepared from hypertensive or normotensive rhesus monkeys, which had an established cohort of spontaneous metabolic syndrome<sup>5</sup>. Cardiac hypertrophy was detected by echocardiography. The experimental protocol for non-human primate was approved by the Institutional Animal Care and Use Committee of Peking University and was in accordance with the principles of laboratory animal care of China National Academy of Sciences/National Research Council (IACUC approval No. IMM-Zhangxq-1).

#### **Transverse aortic constriction (TAC), Isoprenaline minipump and Valproic acid (VPA) treatment**

Male (8-10 weeks old) mice were anesthetised with Ketamine (100mg/kg) and Xylazine (5mg/kg) by intraperitoneal (I.P.) injection and ventilated for TAC surgery, performed as previously described<sup>6</sup>. Briefly, the transverse aorta between right innominate and left common carotid arteries was subjected to ligation by a 7-0 Prolene suture to produce an approximate pressure difference of 30-40 mmHg between the two common carotid arteries. Buprenorphine (0.1mg/kg) was subsequently administered for post-operative analgesia. The method for minipump delivery of Isoprenaline (10mg/kg/day, Sigma) by subcutaneous implantation was described in our previous study<sup>6</sup>. In treatment experiments, mice were treated with I.P. VPA (200mg/kg/day, Sigma Aldrich P4543) or equal volume of water (vehicle) for 3 days along with TAC, or 4 days followed 3 days TAC, or 2 weeks followed 3 weeks TAC as described in the main text, thereafter the mice were subjected to various assessments.



## **Morphological and histological analysis**

Morphological data including body weights, heart and lung weights and right tibia length were measured. Histological analysis following Haematoxylin and Eosin staining for myocyte cross-sectional area measurement, or Masson's trichrome staining for fibrosis assessment was performed as previously described<sup>1</sup>.

## **Echocardiography**

Mice were terminally anesthetized with 2,2,2-Tribromethanol (Avertin, 200mg/kg, Sigma) and echocardiographic assessment of cardiac function was carried out using an Acuson Sequoia C256 (Siemens) ultrasound machine. For each mouse, measurements of the left ventricle end-systolic (LVESD) and end-diastolic (LVEDD) dimensions, end-diastolic posterior wall thickness (dPW), ejection fraction (EF) and left ventricular mass were recorded<sup>7</sup>.

## **In-vivo electrocardiography and programmed electrical stimulation (PES)**

3-leads surface electrocardiographic recordings were carried out using an ML136 'Bio-Amp' differential amplifier connected to Powerlab 4/30 (ADInstruments). ECG signals were digitally stored at 2KHz sampling frequency for blind offline analysis of P wave duration, PR and RR intervals, QRS and QT durations. The QT interval was corrected for heart rate (QTc) using Mitchell equation  $QTc = QT / (RR/100)^{1/2}$ <sup>8</sup>. For in-vivo PES, an EPR-800 catheter (Millar instruments) was introduced through the diaphragm. Electrical stimulation was delivered via DS3 isolated constant-current stimulator (Digitimer Ltd), which was connected with CED Micro3-1401 data acquisition system and controlled by Spike (Cambridge Electronic Design). The PES protocol consisted of a single extra-stimulus (S2) following a train of eight stimuli (S1) at a constant basic cycle length (BCL) of 100ms or 120ms<sup>9</sup>. The S1S2 coupling interval was progressively decreased by 2ms until any of the pre-defined end-points

were reached. Such end-points were ventricular effective refractory period, arrhythmia or S1S2 coupling interval of 30ms. In-vivo electrophysiological data were analyzed with Labchart (ADInstruments).

### **Langendorff perfusion of mouse heart**

Heparinised (200U/Kg, Wockhardt) mice were sacrificed by cervical dislocation and the whole heart was dissected out. The aorta was quickly cannulated and the heart was perfused with carbogen-bubbled (95% O<sub>2</sub>, 5% CO<sub>2</sub>) 37°C-heated modified Ringers solution (NaCl 120mM, KCl 4.5mM, MgCl<sub>2</sub> 1mM, CaCl<sub>2</sub> 1.8mM, NaHCO<sub>3</sub> 25mM, Glucose 10mM; pH 7.4) with a constant flow rate of 4-5ml/min.

### **Ex-vivo monophasic action potential and PES**

ECG electrodes (Harvard apparatus) were placed on the right atria and the ventricular apex for monitoring electrocardiograms. A monophasic action potential (MAP) electrode was placed on the left ventricular epicardium, whilst a bipolar stimulation electrode was placed on the posterior epicardial surface in relation to the A-V junction. ECG and MAP signals were assessed for stability, signal quality and intrinsic rhythms for about 15 minutes. Double-capture threshold stimuli were used firstly for basal stimulation to record paced-MAPs and subsequently for PES protocols to assess pro-arrhythmia. The ex-vivo PES protocol was similar to that described for in-vivo recordings. 3 PES attempts were made for each recording. However, the first attempt was preferably chosen when analysing occurrences of ventricular arrhythmia in order to avoid false positives data. For MAPs, 100 consecutive beats paced at 8Hz were analyzed using the peak-analysis module in LabChart with visual confirmation.

### **Adult cardiomyocyte isolation**

Murine ventricular cardiomyocytes were isolated using enzymatic dispersion optimized from those previously described<sup>10</sup>. Briefly, hearts were perfused with 60U/ml collagenase (type II, Worthington) and 0.042mg/ml protease (Sigma-Aldrich) containing solution<sup>9</sup>. Cells were gently dispersed from sufficiently digested ventricular apex and suspended in modified Tyrodes solution (NaCl 130mM, KCl 5.4mM, MgCl<sub>2</sub> 1mM, CaCl<sub>2</sub> 1mM, NaH<sub>2</sub>PO<sub>4</sub> 0.33mM, HEPES 10mM, Glucose 5.5mM; pH 7.4). Only clearly-striated rod-shaped cells without membrane blebs were used for electrophysiological studies.

### **Electrophysiological studies on mouse single ventricular myocyte**

Patch pipettes (Harvard apparatus) had resistances of 1.1-2.3m $\Omega$  when filled with pipette solution (Potassium L-aspartate 110mM, KCl 20mM, NaCl 8mM, EGTA 10mM, MgCl<sub>2</sub> 1mM, Mg-ATP 5mM, CaCl<sub>2</sub> 1mM, HEPES 10mM; pH 7.4). The electrodes were connected to an Axopatch 200B amplifier (Axon Instruments) and data were acquired at sampling rate 5 kHz using Digidata 1321A interface (Axon Instruments). Current- and voltage-clamping was achieved in the whole cell configuration. Cell membrane capacitance and series resistance was electronically compensated. Data were analyzed using pClamp software (version 10.6, Axon Instruments Inc.).

Action potentials (APs) were elicited in current-clamp by injecting square pulses of 1ms width and 1.5 times threshold current at 1Hz using current clamp. 100 consecutive AP traces were recorded at 37°C. A dual heater controller (TC-324B, Warner Instrument Corp) connected with two temperature sensors was placed in the recording chamber to ensure the on-site temperature. Liquid junction potential of -12 mV was corrected offline in the AP data analysis.

Outward  $K^+$  currents were recorded using voltage clamp in presence of  $CoCl_2$  (5mM) and Tetrodotoxin (0.02mM) to eliminate  $Ca^{2+}$  and  $Na^+$  currents, respectively. Isolation of  $K^+$  currents was subsequently confirmed with inclusion of 4-aminopyridine (4-AP, 5mM). Outward  $K^+$  currents were activated by 4s depolarising voltage steps to potentials ranging between  $-35$  and  $+45$ mV in 10mV increments preceded by a 50ms pre-pulse voltage step to  $-40$ mV (to separate TTX-resistant  $Na^+$  currents) from a holding potential of  $-70$ mV<sup>11</sup>. All currents were normalised to the cell capacitance ( $pA\ pF^{-1}$ ), which was measured from capacitive transient currents elicited by a 10mV depolarising step. To achieve a better separation of outward  $K^+$  currents, all recordings were made at  $22^\circ C$ <sup>12</sup>.

### **Neonatal rat cardiomyocyte isolation and culture**

Primary cultures of neonatal rat cardiomyocytes (NRCMs) were prepared as previously described<sup>13</sup>. Briefly, NRCMs were isolated from 2 days old Sprague-Dawley rats using a standard enzyme solution (30U/100ml Collagenase A, 100mg/ml Pancreatin, NaCl 116mM, HEPES 20mM,  $NaH_2PO_4$  1mM, Glucose 6mM, KCl 5mM,  $MgSO_4$  0.8mM; pH 7.4). Isolated NRCMs were plated in culture medium (79.5% DMEM, 19.5% M199; 1% fetal bovine serum, 1% Penicillin-Streptomycin, 2.5 $\mu$ g/ml Amphotericin-B and 1 $\mu$ M Bromodeoxyuridine) at a field density of  $2 \times 10^6$  cells/well for treatments and subsequent analyses.

### **NRCM transfection with siRNA**

NRCMs were transfected with siRNA (100nM) using Lipofectamine Plus reagent according to the manufacturer's (Invitrogen) recommendation. Rat MKK7 siRNA (gene ID #363855), KLF4 siRNA (gene ID #114505), HDAC2 siRNA (gene ID #84577) and FLNA siRNA (gene ID #293860) were purchased from Dharmacon (si genome SMART pool), and negative control siRNA was obtained from Sigma-Aldrich.

48 hours post-transfection with siRNA, NRCMs were treated with Isoprenaline (ISO, 10 $\mu$ M) for 24 hours. To investigate FLNA protein levels, knockdown of MKK7 was followed with infection of Ad-JNK1 and ISO stimulation. NRCMs were pre-treated with Cycloheximide (CHX, 10 $\mu$ l/ml, 4 hours) followed by treatment with a proteasome inhibitor (MG132, 2.5 $\mu$ M, 16 hours) or cysteine protease inhibitor (E-64D, 5 $\mu$ M, 16 hours). To determine the effects of VPA, NRCMs were treated with ISO or combination of ISO and VPA (20mM) for 48 hours.

### **Lysate preparation and immunoblotting**

Total protein from tissue samples or NRCMs were lysed with triton lysis buffer (Tris 20mM, NaCl 137mM, EDTA 2mM, 1% Triton X-100,  $\beta$ -glycerophosphate 25mM, Na<sub>3</sub>VO<sub>4</sub> 1mM, phenylmethanesulphonylfluoride 1mM, Aprotinin 1.54 $\mu$ M, Leupeptin 21.6 $\mu$ M, 10% Glycerol; pH 7.4). Nuclear proteins were extracted with gradient centrifugation. Briefly, tissue samples were lysed in cytoplasmic buffer (Tris 20mM, NaCl 10mM, MgCl<sub>2</sub> 2mM, EDTA 2mM,  $\beta$ -glycerophosphate 25mM, Na<sub>3</sub>VO<sub>4</sub> 1mM, PMSF 1mM, Aprotinin 1.54 $\mu$ M, and Leupeptin 21.6 $\mu$ M; pH 7.4). The lysates were spun at 5,000g for 5 minutes for the removal of cytoplasmic proteins. The pellets were re-suspended in the nuclear buffer (Tris 50mM, NaCl 500mM, EDTA 2mM, 10% Glycerol, 1% TritonX-100,  $\beta$ -glycerophosphate 25mM, Na<sub>3</sub>VO<sub>4</sub> 1mM, PMSF 1mM, Aprotinin 1.54 $\mu$ M, and Leupeptin 21.6 $\mu$ M; pH 7.4), followed by centrifugation at 10,000g for 10 minutes, leaving the nuclear proteins suspended in the supernatant. Protein concentration was determined by Bradford assay (Bio-Rad).

Protein extracts (30 $\mu$ g) were subjected to immunoblot analyses with antibodies against MKK7 (Cell Signaling, 4172), phospho-MKK7 (Cell Signaling, 4171), KChIP2 (Abcam, ab99041), HDAC2 (Abcam, ab51832), phospho-HDAC2 (Abcam, ab75602, Ser394), HDAC3 (Abcam, ab32369), HDAC8 (Abcam, ab126886), KLF4 (Santa

Cruz, sc20691), TGF $\beta$  (R&D, MAB240), Smad2/3 (Cell Signaling, 3102), phospho-Smad2 (Cell Signaling, 3108, Ser465/467), Bad (BD Biosciences, 610391), Bax (Santa Cruz, sc493), Bcl2 (Cell Signaling, 2876), Tubulin (Sigma-Aldrich, T6199),  $\alpha$ -Actinin (Sigma-Aldrich, A7811),  $\alpha$ -smooth muscle actin (SMA, Abcam, ab7817),  $\beta$ -actin (Abcam, ab20272), Histone-3 (Cell Signaling, 9715), Filamin-A (FLNA, Cell Signaling, 4762), or GAPDH (Abcam, ab9482). Immune-complexes were detected by chemi-luminescence with anti-mouse or -rabbit immunoglobulin-G coupled with horseradish peroxidase as the secondary antibody (Amersham-Pharmacia).

### **Immunoprecipitation**

To investigate the association of KLF4, HDAC2 and FLNA, immunoprecipitations were performed with Pierce Protein A/G Magnetic Beads (Thermo Scientific) following the manufacturer's instruction. Briefly, tissue samples or NRCMs were lysed with immunoprecipitation buffer (Tris 50mM, NaCl 250mM, 0.25% v/v TritonX-100, and 10% Glycerol; pH 7.4) and 2mg of the protein extract was immunoprecipitated with antibody against KLF4 (Santa Cruz, sc20691), HDAC2 (Abcam, ab51832), FLNA (Cell Signaling, 4762, or Abcam, ab80837) or IgG (Cell Signaling, 2729). The interacting protein was detected by SDS-PAGE and immunoblot analyses using antibody against HDAC2 (Abcam, ab51832), phospho-HDAC2 (Abcam, ab75602, Ser394), HDAC1 (Abcam, ab31263), or KLF4 (Santa Cruz, sc20691), respectively. To further determine the MKK7/JNK regulation, NRCMs were infected with recombinant adenovirus encoding JNK1 (Ad-JNK1, a kind gift from Dr, Hiroki Aoki, Kurume University, Japan) followed by 24 hours treatment with ISO (10 $\mu$ M).

To further determine the association of FLNA domain with KLF4 and HDAC2, respectively, we used polymerase chain reaction (PCR) to generate various FLNA



fragments: FLNA (1-337), FLNA (338-991), FLNA (992-1667), FLNA (1716-2436), FLNA (1716-1955), FLNA (1956-2195), FLNA (2196-2436), and FLNA (2437-2648). Fragments were cloned to p3xFlagCMV7.1 (Sigma). V5-KLF4 and V5-HDAC2 constructs were also obtained by cloning of PCR fragment to pcDNA6 V5-His A (Promega). Ventricular myoblast cell line, H9c2 cells, were transfected using Lipofectamine 2000 reagent (Invitrogen) following the manufacturer's protocol. Total protein from H9c2 cells was prepared using immunoprecipitation buffer. For each immunoprecipitation, 1mg protein was precipitated with 10µg of anti-Flag antibody bound to Pierce Protein A/G Magnetic Beads (Thermo Scientific). Anti-FLAG Tag antibody (Cell Signaling, 8416) was used for immunoprecipitation. Immune complexes were eluted in 2xLaemmli sample buffer (65.8mM Tris-HCl, pH 6.8, 2.1% SDS, 26.3% glycerol, 0.01% bromophenol blue). Precipitated and input proteins were subjected to SDS-PAGE and immunoblotted using anti-V5 Tag antibody (Cell Signaling, 13202) as indicated in Results.

#### **Human induced pluripotent stem cell (iPSC) differentiation and treatment**

Human iPSCs were derived from peripheral blood cells. The pluripotency was proven according to the previous study<sup>14</sup>, and were maintained in feeder-free culture conditions with E8 medium (Thermo Fisher Scientific) on Geltrex-coated plates. Standard directed cardiomyocytes differentiation of iPSCs was initiated at confluence of 90-100% via WNT signaling modulation with cardiac differentiation medium (RPMI1640 HEPES Glutamax, 500mg/L human recombinant albumin, 200mg/L L-ascorbic acid 2-phosphate) and progressive treatment with 4µM CHIR99021 (inhibitor of Glycogen synthase kinase 3) for 48h and 5µM IWP2 (Wnt Inhibitor) for further 48h. Medium was changed to cardiac culture medium (RPMI1640 HEPES Glutamax, B27) at day 10. Metabolic cardiomyocytes selection was performed using

cardiac selection medium (RPMI 1640 minus Glucose, 4mM Lactate, 500mg/L human recombinant albumin, 200mg/L L-ascorbic acid 2-phosphate) for 5 days. iPSC-derived cardiomyocytes (iPSC-CM) were cultured in cardiac culture medium up to day 120 for further maturation. Immunocytochemistry was applied using alpha-actinin (Sigma A7811), Cx43 (Abcam AB11370), and Alexa Fluor 555-Phalloidin (Thermo Fisher Scientific A34055). To examine the expression of K<sup>+</sup> channels, qPCR were performed on the iPSC-CM transfected with human MKK7 siRNA (Gene ID # 5609) followed by ISO (5μM) stimulation for 48 hours, or ISO stimulation for 24 hours followed by an addition of VPA (4mM) for further 24 hours.

For single iPSC-CM action potential recordings, glass coverslips were coated with Geltrex and placed into 60 x 15 mm peril dish. A low density of 6000–10,000 iPSC-CM were plated to each coverslip and cultured for 7 days followed by various treatments: iPSC-CMs were knocked down MKK7 by siRNA followed by the treatment of 5μM ISO alone, or in combination with 4mM VPA as above described. Thereafter, single cell APs were recorded by patch clamping. Patch pipettes (Harvard apparatus) had resistances of 5.5-6.5mΩ when filled with pipette solution (KCl 150mM, NaCl 5mM, CaCl<sub>2</sub> 2mM, EGTA 5mM, HEPES 10mM, Mg-ATP 2mM; pH 7.2)<sup>15</sup>. The external solution for recording (NaCl 150mM, KCl 5.4mM, CaCl<sub>2</sub> 1.8mM, MgCl<sub>2</sub> 1mM, Glucose 15mM, HEPES 15mM, Na Pyruvate 1mM; pH 7.4) was used<sup>15</sup>. The recording procedure was described as above.

### **Quantitative real-time polymerase chain reaction (qPCR)**

Total RNA was extracted from tissues or NRCMs using Trizol (Invitrogen), followed by immediate conversion to cDNA. Primers used in this study were purchased from Qiagen or designed using Roche online program Universal ProbeLibrary Assay Design Center. Polymerase reactions were performed using SensiMix<sup>TM</sup> SYBR No-

ROX Kit (Bioline) according to the manufacturer's recommendations or TaqMan method by Roche Universal ProbeLibrary on a ViiA 7 Real-Time, in the Chromo-4™ real-time detection system (Bio-RAD), and the results were analyzed using the 2- $\Delta\Delta C_T$  method<sup>16</sup>. The level of expression of mRNA was normalised to reference gene glyceraldehyde-3-phosphate dehydrogenase (*Gapdh*) mRNA, and validated by reference gene s18 mRNA (Supplementary Fig. 22).

### **Chromatin immune-precipitation (ChIP)**

ChIP was performed using the SimpleChip Plus ChIP kit (Cell Signaling) following manufacturer's instruction. In brief, 75mg of ventricular tissues were cross-linked with 1.5% formaldehyde and homogenized for preparation of nuclei suspension. Nuclear membrane was lysed by sonication and micrococcal nuclease was used to digest DNA to 1-5 nucleosome lengths. 9µg of chromatin was used for immunoprecipitation. Following overnight incubation with KLF4 (Santa Cruz, sc-20691), acetyl-histone3 (Millipore, 06-599), histone (Cell signaling, 4620) or rabbit IgG (Cell signaling, 2729) antibody; immunoprecipitated samples were incubated with ChIP grade protein G agarose beads.

Chromatin was eluted from immunoprecipitated samples, and protein-DNA crosslink was sheared by 65°C incubation. DNA was purified using isopropanol-ethanol extraction in spin-columns and eluted for subsequent analysis. Quantitative PCR was performed using the following primers for *Kcnip2* (Forward: 5'-CTTCTGCTCCGCTCTCACTT-3', Reverse: 5'-GATAGGGCGCTCACACAGT-3'); primers for *Kcnh2* (Forward: 5'-ATCAGCTGGTGGAGCCACCT-3', Reverse: 5'-AACACTAAGGCCAAACAGG-3'); primers for *Kcna5* (Forward: 5'-CATCCCAGCCTAGAACCCAA-3', Reverse: 5'-CAACGCTGCAATTCAAACCC-3'); primers for *Kcnd2* (Forward: 5'-AACTGTCACACTGCACCTG-3', Reverse: 5'-

AGATGGAGGTGAAGTGCAGG-3'); and primers for *Kcnj11* (Forward: 5'-CCCAAATCCCTCCACAACGA-3', Reverse: 5'-AAGGAGCCATGACTAGCAGG-3').

Data was normalised to the amount of input chromatin.

### **HDAC activity assay**

NRCMs were treated with vehicle (injection water), VPA (4mM) for 24 hours and extracts were processed using the Activemotif assay kit following manufacturer's protocol, with Pan-HDAC inhibitor (Trichostatin-A, 1 $\mu$ M) added as control for HDAC inhibitor activity. HDAC activity was determined as fluorescent intensity in a BMG Fluostar Optima micro-plate reader.

### **Proximity ligation assay**

Duolink staining based on *in situ* proximity ligation assay (PLA) was performed on NRCMs according to the manufacturer's instruction (Sigma, DUO92101). NRCMs with MKK7 deficiency were treated with vehicle or ISO (Sigma, 10 $\mu$ M) for 24 hours. After fixation with 3.7% of formaldehyde and permeabilization with 0.1% Triton X-100, NRCMs were incubated with the mixture of two corresponding PLA probes in the antibody diluent. Probes were ligated with circle-forming DNA oligonucleotides, rolling circle amplification was then occurred with polymerase solution. Finally, the fluorescently labelled oligonucleotides hybridized to the amplification product. For FLNA/KLF4 interaction, mouse anti-FLNA (Abcam, ab80837) and rabbit anti-KLF4 (Santa Cruz, sc20691) primary antibodies were used; for FLNA/HDAC2 interaction, rabbit anti-FLNA (Cell Signaling, 4762) and mouse anti-HDAC2 (Abcam, ab51832) were used. Images were obtained via fluorescence microscopy (Olympus).

### **Experimental design and statistical analysis**

Sample sizes were calculated based on available comparable data to achieve 80% power at a 5% significance level. Samples were randomly assigned to experimental

groups. Data are expressed as mean  $\pm$  S.E.M. and analyzed using Student's t-test for comparisons between two experimental groups or one- or two-way ANOVA with Bonferroni post-hoc tests for comparisons among multiple experimental groups. P values  $p < 0.05$  were considered statistically significant. When screening 19 ion channel genes in myocardium, multiple testing correction by the Bonferroni method was used. Genes that were differentially expressed between MKK7-Flox/3d-TAC group versus MKK7-CKO/3d-TAC group with ANOVA P-value  $< 0.0026$  ( $0.05/19$ ) were selected. Expression of the selected genes (*Kcnip2*, *Kcnd2*, *Kcnh2*, *Kcna5* and *Kcnj11*) in 4 experimental groups (MKK7-CKO/Sham, MKK7-CKO/3d-TAC, MKK7-Flox/Sham, MKK7-Flox/3d-TAC) was further analyzed by two-way ANOVA with Bonferroni correction for post-hoc comparisons.

## References

1. Liu W, Zi M, Chi H, Jin J, Prehar S, Neyses L, Cartwright EJ, Flavell RA, Davis RJ, Wang X. Deprivation of MKK7 in cardiomyocytes provokes heart failure in mice when exposed to pressure overload. *J Mol Cell Cardiol.* 2011; 50: 702-711.
2. Minamisawa S, Gu Y, Ross J, Chien KR, Chen J. A post-transcriptional compensatory pathway in heterozygous ventricular myosin light chain 2-deficient mice results in lack of gene dosage effect during normal cardiac growth or hypertrophy. *J Biol Chem.* 1999; 274: 10066–10070.
3. Kaiser RA, Liang Q, Bueno O, Huang Y, Lackey T, Klevitsky R, Hewett TE, Molkentin JD. Genetic inhibition or activation of JNK1/2 protects the myocardium from ischemia-reperfusion-induced cell death in vivo. *J Biol Chem.* 2005; 280: 32602–32608.
4. Liao X, Zhang R, Lu Y, Prosdocimo DA, Sangwung P, Zhang L, Zhou G, Anand P, Lai L, Leone TC, Fujioka H, Ye F, Rosca MG, Hoppel CL, Schulze PC, Abel ED,

- Stamler JS, Kelly DP, Jain MK. Kruppel-like factor 4 is critical for transcriptional control of cardiac mitochondrial homeostasis. *J Clin Invest*. 2015; 125:3461-3476.
5. Zhang X, Zhang R, Raab S, Zheng W, Wang J, Liu N, Zhu T, Xue L, Song Z, Mao J, Li K. Rhesus macaques develop metabolic syndrome with reversible vascular dysfunction responsive to pioglitazone. *Circulation*. 2011; 124:77-86.
6. Liu W, Zi M, Jin J, Prehar S, Oceandy D, Kimura TE, Lei M, Neyses L, Weston AH, Cartwright EJ, Wang X. Cardiac-specific deletion of mkk4 reveals its role in pathological hypertrophic remodeling but not in physiological cardiac growth. *Circ Res*. 2009; 104:905-914.
7. Gardin JM, Siri FM, Kitsis RN, Edwards JG, Leinwand LA. Echocardiographic assessment of left ventricular mass and systolic function in mice. *Circ Res*. 1995; 76: 907–914.
8. Mitchell GF, Jeron A, Koren G. Measurement of heart rate and QT interval in the conscious mouse. *Am J Physiol*. 1998; 274: H747-751.
9. Gutstein DE, Danik SB, Sereysky JB, Morley GE, Fishman GI. Subdiaphragmatic murine electrophysiological studies: sequential determination of ventricular refractoriness and arrhythmia induction. *Am J Physiol Heart Circ Physiol*. 2003; 285: H1091–1096.
10. Schlüter KD, Schreiber D. Adult ventricular cardiomyocytes: isolation and culture. *Methods Mol Biol*. 2005; 290: 305–314.
11. Xu H, Guo W, Nerbonne JM. Four kinetically distinct depolarization-activated K<sup>+</sup> currents in adult mouse ventricular myocytes. *J Gen Physiol*. 1999, 113: 661–678.
12. Zhou J, Jeron A, London B, Han X, Koren G. Characterization of a slowly inactivating outward current in adult mouse ventricular myocytes. *Circ. Res*. 1998; 83: 806-814.



13. Armesilla AL, Williams JC, Buch MH, Pickard A, Emerson M, Cartwright EJ, Oceandy D, Vos MD, Gillies S, Clark GJ, Neyses L. Novel functional interaction between the plasma membrane  $\text{Ca}^{2+}$  pump 4b and the proapoptotic tumor suppressor Ras-associated factor 1 (RASSF1). *J Biol Chem*. 2004; 279: 31318–31328.
14. Streckfuss-Bömeke K, Wolf F, Azizian A, Stauske M, Tiburcy M, Wagner S, Hübscher D, Dressel R, Chen S, Jende J, Wulf G. Comparative study of human-induced pluripotent stem cells derived from bone marrow cells, hair keratinocytes, and skin fibroblasts. *Eur Heart J*. 2013; 34: 2618-2629.
15. Ma J, Guo L, Fiene SJ, Anson BD, Thomson JA, Kamp TJ, Kolaja KL, Swanson BJ, January CT. High purity human-induced pluripotent stem cell-derived cardiomyocytes: electrophysiological properties of action potentials and ionic currents. *Am J. Physiol. Heart Circ Physiol*. 2011; 301:H2006–H2017.
16. Livak KJ, Schmittgen TD. Analysis of relative gene expression data using real-time quantitative PCR and the  $2^{-\Delta\Delta\text{CT}}$  method. *Methods*. 2001; 25:402–408.

### **Supplementary Figure Legends**

Supplementary Figure 1. MKK7 expression in cardiac hypertrophy. (A) Expression and phosphorylation of MKK7 is down-regulated in hypertrophied hearts of non-human primates (*Macaca mulatta*) and in mice received TAC stress at 1-day, 3-day, 7-day and 5-week. GAPDH used as loading control. (B) Mean echocardiographic left ventricular posterior wall (PW), inter-ventricular septum (IVS) thickness and fractional shorting (FS%) in normal (n=3) and hypertrophied monkey hearts (n=7).

Supplementary Figure 2. Pressure overload by TAC for 3 days in MKK7-CKO mice. (A) Heart weight / tibia length ratio and lung weight / tibia length ratio following pressure overload (n=10 mice/group). (B) Quantitative measurements of myocyte cross-sectional area and fibrosis area after TAC (representative images in left panel, quantitation in bar graph, n=6 mice/group). (C) Cardiac function analysis by echocardiographic assessment of ejection fraction (EF), end-diastolic left ventricular posterior wall thickness (dPW), left ventricular end-systolic dimension (LVESD), left ventricular end-diastolic dimension (LVEDD), and left ventricular mass (LV mass) following TAC (n=10 mice/group). Data presented as mean  $\pm$  S.E.M, ns = not significant.

Supplementary Figure 3. ECG analysis of MKK7-CKO mice after 3-day TAC. Surface ECG parameters show comparable heart rate, R-R interval, P-R interval, P duration and QRS duration between MKK7-Flox and MKK7-CKO mice following 3-day TAC (n=10 mice/group). \*P<0.05, vs Flox/3d-TAC. Data presented as mean  $\pm$  S.E.M. ns = not significant.

Supplementary Figure 4. Arrhythmia vulnerability in MKK7-CKO mice following chronic ISO stimulation of 2 weeks. (A) Representative ex-vivo PES traces showing ventricular tachycardia (VT) events after 2-week ISO stimulation (10mg/kg/day) (n=6/group). (B) Monophasic action potential durations at 90% (APD<sub>90</sub>) of repolarizations recorded from ex-vivo Langendorff perfused hearts (n=6 mice/group). Data presented as mean  $\pm$  S.E.M.

Supplementary Figure 5. MKK7-Tg mice show no cardiac dysfunction, repolarization delays or induced arrhythmias. (A) Representative ex-vivo PES traces showing absence of ventricular arrhythmia after 3-day TAC, 7-day TAC, and 5-week TAC (n=9/group). (B) Monophasic action potential durations at 90% (APD<sub>90</sub>) of repolarizations recorded from ex-vivo Langendorff perfused hearts from 3-day TAC stressed MKK7-Tg mice (n=9 mice/group). (C) Morphological and echocardiographic measurements of heart weight/tibial length ratio (HW/TL), left ventricular mass (LV mass), ejection fraction (EF), left ventricular end-diastolic dimension (LVEDD), left ventricular end-systolic dimension (LVESD), and end-diastolic left ventricular posterior wall thickness (dPW) are comparable between the wild-type and MKK7-Tg mice under 3-day TAC (n=9 mice/group). (D) APD<sub>90</sub> of repolarizations recorded from ex-vivo Langendorff perfused hearts after 7-day TAC (n=9 mice/group). (E) Echocardiographic measurements show comparable cardiac function between wild-type and MKK7-Tg mice after 7-day TAC (n=9 mice/group). (F) APD<sub>90</sub> of repolarizations recorded from ex-vivo Langendorff perfused MKK7-Tg hearts after 5-week TAC (n=9 mice/group). (G) Echocardiographic measurements of wild-type and MKK7-Tg mice after 5-week TAC (n=9 mice/group). Data normalized to *Gapdh* and presented as mean ± S.E.M, ns = not significant.

Supplementary Figure 6. qPCR analyses of K<sup>+</sup> channel expression in hypertrophied models. qPCR detection of mRNA levels of *Kcnp2*, *Kcnd2*, *Kcnh2*, *Kcna5* and *Kcnj11* in (A) MKK7-CKO myocardium under 2-week ISO stimulation (n=4 mice/group), in (B) MKK7-Tg after 3-day TAC (n=4 mice/group), in (C) C57BL/6N mice under 5-week TAC (n=5-6 mice/group). (C) mRNA levels of *Kcnp2*, *Kcnh2*, *Kcna5* and *Kcnj11* in hypertrophied primate hearts (n=3 for normal hearts, n=7 for

hypertrophied hearts). Data normalized to *Gapdh* and presented as mean  $\pm$  S.E.M, ns = not significant.

Supplementary Figure 7. Representative immunoblot shows decreased KChIP2 protein in MKK7-CKO myocardium following 3 days of TAC, while MKK7 protein level remained unaltered, but its phosphorylation level was increased in the MKK7-Flox hearts. GAPDH used as loading control.

Supplementary Figure 8. Expression of ion-transporters in MKK7-CKO mice following 3-day TAC. Genes encoding for sodium channel (*Scn5a*), calcium channel (*Cacna1c*, *Cacna2d2*), potassium channels (*Kcna4*, *Kcnb1*, *Kcne1*, *Kcnj2*, *Kcnj12*, *Kcnq1*), exchangers (*Slc8a1*, *Atp1a4*), gap junction (*Gja1*), and key receptors (*Irpt2*, *Ryr2*) were assessed by quantitative real-time PCR and analyzed by multiple testing Bonferroni correction and two-way ANOVA with Bonferroni post-hoc tests that showed their levels were comparable between the groups of MKK7-CKO/3d-TAC versus MKK7-Flox/3d-TAC. (n=12 mice/group). Data normalized to *Gapdh* and presented as mean  $\pm$  S.E.M, ns = not significant.

Supplementary Figure 9. qPCR analyses of *Kcnip2*, *Kcnd2*, *Kcnh2*, *Kcna5* and *Kcnj11* in NRCMs. Data derived from 4 independent experiments performed in triplicates, normalized to *Gapdh* and presented as mean  $\pm$  S.E.M.

Supplementary Figure 10. K<sup>+</sup> channel promoter regions contain KLF binding sites. Schematic diagram of consensus KLF binding sites in promoter regions of *Kcnip2*, *Kcnd2*, *Kcnh2*, *Kcna5* and *Kcnj11* genes.

Supplementary Figure 11. Characterization of HDAC2 and JNK in response to hypertrophic stress. Representative immunoblots show increased phosphorylation of HDAC2 and JNK1/2 along with TAC (1-day to 7-day) in wild-type hearts, but is declined in 5-week TAC stressed hearts. Similarly, ISO is able to induce phosphorylation of HDAC2 and JNK1/2 (30mins to 12h), but reduced their phosphorylation thereafter.

Supplementary Figure 12. Proximity ligation assay (PLA) detection of *in situ* FLNA association with KLF4 and HDAC2 in NRCMs. Representative images of NRCMs being fixed and probed with anti-FLNA antibody (mouse) and anti-KLF4 antibody (rabbit) or anti-FLNA antibody (rabbit) and anti-HDAC2 antibody (mouse) indicate KLF4/FLNA association and HDAC2/FLNA association in the nuclei of MKK7-knockdown NRCMS following ISO stress (upper panels, scale bar: 10µm). Lower panels show controls using only anti-KLF4 antibody (rabbit) or anti-HDAC2 (mouse). Arrows indicate the association in nuclei.

Supplementary Figure 13. Detection of FLNA association with KLF4 and HDAC2 in MKK7-Tg hearts. Immunoprecipitation analyses show no FLNA interaction with KLF4 or HDAC2 in MKK7-Tg hearts of 3-day TAC or 7-day TAC. GAPDH used as the loading control.

Supplementary Figure 14 ChIP assays reveal increased KLF4 binding and higher H3ac level at the promoter regions of *Kcnip2*, *Kcnd2*, *Kcnh2*, *Kcna5* and *Kcnj11*

following VPA treatment in MKK7-CKO/3d-TAC mice (n=4 mice/group, data normalized to % input DNA and expressed as fold change relative to control).

Supplementary Figure 15. VPA treatment profile in MKK7-CKO mice of 3-day TAC. (A) Measurement of transcript levels of *Scna5*, *Cacna1c*, and (B) *Nppa*, *Nppb*, *Col3a1* (n=5 mice/group). (C) Cardiac morphology and function is comparable between vehicle and VPA treatment, shown by HW/TL, EF, and LV mass after treatment (n=10 mice/group). Data presented as mean  $\pm$  S.E.M, ns = not significant.

Supplementary Figure 16. Detection of expression of cJun, KLF4 and HDAC2 in prolonged TAC-stressed hearts. Representative immunoblots show comparable protein expression of cJun, KLF4 and HDAC2 in TAC- and sham-hearts of MKK7-Flox versus MKK7-CKO, or in TAC- versus sham-hearts of C57BL/6N mice. GAPDH used as loading control.

Supplementary Figure 17. Characterization of MKK7-CKO mice after 7-day TAC with VPA or vehicle treatment. (A) Heart weight / tibia length ratio following 7-day TAC (n=7 mice/group). (B) Quantitative measurements of myocyte cross-sectional area and fibrosis area after TAC (n=7 mice/group). (C) qPCR analyses of *Nppa*, *Nppb*, *Myh7*, *Col1a2* and *Col3a1*. The data are normalized to *Gapdh* content (n=7 mice/group).

Supplementary Figure 18. Characterization of C57BL/6N mice after 5-week TAC with VPA or vehicle treatment. (A) Heart weight / tibia length ratio following 5-week TAC (n=6 mice/group). (B) Quantitative measurements of myocyte cross-sectional area

and fibrosis area after TAC (n=6 mice/group). (C) qPCR analyses of *Nppa*, *Nppb*, *Myh7*, *Col1a2* and *Col3a1*. The data are normalised to the *Gapdh* (n=6 mice/group).

Supplementary Figure 19. VPA treatment improves cardiac function in MKK7-CKO hearts stressed by 7-day TAC. Cardiac function analyses by echocardiographic assessment show deterioration in MKK7-CKO hearts after 7-day TAC, whereas VPA treatment for 4 days notably improves cardiac function (n=7 mice/group). Data presented as mean  $\pm$  S.E.M values.

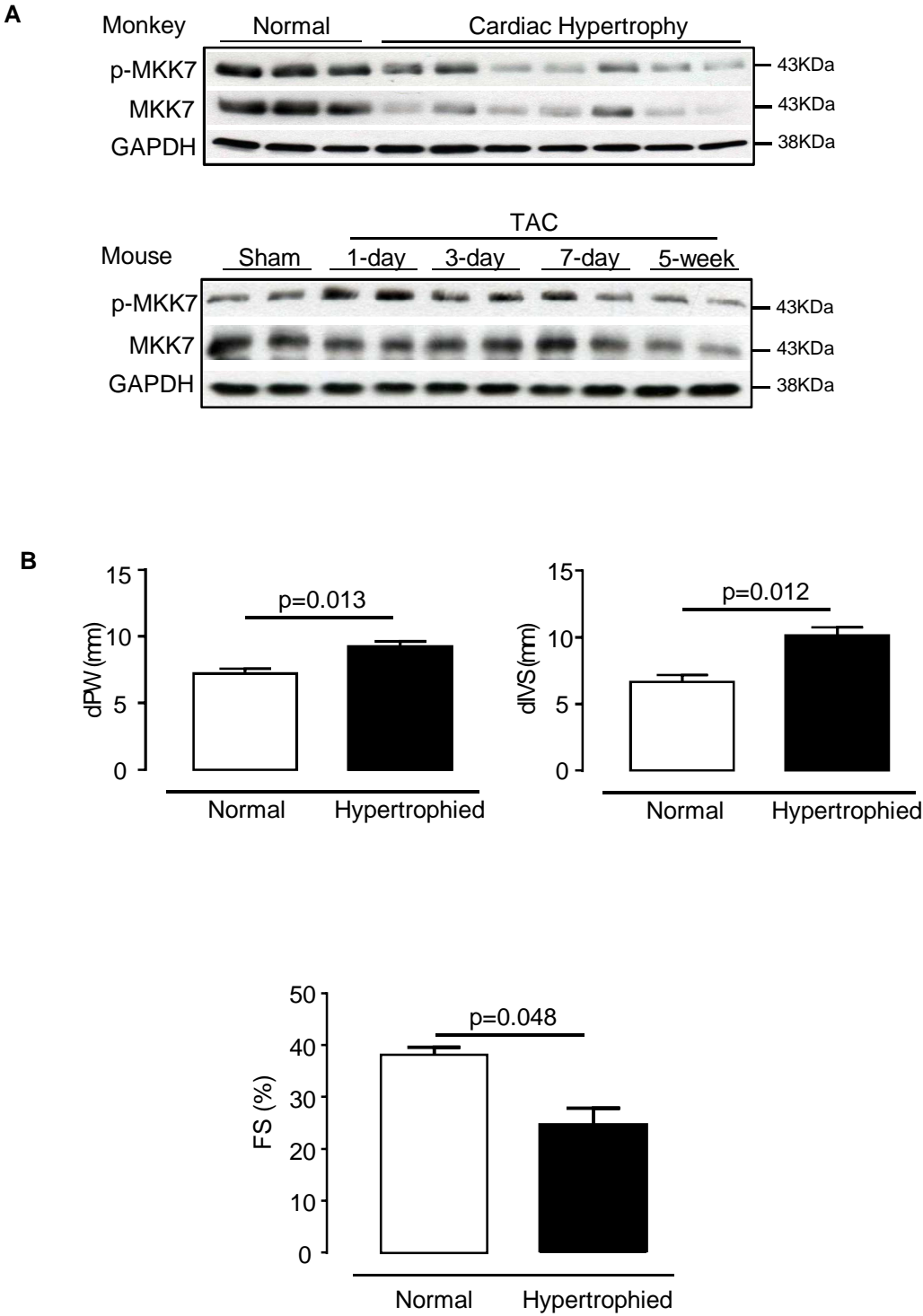
Supplementary Figure 20. VPA treatment improves cardiac function in the hearts of C57BL/6N mice stressed by 5-week TAC. Echocardiographic assessments show deteriorated cardiac function in C57BL/6N mice after 5-week TAC, whereas VPA treatment for 2 weeks improves their cardiac function (n=6 mice/group). Data presented as mean  $\pm$  S.E.M, ns = not significant.

Supplementary Figure 21. Functional characterization of MLC2v-Cre mice following TAC stress. (A) Echocardiographic assessments show normal cardiac function of MLC2v-Cre mice after 3-day TAC compared with MKK7-Flox mice. (B) ECG parameters show normal cardiac electrical activity of MLC2v-Cre mice. n=5 mice/group, data presented as mean  $\pm$  S.E.M, ns = not significant.

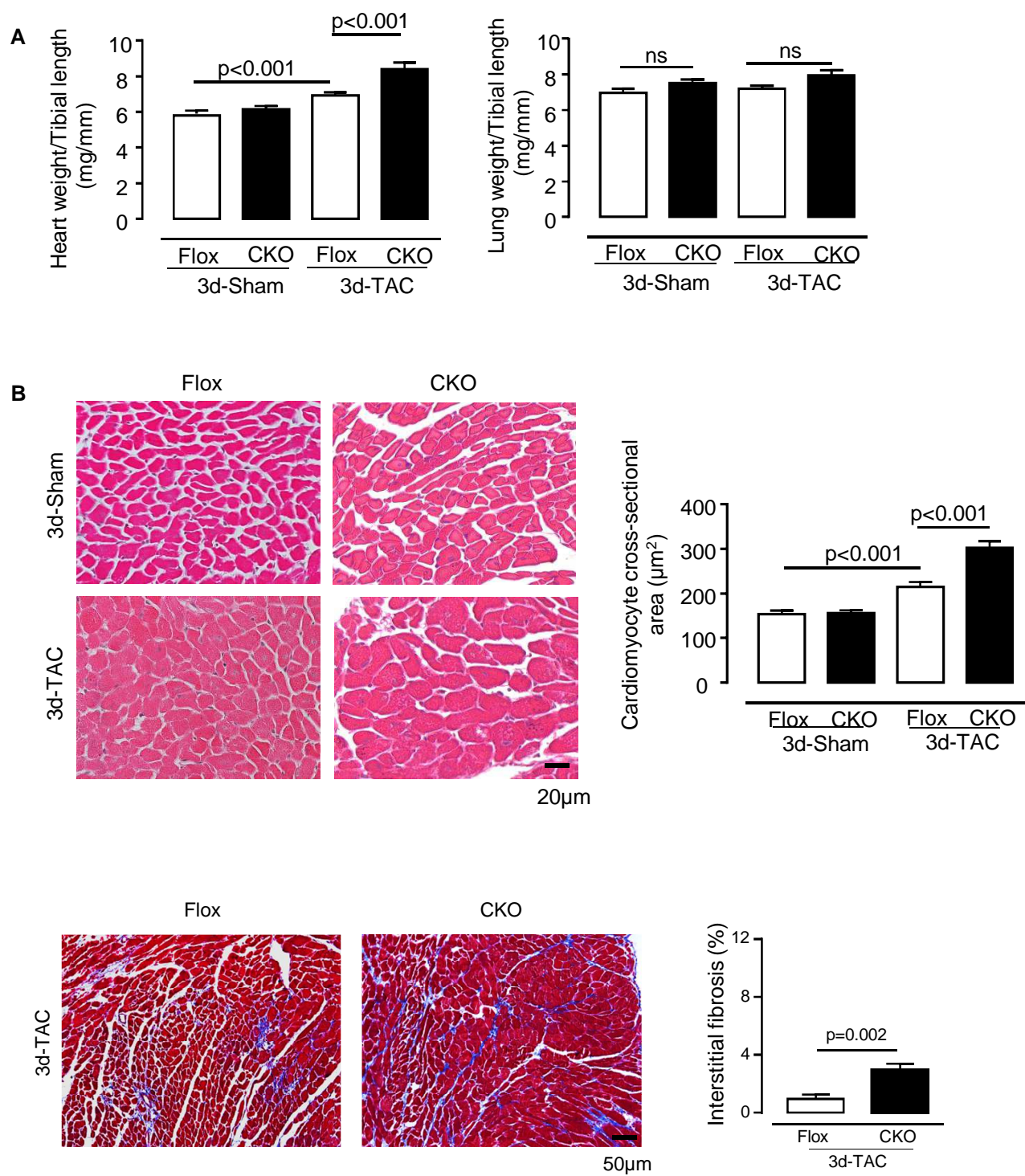
Supplementary Figure 22. Validation of qPCR data. qPCR analyses of *Kcnip2*, *Kcnd2*, *Kcnh2*, *Kcna5* and *Kcnj11* in the hearts of MKK7-CKO mice after 3-day TAC. n=5 mice/group, normalised to *s18* as a reference gene, data presented as mean  $\pm$  S.E.M.



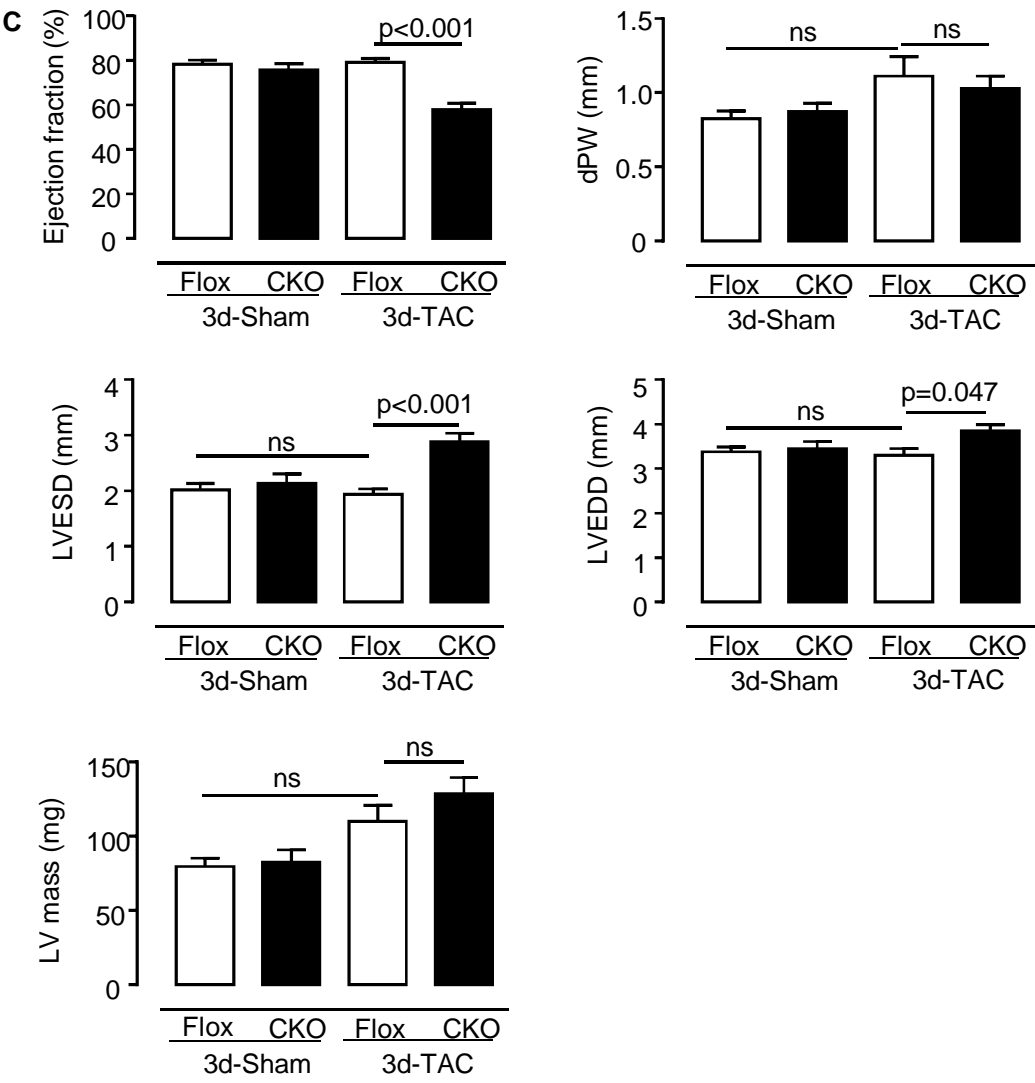
Supplementary Figure 1



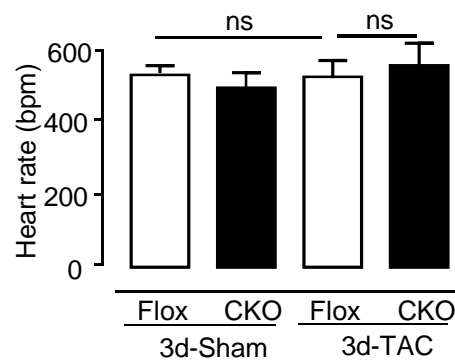
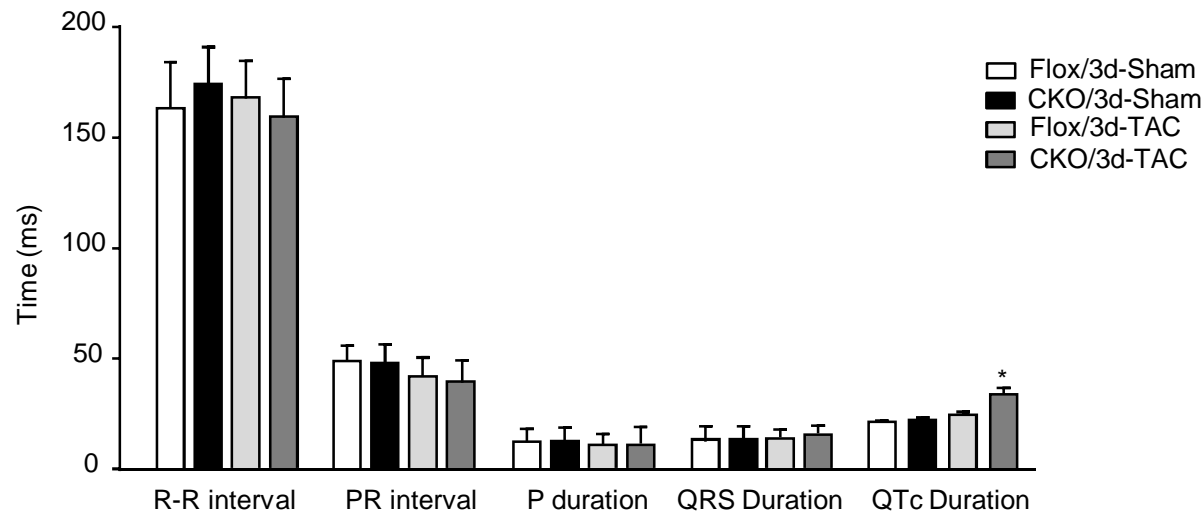
Supplementary Figure 2



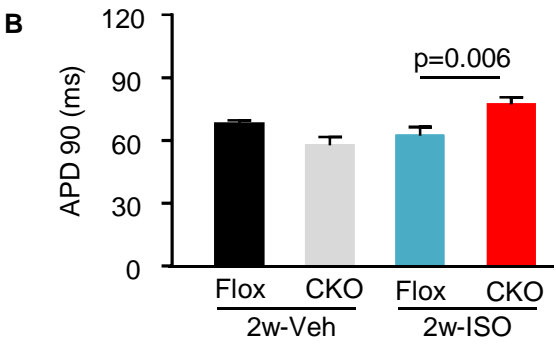
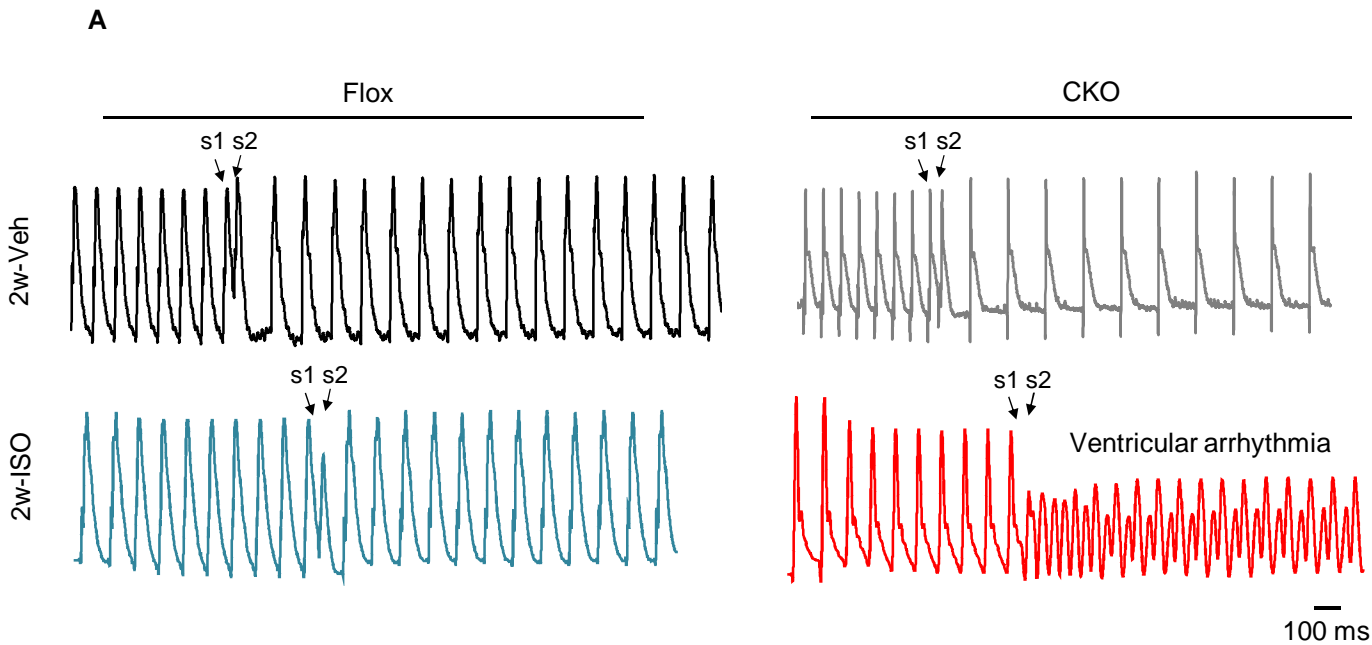
Supplementary Figure 2 (cont.)



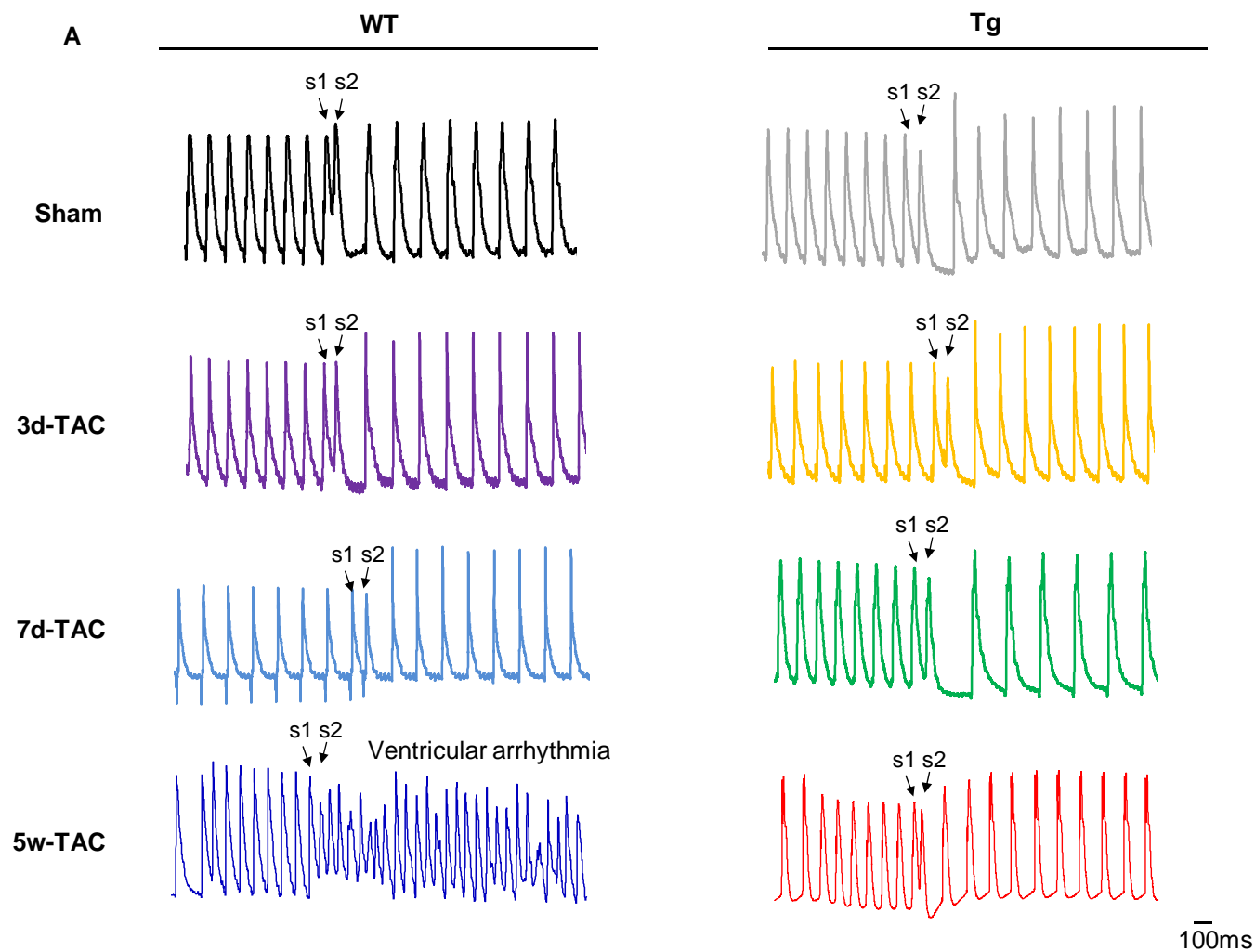
Supplementary Figure 3



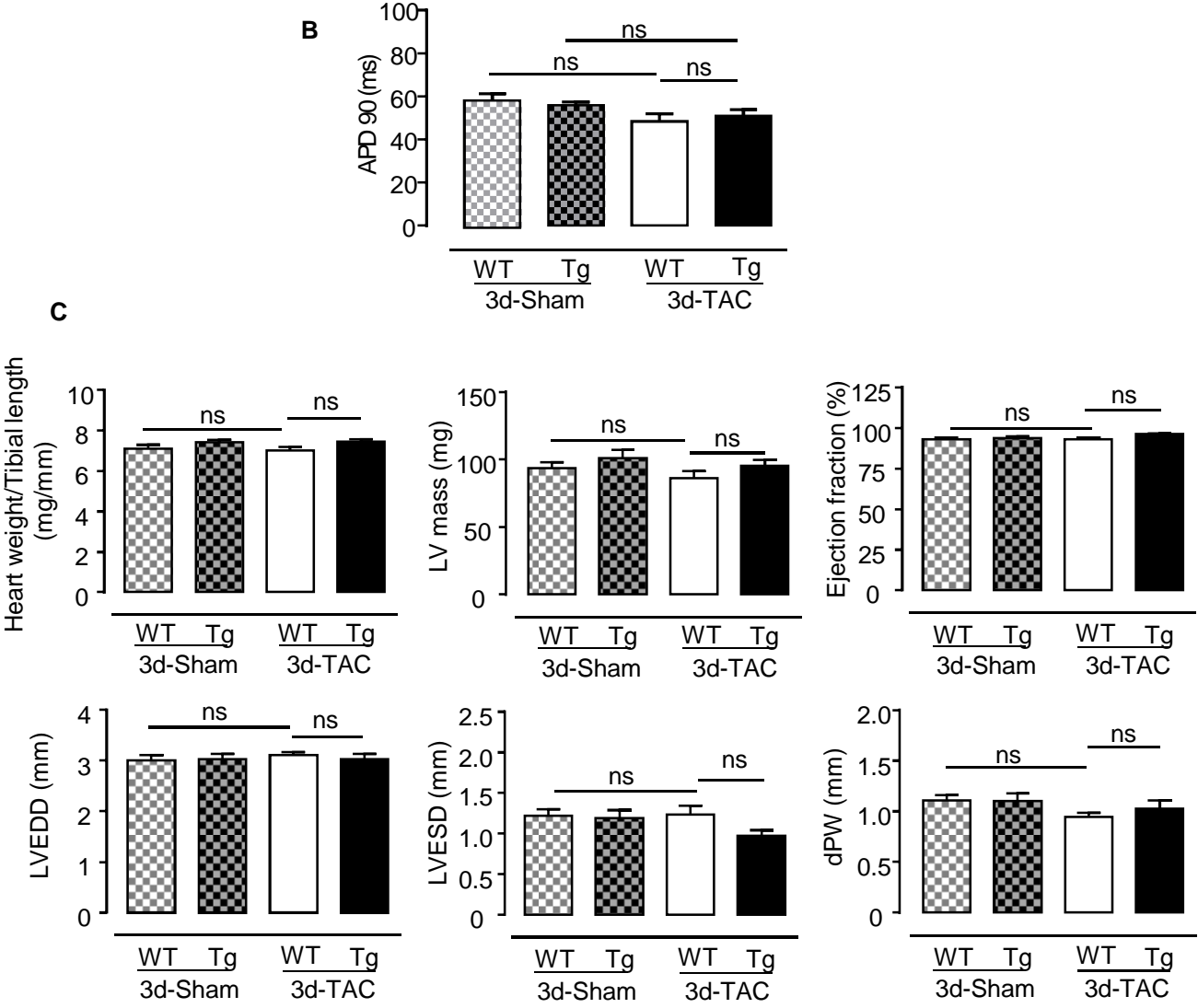
Supplementary Figure 4



Supplementary Figure 5

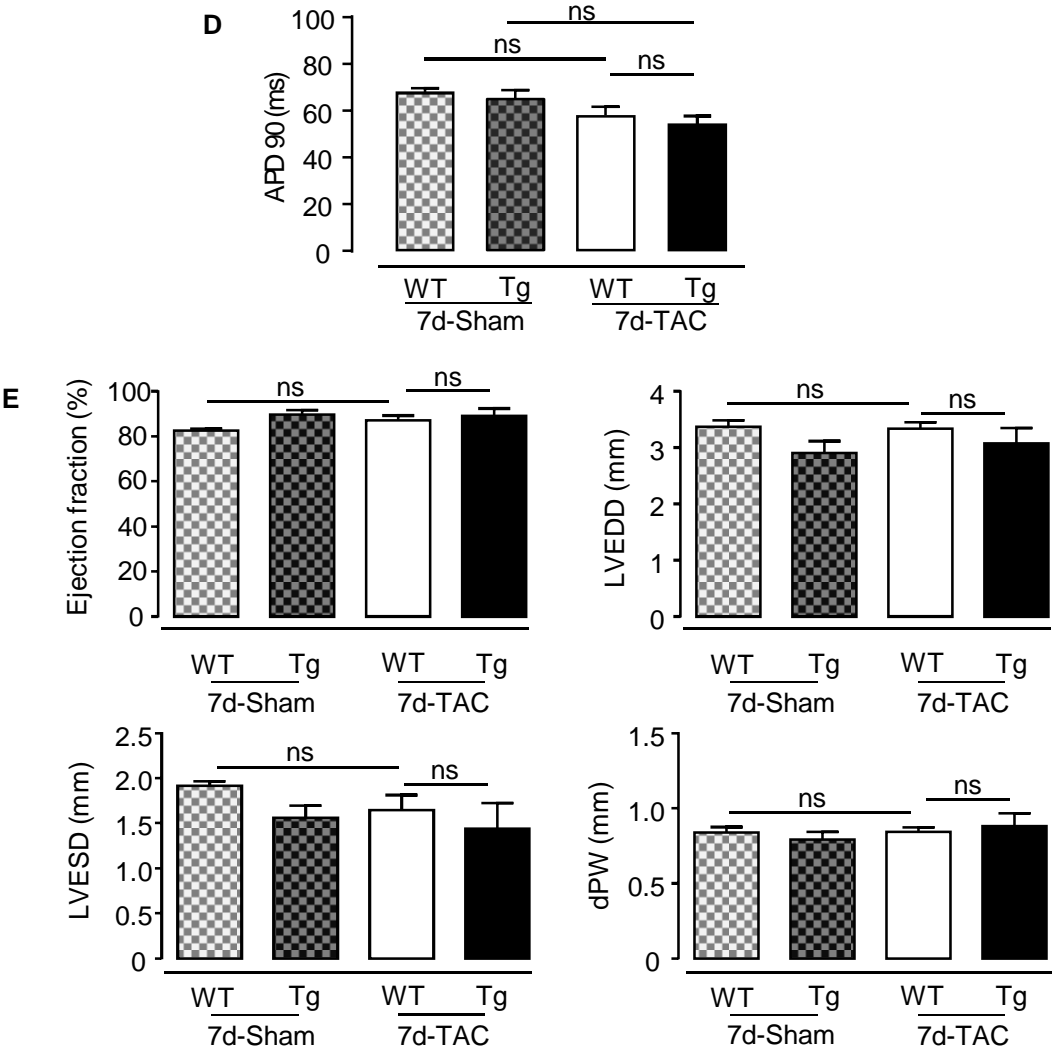


Supplementary Figure 5 (cont.)

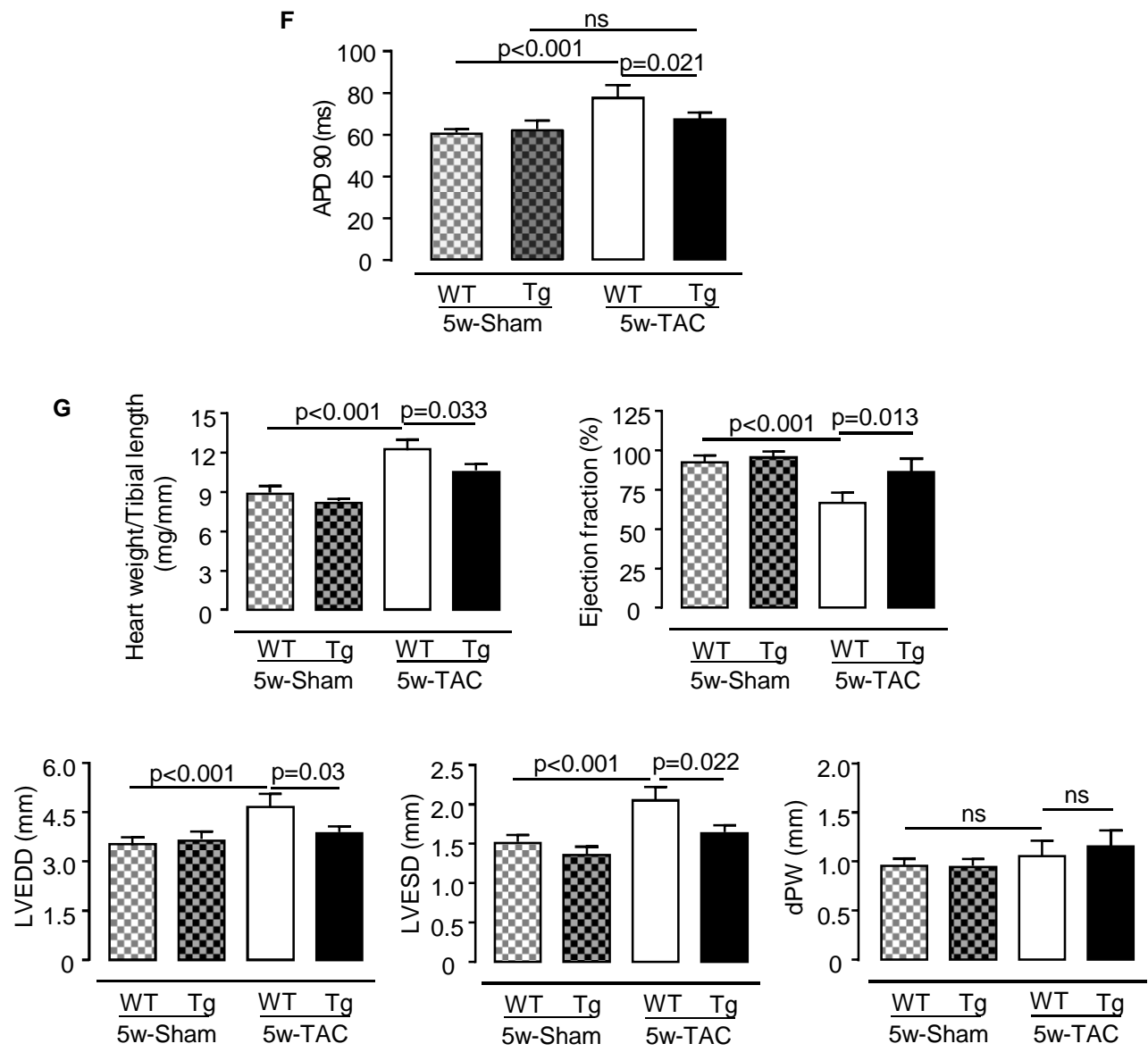




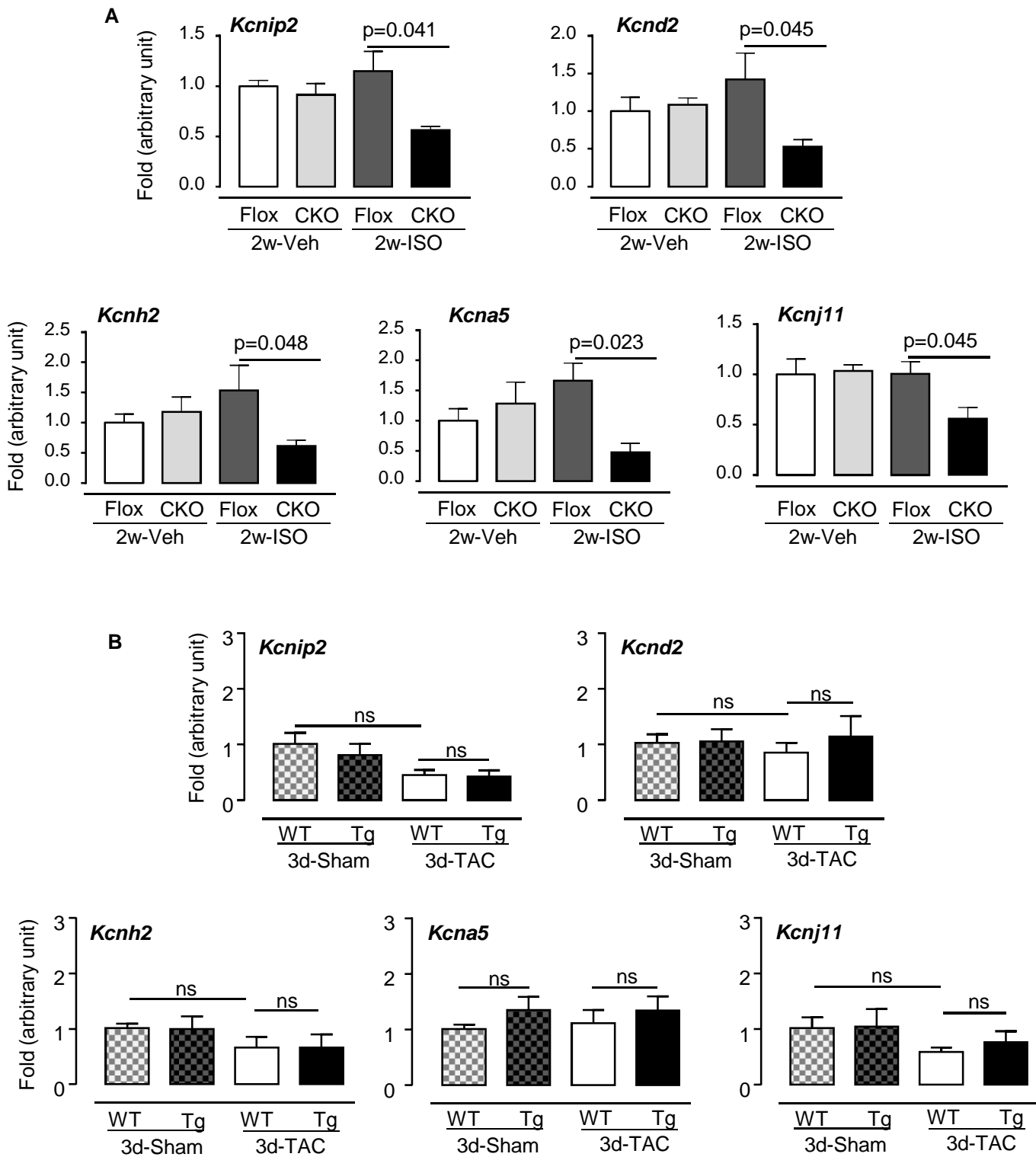
Supplementary Figure 5 (cont.)



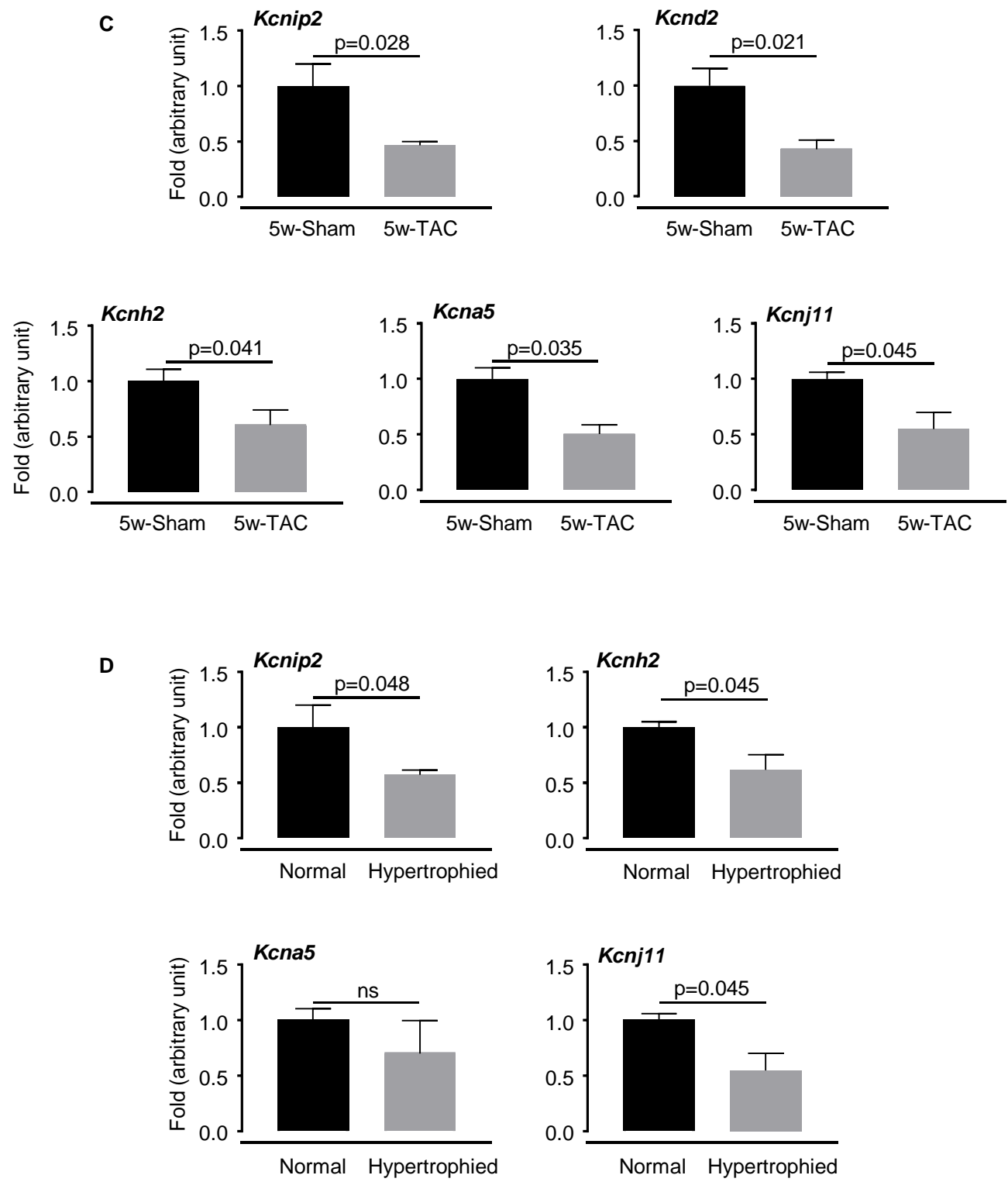
Supplementary Figure 5 (cont.)



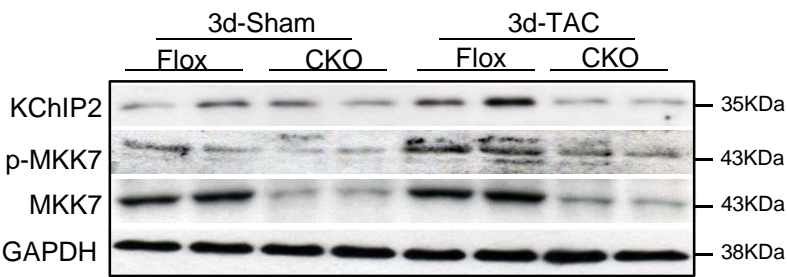
### Supplementary Figure 6



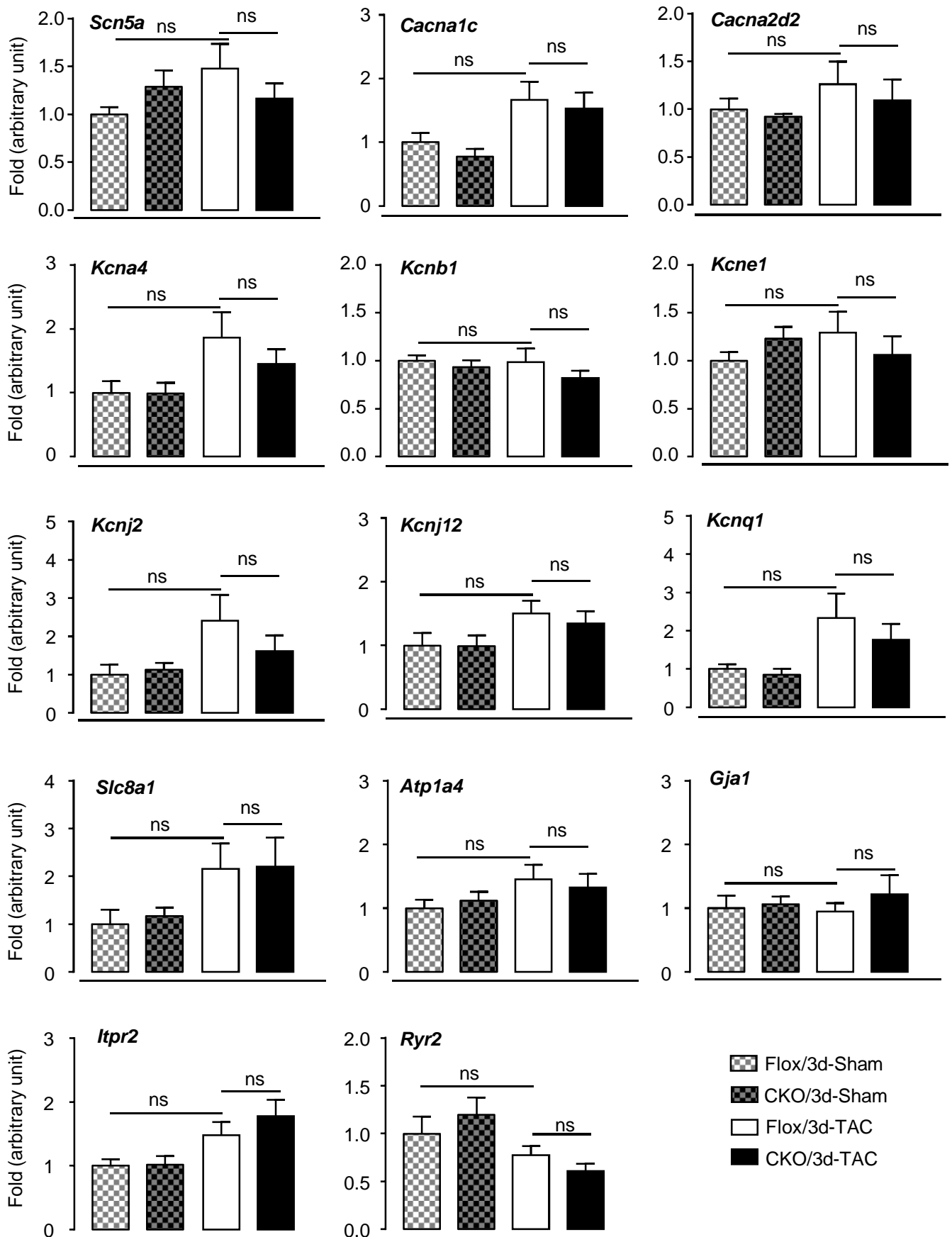
Supplementary Figure 6 (cont.)



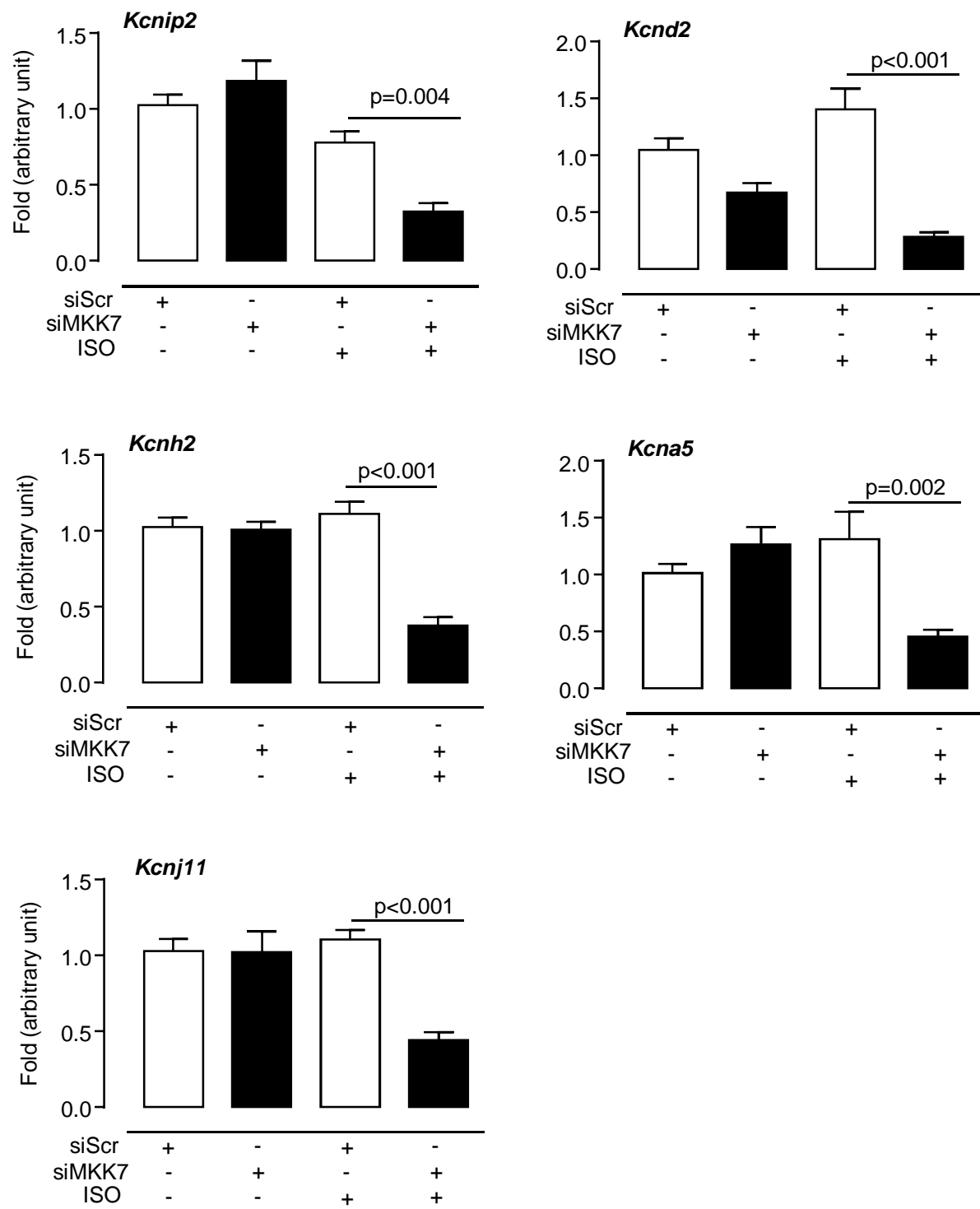
Supplementary Figure 7



**Supplementary Figure 8**

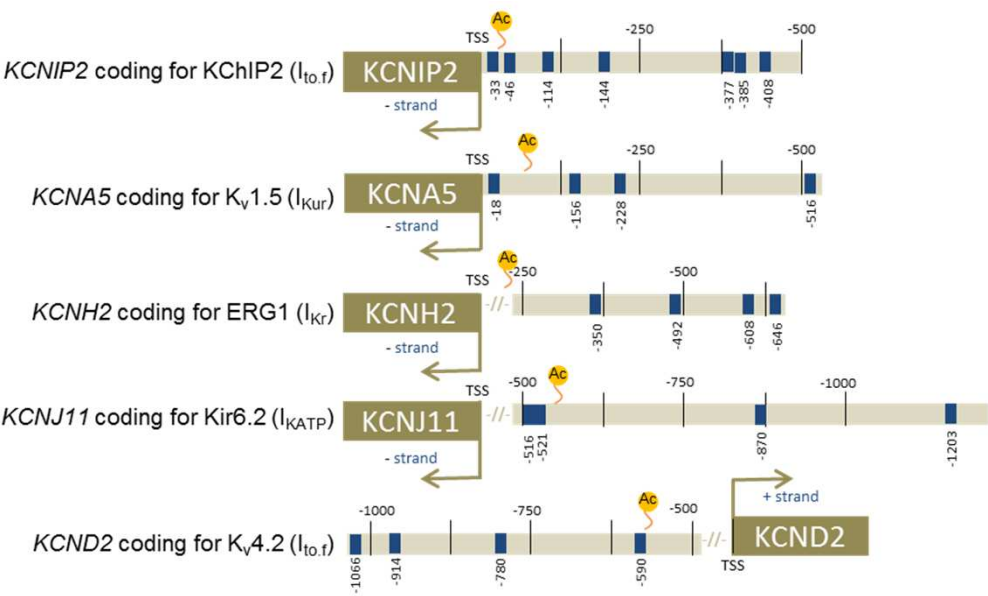


Supplementary Figure 9

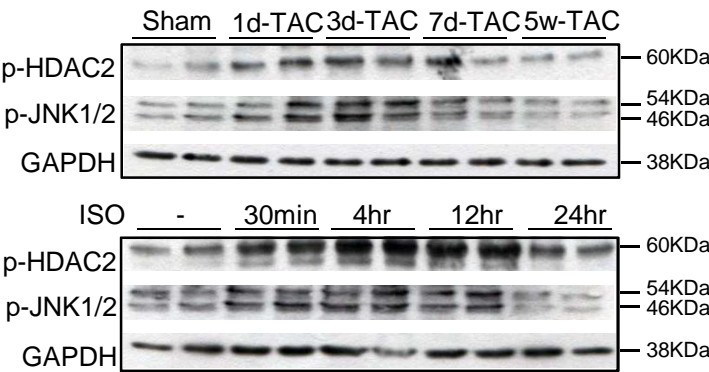




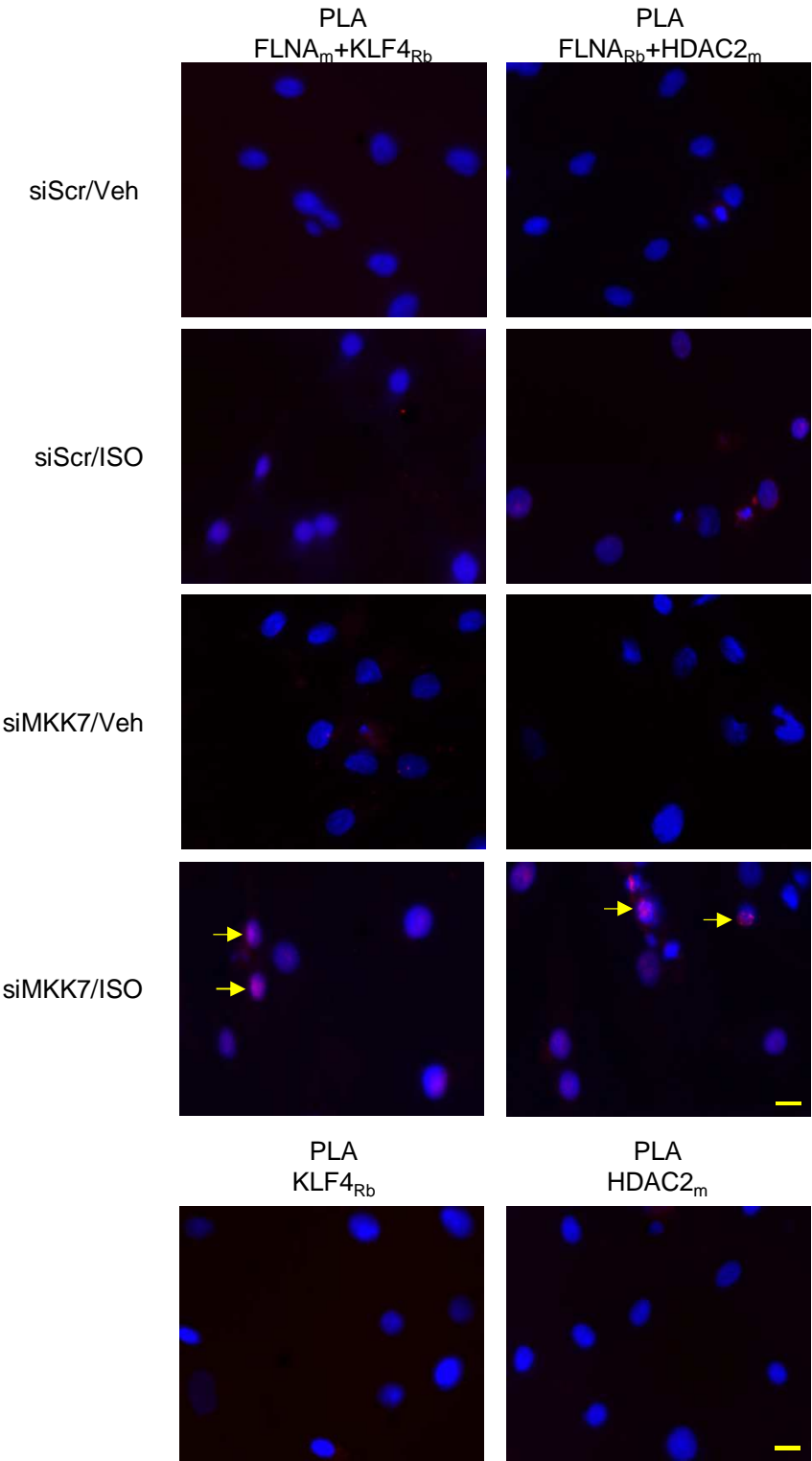
Supplementary Figure 10



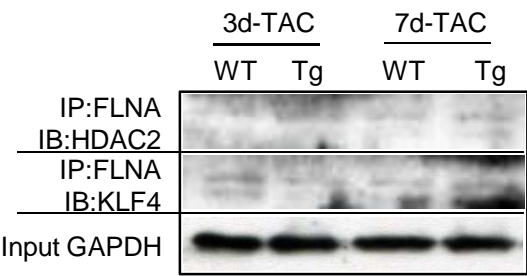
Supplementary Figure 11



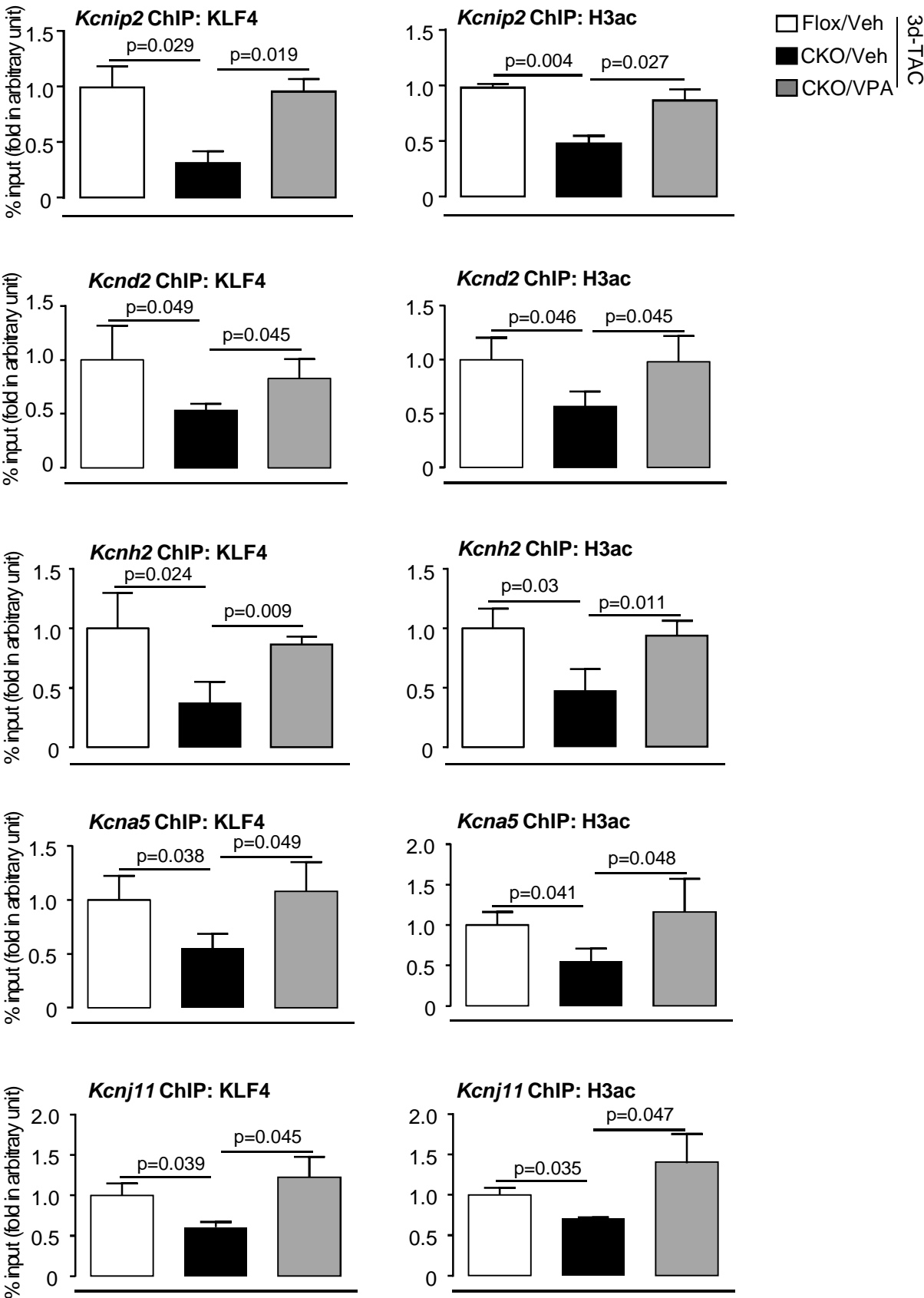
Supplementary Figure 12



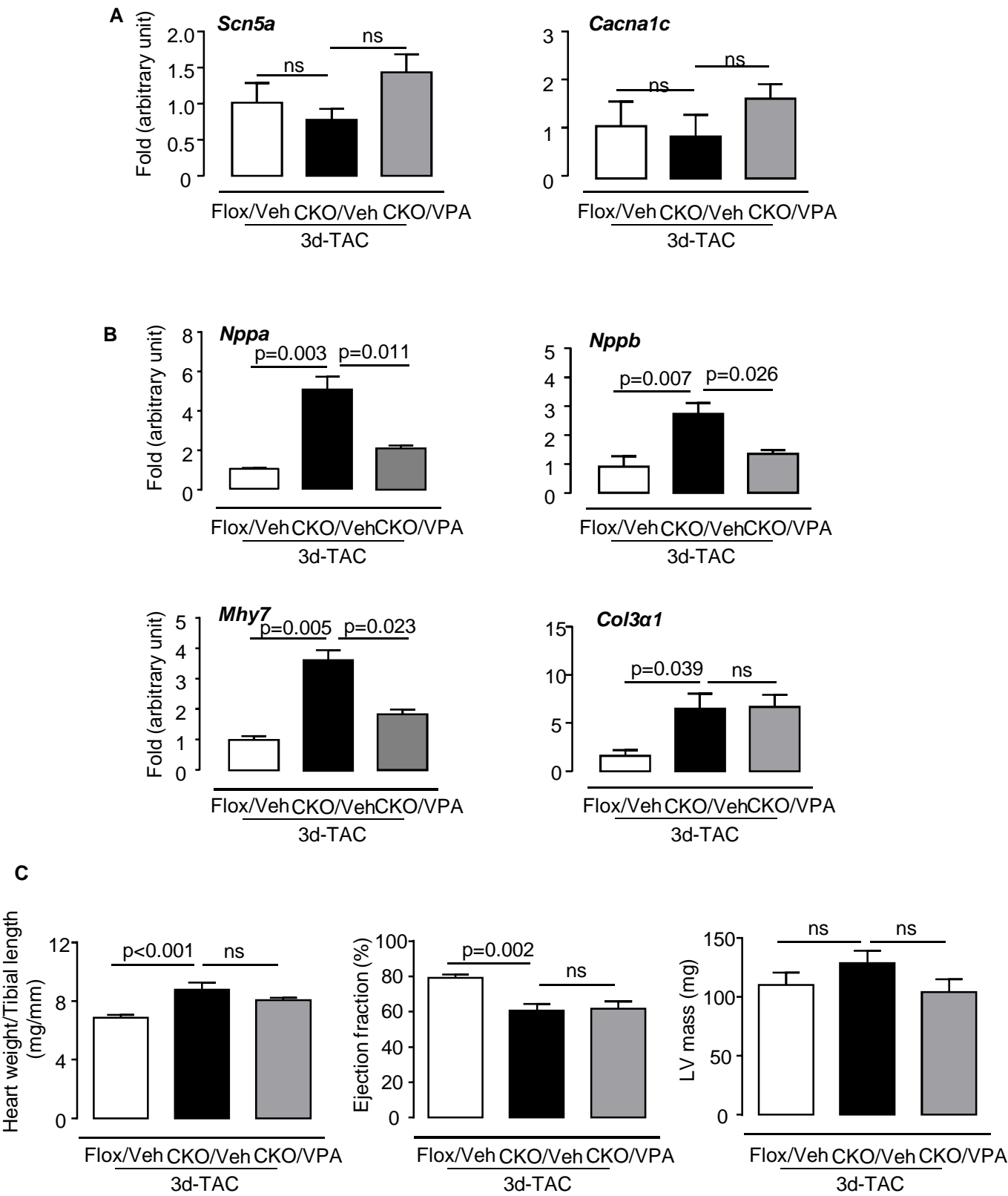
Supplementary Figure 13



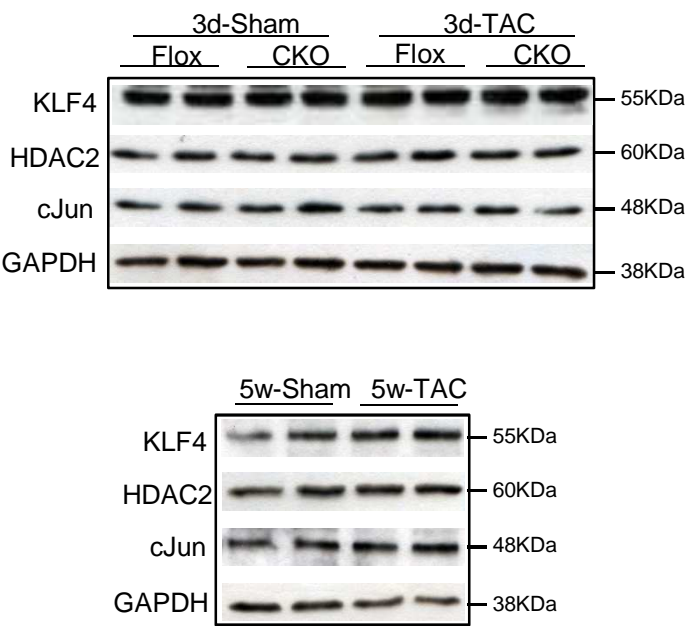
Supplementary Figure 14



Supplementary Figure 15

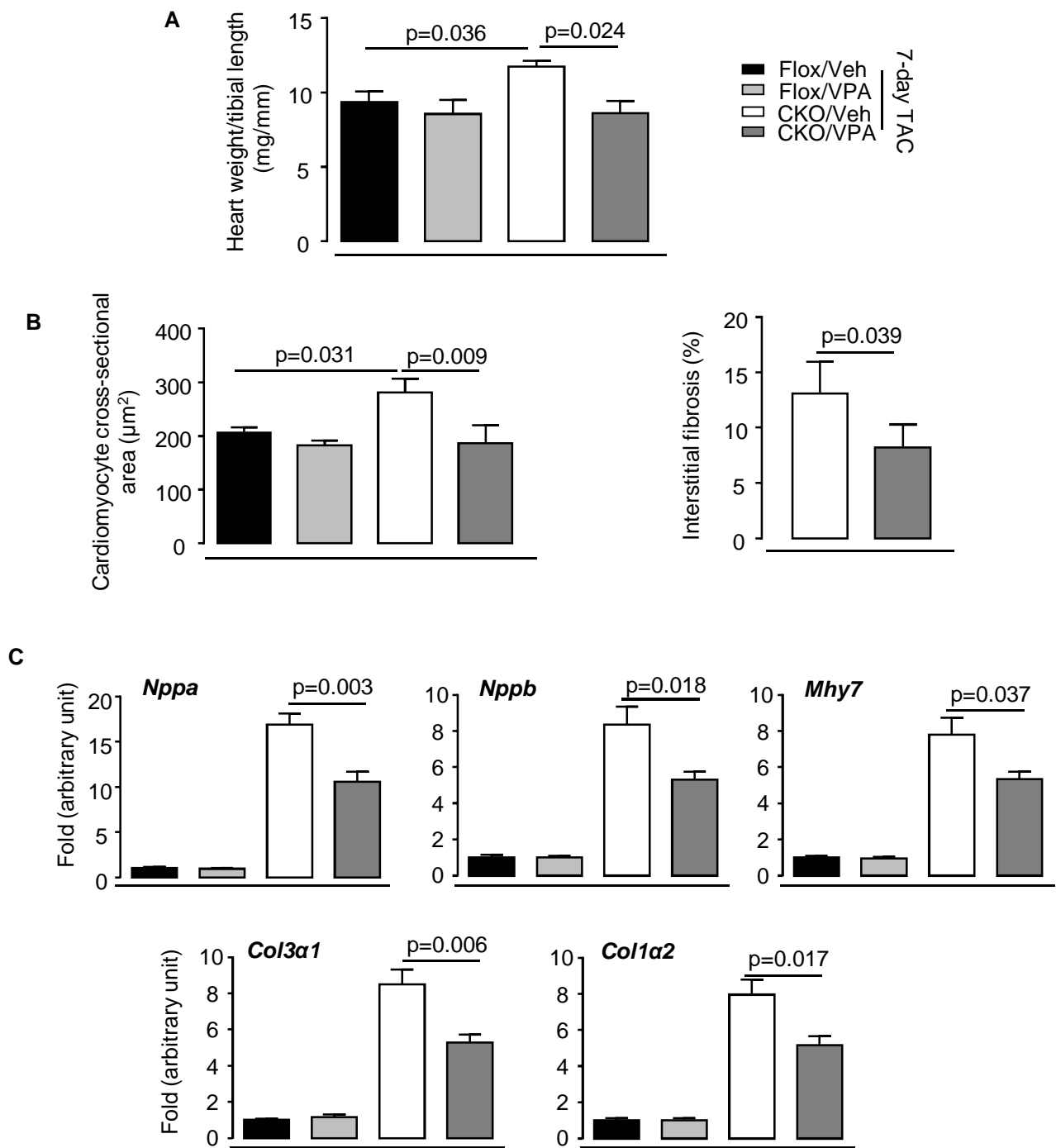


Supplementary Figure 16

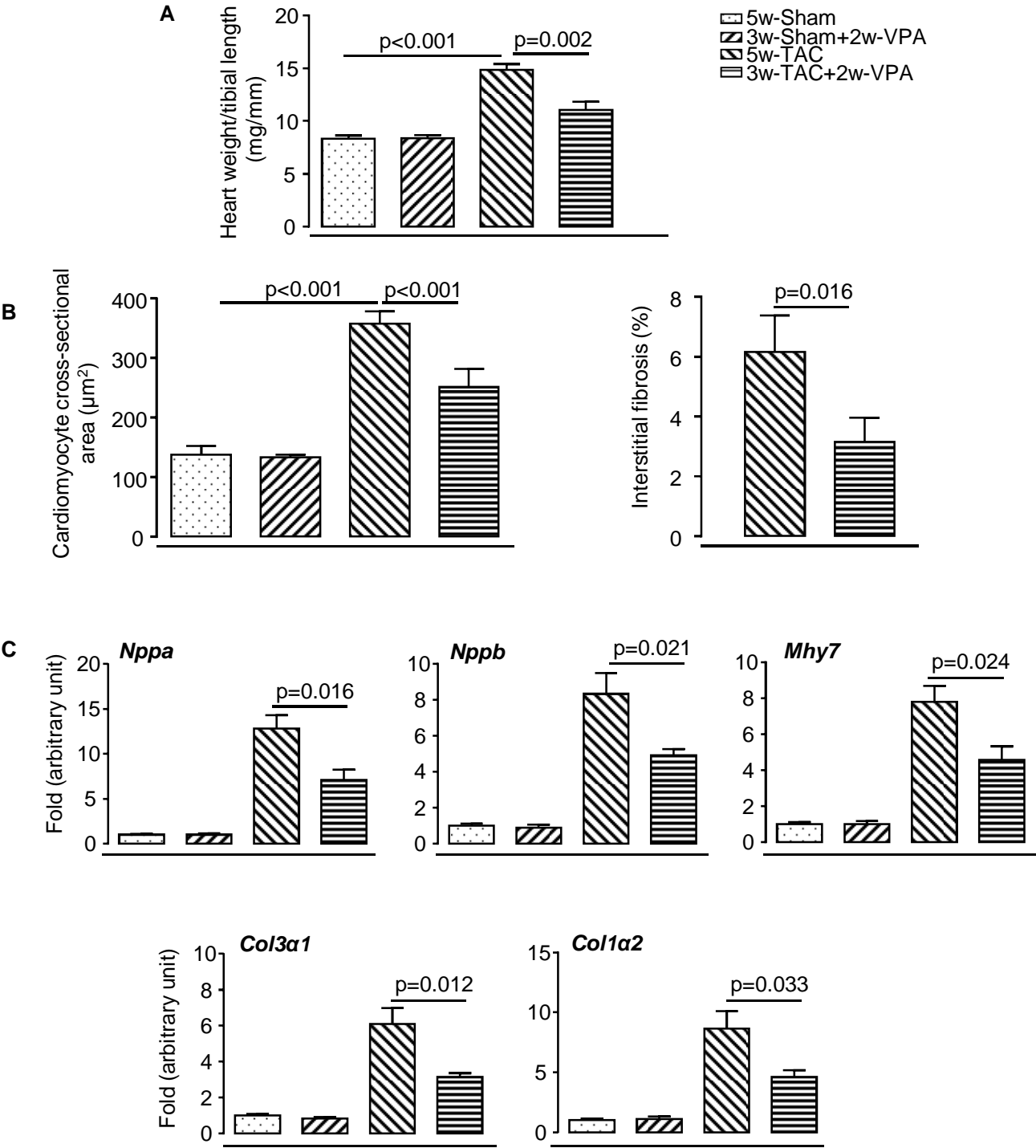




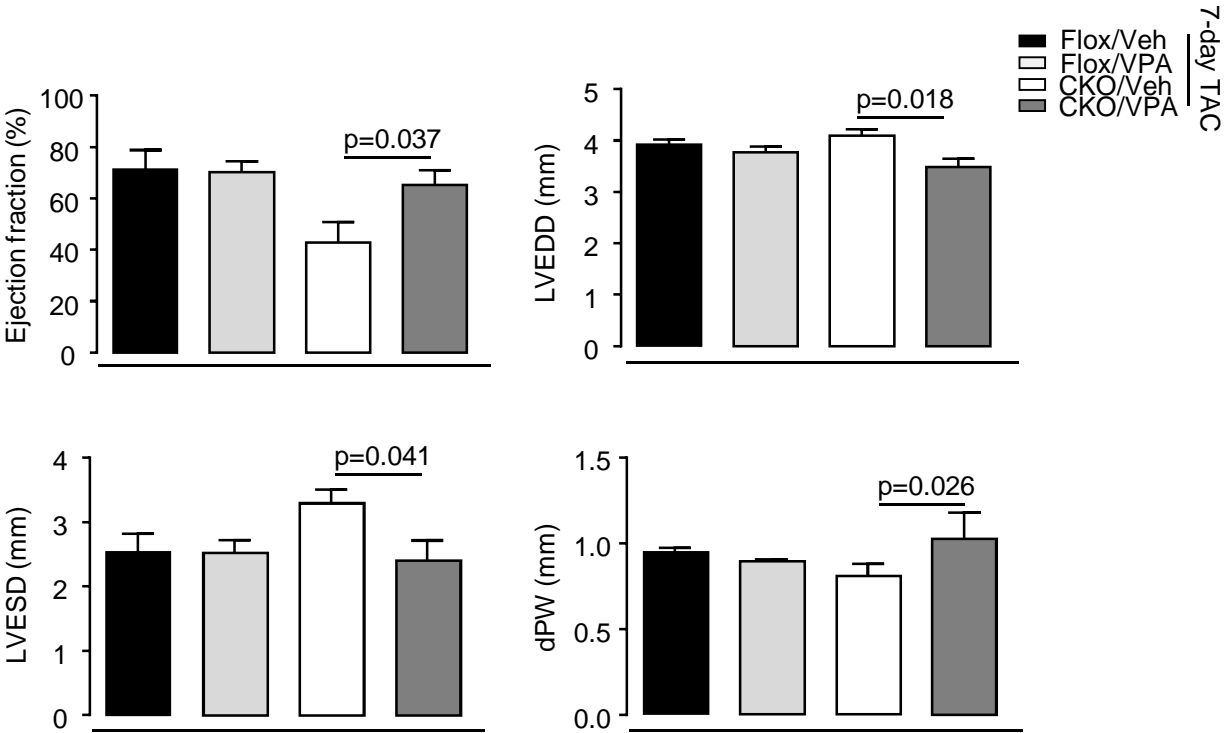
Supplementary Figure 17



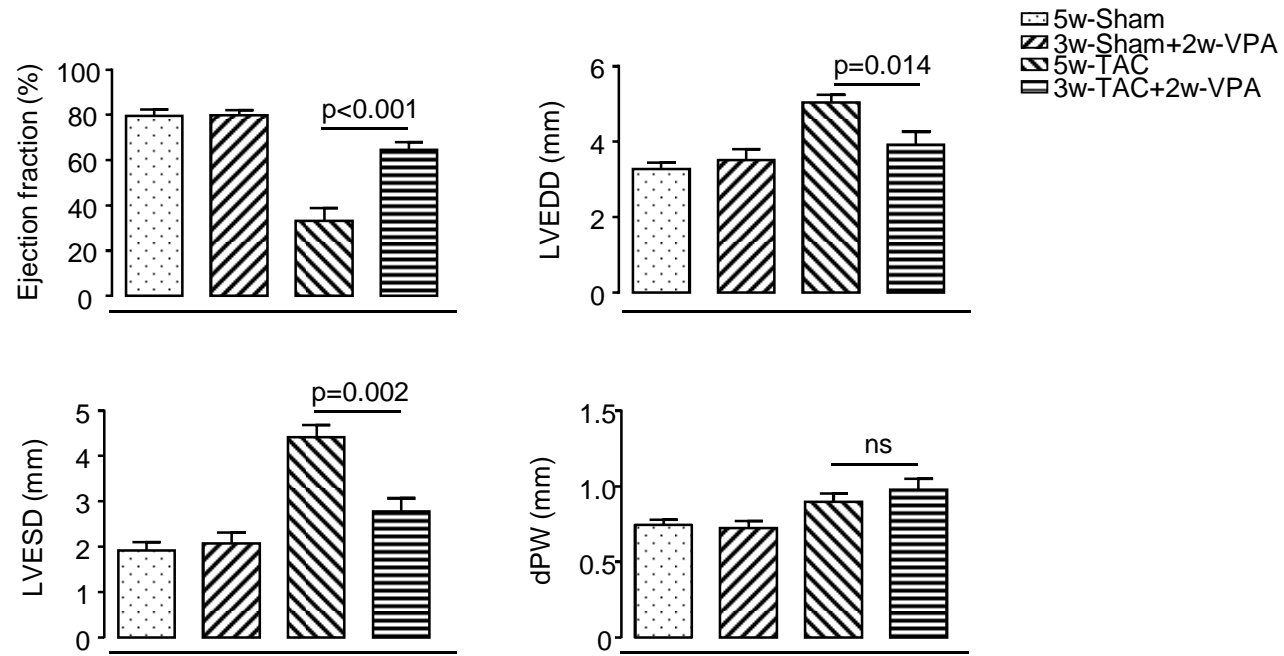
Supplementary Figure 18



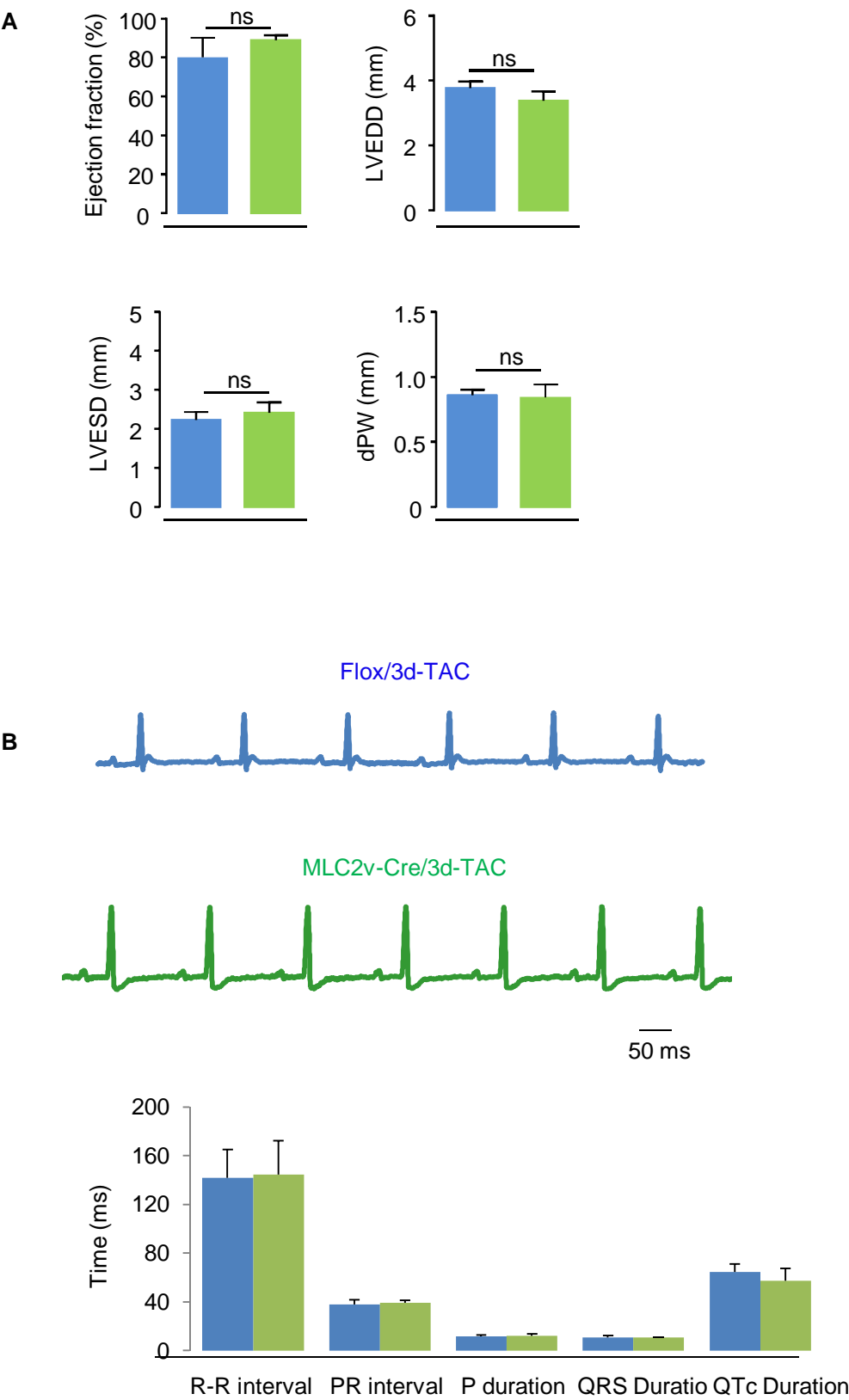
Supplementary Figure 19



Supplementary Figure 20



Supplementary Figure 21



Supplementary Figure 22

